CHALMERS
UNIVERSITY OF TECHNOLOGY

Impacts of integrating solar PV power to an existing grid

Case Studies of Mölndal and Orust energy distribution (10/0.4 kV and 130/10 kV) grids

Master's thesis in Electric Power Engineering

Enock Mulenga

Department of Energy and Environment
Division of Electric Power Engineering
Chalmers University of Technology
Gothenburg, Sweden 2015

Master's thesis

Impacts of integrating solar PV power to an existing grid:

Case studies of Mölndal and Orust energy distribution (10/0.4 kV and 130/10 kV) Grids

Enock Mulenga

In partial fulfilment for the award of Master of Science degree in Electric Power Engineering, in the Department of Environment and Energy, Division of Electric Power Engineering, Chalmers University of Technology, Gothenburg, Sweden

Supervisors: Jacob Edvinsson
WSP-Sverige SE-402 51
Department-Electrics
Gothenburg -Sweden
Email: jacob.edvinsson@wspgroup.se

Martin Skoglund
WSP-Sverige SE-402 51
Department-Electrics
Gothenburg -Sweden
Email: martin.skoglund@wspgroup.se

Examiner: Tuan Anh Le
Division of Electric Power Engineering
Chalmers University of Technology SE-412 96
Gothenburg-Sweden
Email: Tuan.le@Chalmers.se

Department of Energy and Environment
Division of Electric Power Engineering
CHALMERS UNIVERSITY OF TECHNOLOGY
Gothenburg, Sweden 2015

Impacts of Integrating Solar PV Power to an Existing Grid: Case Studies for Mölndal and Orust Energy distribution (10/0.4 and 130/10 kV) grids

Master's Thesis within the Master's programme in Electric Power Engineering

Enock Mulenga

Department of Energy and Environment
Division of Electric Power Technology
Chalmers University of Technology
SE-412 96 Gothenburg
Sweden
Telephone: + 46 (0)31-772 1000
Fax: +46 (0)31-7721633

Cover: Photo of Photovoltaics (PV) Panels taken at Swedish 1MW PV Plant at Västerås

Chalmers Bibliotek, Reproservice
Gothenburg, Sweden 2015

Impacts of Integrating Solar PV Power to an Existing Grid
Case Studies for Mölndal and Orust Energy Distribution (10/0.4 and 130/10 kV) grids
Master's Thesis within the Master's programme in Electric Power Engineering

Enock Mulenga

Department of Energy and Environment
Division of Electric Power Engineering
Chalmers University of Technology

Abstract

Abundance existence of solar energy from the sun on the globe has brought potential for rapid growth of solar photovoltaic (PV) rooftops/power plants connection to existing grids at transmission and distribution levels. The connections are likely to bring impact challenges of integration and operations of the grids by utility companies. The steady state integration impacts of solar PV power to existing grids were studied with focus on the distribution grids of Mölndal energy (10/0.4 kV) residential distribution grid and Orust energy (130/10 kV) distribution grid. The steady state impacts on voltage level, voltage profile, voltage drop, losses, line loading and voltage stability on the distribution grids were studied. The study approached the integration impacts by comparison method of the distribution grids without solar PV power integrated, with solar PV power integrated and with different penetration levels (0%, 30%, 60% and 90%) of integrated solar PV power with aid of simulation software NEPLAN, Paladin Designbase and PVSyst for solar PV power production for the grid areas. The impacts study revealed that integration of solar PV power for the distribution grids studied in general caused an increase in voltage profile, voltage level, decrease in voltage drop and losses, and improvement in steady state voltage stability of the studied grids. In addition, integration of rooftop PV systems caused a decrease in line loading of feeder cables while integration of large ground utility PV systems caused an increase in line loading of the feeder cable/line to the coupling substation to the grid. The increase in PV power penetrations caused similar latter results in voltage level, voltage drop and voltage stability. However, the grid losses decreased for 40% penetrations level and below for Orust energy distribution grid. The losses started to increase at penetrations higher than 40%. From these results, there is a limit to how much maximum PV power (hosting capacity) a grid could allow. For the grids under study, the hosting capacities were determined. Hosting capacities of 30%, 40% and 25% penetration levels were found for Mölndal area 1, Mölndal area 2 and Orust area distribution grids.

Key Words: Solar Integration, Grid Impacts, Hosting Capacity, Solar PV power, NEPLAN, Paladin designbase, Steady State Voltage Stability, Distribution Grid.

Acknowledgments

This study thesis work would not have been possible without aid and influence of so many people and organisations. Of utmost importance, the thesis work was done and published during the Swedish Institute (SI-Sweden) scholarship award period of August 2013 to June 2015. I express my epitome gratitude to the Swedish Institute for the gesture of scholarship award. SI has made it possible to having this work published at Chalmers University of Technology.

I would like to thank my ever loving family for the support and patience you have had with me during the period of studying for my masters' degree at Chalmers University of Technology. In particular, I thank my wife Rhoda (Mwakhalandiyani), my daughter Bwalya, my elder brother William and my son Kasongo, you have sacrificed a lot for me and only God can reward you.

In addition, this work was done at WSP-Sweden, department of electrics in Gothenburg and collaboration with Chalmers University of Technology-Electric Power Engineering division. I thank with deepest gratitude Dr. Tuan Le, Jacob Edvinsson (WSP), Martin Skoglund (WSP) and WSP (Gothenburg-Sweden) for the opportunity, supervision and guidance of the thesis work. To Mölndal Energy and Orust Energy for provision/permission of using your grid data for the studies, I thank you very much. The evergreen and vibrant classmates and everyone within the electric power engineering department who helped with my master thesis, I say my thank you. I thank my Zambian contingent (In Sweden and Zambia) and friends who have been behind me throughout my stay/study in Sweden. In addition, I thank Kawanga C, Mwambazi B, Chiumya F, Jagger B and all (Zambia and Sweden) for being there for me and encouraging me to forge ahead with studies.

Contents

List of Figures

List of Tables

List of Symbols, Abbreviations and Acronyms

CSP:	Concentrated Solar Power
CST:	Concentrated Solar Thermal
PV:	Photovoltaics
U:	Voltage
ΔV:	Voltage drop
P:	Active power
Q:	Reactive power
Z:	Impedance
R:	Resistance
X:	Reactance
Y:	Admittance
***J*:**	Jacobian matrix
δ:	Load angle
AC:	Alternating current
DC:	Direct Current
P-U Curve:	Active power versus voltage curve
Q-U Curve:	Reactive power versus voltage curve
G:	Solar irradiation
C:	Photovoltaic cell constant
MPP:	Maximum Power Point
MPPT:	Maximum Power Point Tracking
VI:	Variability Index
CI:	Clearness Index
SVC:	Static Var Compensator
STACOM:	Static Compensator
D-STATCOM:	Distribution STATCOM
PVSyst:	Solar design software
NEPLAN:	Power system simulation software
Paladin designbase:	Power system simulation software
%:	Percentage
OLTC:	On Load Tap Changer
S.S:	Steady State
SPPT	Sustainable Power Production and Transportation

1 Introduction

This chapter introduces the background to the impacts of integrating solar PV power to an existing grid. It describes the aims, problem tasks and scope that were used in studying the topic of solar PV power integration. It introduces the skeleton structure of the thesis report.

1.1 Background

Solar power is the production of electric power by utilizing thermal energy of sunlight rays from the sun. It consists of a solar power source and a converter of the energy from sunlight to electric energy. This power can be independent of a conventional power grid or can be integrated to an existing conventional electricity grid at transmission or distribution level. Solar power is divided into two branches of technology that are popular today. These are Concentrated Solar Power (CSP) and Photovoltaic (PV) solar power systems.

Solar power in form of CSP operates similar to thermal power plants and is sometimes referred to as Concentrated Solar Thermal. It uses reflecting mirrors that reflect sunlight to a common point and heat a fluid that can further drive a turbine to generate electricity. It is an indirect solar power system. In a solar PV power, sunlight is converted to electrical energy directly by using a photovoltaic material (semiconductor material). The sun hits this material and by photovoltaic action in the material, electrical energy is generated. Concentrated Solar Power system operates like conventional thermal power plants and their effects on the grid can be understood by understanding a thermal power plant. Of much interest is the Photovoltaic (PV) solar power system that operates different from conventional generating systems and the effects to an existing transmission or distribution system need to be fully understood before much integration can be made to any distribution or transmission system in power system.

A solar photovoltaic (PV) power system can operate in isolation or connected to a power grid. The system normally consists of a micro power source (solar) and some local loads. Additionally, it can be a solar system without any loads connected but connected to a power grid. When connected to a grid, the operating conditions of the grid are altered in either a positive or negative way.

There has been rapid increase of grid connected solar PV power in rural, urban and city areas around the globe (e.g. Sweden, Germany, India and some parts of Africa) [1]. This is to enable solar PV Power systems to supply generated power locally and to other places through the existing transmission and distribution power grid. This integration of solar PV power can result in improvements of the grids or can have negative impacts on the steady state system operation parameters.

Integration of solar PV power can have impact on the active and reactive power reliability due to variations of power production and this could in turn impact on the voltage profile, voltage stability and protection of the transmission and /or Distribution power grid after integration.

A study, [2], was conducted at Uppsala University that looked at the hosting capacity of PV and some integration issues in the Swedish distribution grid using Matlab and it was proposed that software such as power system simulation software could be used to further investigate the integration challenges and how much could be ok for a distribution grid.

It was with this background that the thesis was done to investigate the steady state impacts of integrating solar PV power on a distribution power grid. After investigations at minimum and maximum load demand, possible solutions to mitigating the impacts that the integration caused are proposed.

1.2 Aim

The aim of the thesis was to investigate the impacts of integrating solar PV power to an existing distribution power grid. This was done by modelling the distribution grids with and without solar PV power in power system simulation software (Paladin designbase and NEPLAN [28], [29]) to investigate steady state impacts on the distribution grid. The thesis analysed the impacts of the different solar PV penetration levels and their impacts from zero percent to ninety percent (0%, 30%, 60% and 90%). In the process, the hosting capacity of the distribution grid under study is determined. The thesis attempted to answer the following research questions:

1. What are the impacts of solar PV integration with different penetration levels of 0%, 30%, 60% and 90% on voltage level, voltage profile along a feeder, line losses and loading and voltage stability (P-U and Q-U curves)? According to [3], penetration level is defined as in equation (1.1):

$$PV\ Penetration\ Level = \frac{PV\ Generated\ Capacity\ (kWh\ or\ MWh)}{Network\ Peak\ Load\ (kWh\ or\ MWh)} \quad (1.1)$$

2. What is the maximum level of PV power capacity that can penetrate the distribution grid before it causes unstable operation condition.
3. What are the mitigation solutions to the impacts and increasing of the hosting capacity at maximum and minimum load demand?

1.3 Problem/Task

The task was to investigate the steady state impacts of integrating solar PV power to an existing distribution grid in Sweden i.e. Mölndal Energy (mostly urban cable grid) and Orust Energy (mostly rural grid) and propose some mitigation solutions. The thesis involved literature studies/review of related studies on solar PV power impacts and modelling of distribution grids. The task involved the following;

1. Literature review of solar PV power, theoretical integrating issues/challenges, and voltage stability and profile.

2. Software familiarization on use, functions and capabilities of Paladin design base, NEPLAN and PVSyst.
3. Analysis of normal case (without PV Integration).
4. Analysis of PV Integration (with aid of PVSyst software).
5. Analysis of PV Integration scenarios (0%, 30%, 60% and 90% Penetration levels).
6. Hosting Capacity Determination.
7. Mitigation Solutions for PV Integration and Hosting capacity increase.
8. Thesis Report writing.

1.4 Scope

The thesis covered integration of solar power to an existing grid and study of the impacts that the integration can cause on an existing grid. In the integration process, different penetration levels (0%, 30%, 60% and 90%) of the solar PV power were integrated and analysed. It involved literature studies and modelling of power distribution grids in power system simulation software without solar PV power. The loading capacity and voltage profile/stability in steady state of buses at point of connection were studied. Solar PV power was modelled and added to the grid at different penetration levels. The steady state impacts were investigated.

In this scope, steady state impacts on the line loading, losses, voltage level, voltage profile and voltage stability of the distribution grid using power system simulation software of Paladin Design Base and NEPLAN were studied.

1.5 Structure of the Thesis

The thesis is organized in a total of five (5) chapters. These are Introduction, Literature study, Grid Modelling and System Study, Results and Discussions, and Conclusions and Future work. The chapters present the topic of impacts of integrating solar PV power to an existing grid.

The first chapter gives background, aim, tasks, scope and method of executing the study topic. The second chapter reviews literature and theoretical background to the topic. It further explains some concepts in understanding the problem and some expected outcome of the integration of solar PV power.

The third chapter describes the method and approach to grid modelling of the grids to be studied. It presents the processing of data, models built in the software environment, the software used and the system studies to be performed in the studies.

The fourth chapter presents the results of simulations for the normal case and with solar PV power integrated. The impacts in terms of results for Solar PV power integration and scenario simulations of solar PV power penetration levels (0%, 30%, 60% and 90%) are presented. Possible solutions to mitigating the possible problems and increasing the hosting capacity are presented in this chapter. Finally, simulation results are discussed

The fifth and last chapter presents conclusions to the study and suggests future work that can be carried out on the study topic presented.

2 Literature Study

This chapter introduces the concepts of literature that is in line to the subject of integrating solar PV power to an existing grid. It describes the concept of solar PV power, voltage profile, steady state voltage stability and related studies that have attempted to study some impacts of distributed generation in various parts of the world. It will show the concept of two port equations and attempt to explain integration issues of solar PV power to a bus voltage level/profile, voltage drop, line losses and voltage stability.

2.1 Literature Review

The increase in the potential of solar power across the globe due abundant sunlight and aim to reduction in carbon emitting generating systems has sparked interest in research and development of solar PV power systems. This potential coupled with an increase in energy demand and use that is estimated to reach 41% by 2035, [4], has led to an increase in investment of research in Solar systems and the integration to already established grids.

To begin with, the sun does not shine equally on all parts of the earth due to difference in latitude of places. The natural seasons and cloud cover reduces the amount of sunlight reaching the surface of the earth. According to [5], it was discovered that cloud cover has a huge impact on large scale PV power plant output and that the variability of clouds causes variable output of the power from the generating PV plant. Furthermore, [6] explains the modelling of the systems for better operations with varying climatic conditions. Therefore, it is very important to consider the variability of cloud cover as an important parameter on the power production when studying the effects or impacts of integrating solar PV power to a grid.

In addition, integration of solar PV power is rising across the globe and this is a challenge for power utility companies, transmission and distribution system operators. This is because, the impacts of integration are not yet fully understood at both transmission and distribution level. According to studies conducted by [1], the integration of solar PV has a lot of challenges from the systems modelling and simulation point of view. The study looked at the stochastic processes study of the impact of solar PV power voltage levels with extensive use of Matlab.

2.1.1 Impacts on Voltage Level and Profile

According to studies in [1], [2], and [7], the integration of solar photovoltaics to an existing grid is likely to cause impacts on the voltage level and profile. Studies presented in [1] and [2] attempted to establish the impacts of on voltage and determination the maximum distributed photovoltaics generation to the distribution grids in Sweden. Three grids were considered in the studies and showed increase in voltage rise at the bus. Of the three grids, two had voltage rise but without voltage violation and one of the grids experienced overvoltage at some buses. Additionally, the studies in [2] showed that voltage level and profile is not the ultimate factor in determining the maximum penetration level. Other

parameters, for example line loading and losses, should be analysed together with voltage level and profile in determining the hosting capacity of the grids. Furthermore, in [8], [9] and [10], the studies and report presented issue that are related with integration of photovoltaics to a grid. One of the challenges of photovoltaics integration discussed in the papers was voltage level and profile. The integration could cause an increase in voltage level and profile but dependant on the grid configuration and how it is from the source of main power. According to [11] and [12], feeders away from the main power source experience lower voltage than the sending end voltage. Integration of photovoltaics in this case improves the voltage profile along the feeders.

2.1.2 Impacts on Losses and Line Loading

Losses and line loading are very important parameters of a power system. Photovoltaics integration to a grid has potential to alter the two parameters. Transmission lines and feeders have a limit to which they can be loaded. Additionally, losses can either reduce or increase the operation costs of a distribution grid [11]. The studies conducted in [1] and [13] presented the effects of photovoltaics integration on the grid losses. Different penetration levels were used to determine the impact of increased PV penetration on grid losses. According to [1], grid losses decreased at lower photovoltaics penetrations and showed increase in grid losses with increased penetration. However, according to [13], the increase in grid losses with increased penetration levels were correlated with the likely of reverse power flow in a radial grid. This is because reverse power flow increases the feeder line loading and consequently the losses. In addition, it could interfere with protection operations in the grid.

In terms of feeder line loading, [13] and [12] presents the changes in line loading with integration of photovoltaics. They present feeder line loading in a radial grid. With distributed photovoltaics, the line loading reduces with increased photovoltaics penetration until reverse power flow occurs. Reverse power flow increases the line loading with additional increase in penetration levels.

2.1.3 Impacts on Steady State Voltage Stability

Voltage stability of a grid determines the potential of the grid to restore initial operating voltage levels after being subjected to a disturbance [14], [15]. The integration of photovoltaics at a feeder provides active power locally for a power factor of 1 and has potential to provide added reactive power support for a power factor less than 1 [10], [12]. Studies in [7] investigated the effect on voltage stability for a grid in Saudi Arabia and in [16] the steady state voltage stability was investigated. In these studies, it was found that the integration of photovoltaics to a grid improved the steady state stability of the grids. The studies also proposed methods that can used to determine the steady state voltage stability of a grid. The method proposed in addition to Q-U and P-U curves are modal analysis and sensitivity analysis. These are described in [14] and [15].

2.1.4 Summary of Photovoltaics Integration Impacts

In summary, the impacts of solar PV Power integration to a grid need extensive attention from researchers and utility companies due to rapid growth of this renewable energy resource. The effects/impacts cannot be generalized for all types of grids across the globe. For effective understanding of the effects before integration, studies are needed to be carried out for a particular grid in countries in which there is need to integrate more and more solar PV system to their power transmission or distribution grids [12], [17]. The impacts of photovoltaics integration has potential to cause:

- Changes to the feeder voltage level, voltage profile, line loading, power quality of the system, system losses, power factor, fault currents, system stability (transient and voltage stability), inertia of the system and mismatch in generation and load.
- Changes in operations of voltage-control and regulations devices (frequent operations). This can in turn, impact on maintenance costs, reliability and life span of the devices.
- Change in direction of power flow. There is a very high chance of reverse power flow and this can impact on protections relays (directional).

2.2 Solar Power

Solar power, an important renewable power, has been on the increase in most parts of the world in terms of installations [1]. This is as a result of abundant sunlight shining on the earth from the sun every year and making conversion of this source to usable sustainable electric power a top priority for most developed and developing countries. In Europe, Germany has taken a major leading role in the installation and integration of solar power while Sweden lags behind. Various technologies of solar power harnessing can be used, but today the concentration has been more on two technologies. A technology utilizing the principle of thermal power plants called concentrated solar power (CSP) or solar thermal (CST) is one of them [18]. The other technology uses the photovoltaic effect and is known as solar photovoltaic (PV) power.

In a concentrated solar power (CSP), thermal energy is reflected to a receiver and makes the point on the receiver concentrated with thermal energy. The concentrated thermal energy is used to heat a fluid that drives a turbine that is coupled to an alternator. The alternator generates electric power. A CSP system operates and behaves like a conventional thermal power plant [18].

In a solar PV system, a solar cell is used to convert energy (e.g. thermal and radiant) in sunlight into a direct current (dc) power [12]. Figure 2.1 shows a simple process of conversion from sunlight to electric power.

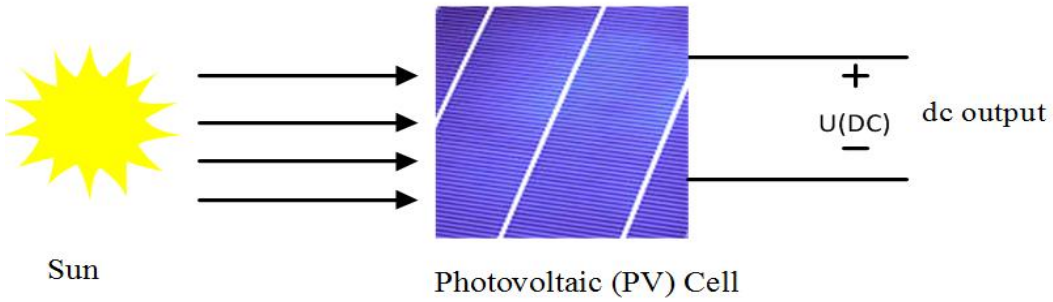

Figure 2.1: Photovoltaic (PV) Cell System [12]

The material used in this solar cell is silicon and semi-conductive in nature. The materials in use today for majority of solar cells are mono-crystalline, poly-crystalline and amorphous silicon [35].

The current and voltage from a single cell is very small. For higher voltage and current, the cells are connected in series to increase the output voltage and in parallel to increase the output current. A combination of cells make up a solar PV module and a combination of modules make up a PV array for high voltage, current and power output. A solar PV array consists of series-parallel arrangement of modules. Since a direct current power is generated, it can be used in two ways. The first way is to have a grid of dc loads that are able to utilise the generated dc power. The second way is to connect power conditioning devices (power electronics converters) to transform generated dc power to alternating current (ac) power. This is because most of the electrical loads today operate with alternating current (ac) power. Figure 2.2 shows a complete arrangement of a solar PV array with power conditioning devices for conversion to alternating current output power.

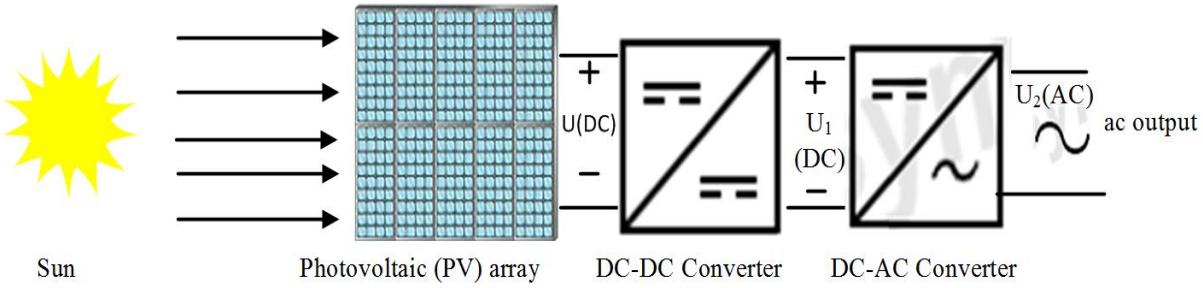

Figure 2.2: Typical Complete Solar PV System [7]

The output dc voltage (U) and current varies with irradiation reaching the array and temperature changes. The DC-DC converter ensures that the dc (U_1) fed to the dc-ac inverter is stable. The inverter converts DC to AC (U_2) which can be either single phase or three phases depending on the requirement. For integration to a grid, cables, filter circuits and a transformer are added at the output of the inverter.

2.2.1 Photovoltaic (PV) Solar Cell Theory

A PV solar cell made of silicon, a semiconductor, has properties similar to a p-n junction diode. It has a p-region and an n-region. The p-region has more holes (+ positive particles) than electrons (- negative particles) and the n-region has the opposite of the p-region [19]. Because of this, the natural movement of holes and electrons in the material create an electric field in the p-n junction material. When a photon from sun's radiation hits a p-n junction and an electron is dislodged across the depletion region in the n-side, it is accelerated by the field and pushed towards the n-region while the corresponding hole is pushed towards the p-region. Figure 2.3 shows an arrangement of a p-n junction and the depletion layer with the created electric field.

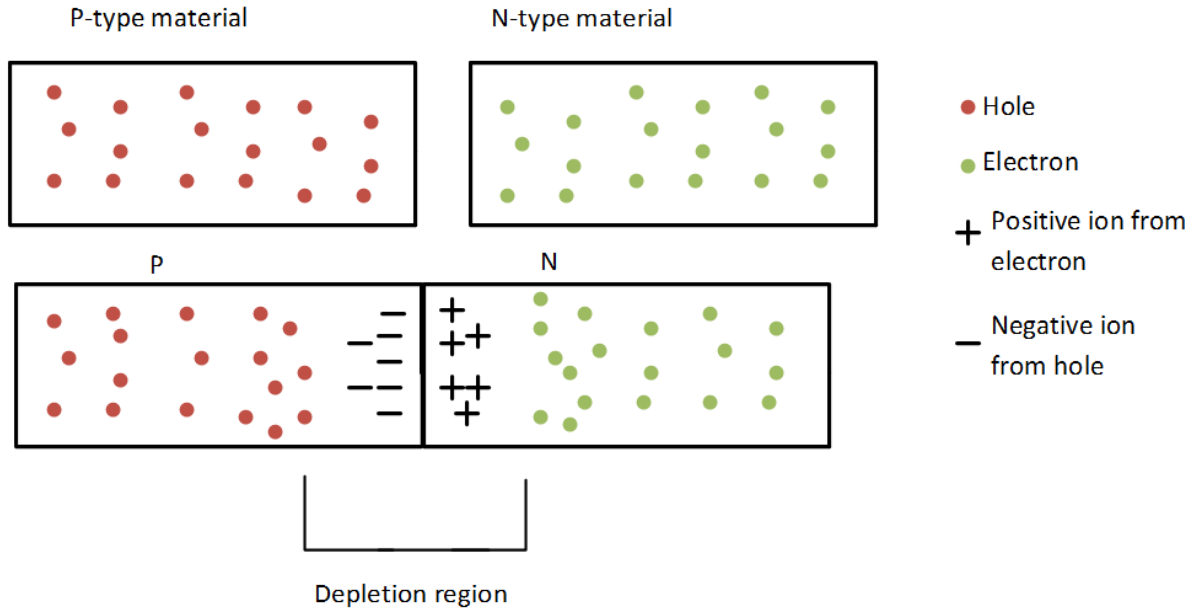

Figure 2.3: P-N Junction [19], [20], [21]

As shown in Figure 2.3, more dislodgement of holes and electrons by photons from sun's radiation creates a field in the depletion region and a difference in polarity of the P and N regions. If an external circuit is connected to the P and N regions, there is poised to be recombination and a dc electric current would flow.

2.2.2 Solar PV Cell Circuit Representation

A solar PV cell for analysis is presented in Figure 2.4 as a constant current source which is a function of the sun's radiation, a diode with a series resistance (R_S) and a parallel resistance (R_P).

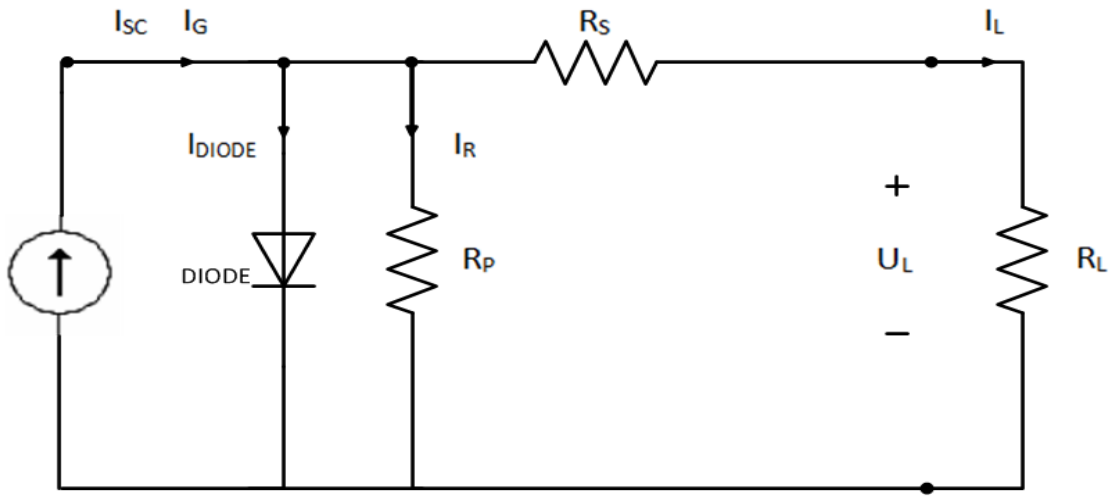

Figure 2.4: Solar Cell Circuit Model

When there is no solar radiation (G) from the sun, there is a backward current that flows in a p-n junction called a dark current (I_o). When there is radiation from the sun, the current I_G is produced by the cell and with a load connected; an electric current can flow and be measured in the external circuit (I_L). The resistor, R_L, is depicting a load connected to the solar cell, which for now assumed resistive, and the voltage U_L is the open circuit voltage that can be recorded when there is no load connected. The current I_G is the maximum current that the cell can produce at a particular solar radiation (G) and I_{SC} is a current that can be produced with shorted cell terminals. The output current I_L is the current that can be recorded for a particular load and solar irradiation (G). This is shown as a block model with power as the output in Figure 2.5.

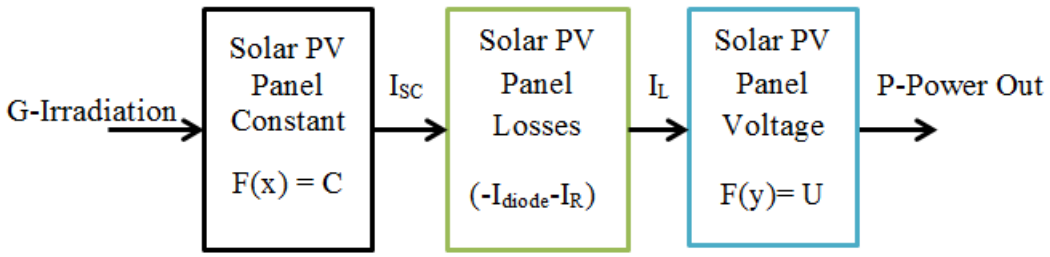

Figure 2.5: Solar PV Block Model Representation

The current for a diode representation is given by the following equation [19]:

$$I_{DIODE} = I_O(e^{\frac{qU_{DIODE}}{n.k.T}} - 1) \quad (2.1)$$

where, I_{DIODE} is diode current, k is the Boltzmann's constant (8.62 x 10^{-5} eV/K), q is the number of electron charges per electron, U_{DIODE} is the diode voltage, n: a material constant between 1 and 2, T is the diode temperature in kelvin (K) and I_0 is the dark current.

By using Figure 2.4 and Figure 2.5, the output current (I_L) can be calculated as follows:

$$I_L = I_{SC} - I_{DIODE} - I_R \quad (2.2)$$

The short current I_{SC} at a particular solar radiation G in equation (2.2) is given by equation (2.3):

$$I_{SC} = C.G \quad (2.3)$$

where G is the solar irradiation and C is a constant for the solar cell.

By varying the irradiation on the solar cell and measuring the voltage and current output, a current-voltage (I-U) characteristic of the solar cell can be plotted as shown in Figure 2.6.

By multiplying the output voltage and current, power of the solar cell can be calculated and a plot of power against voltage (P-U) obtained. It is also shown in Figure 2.6.

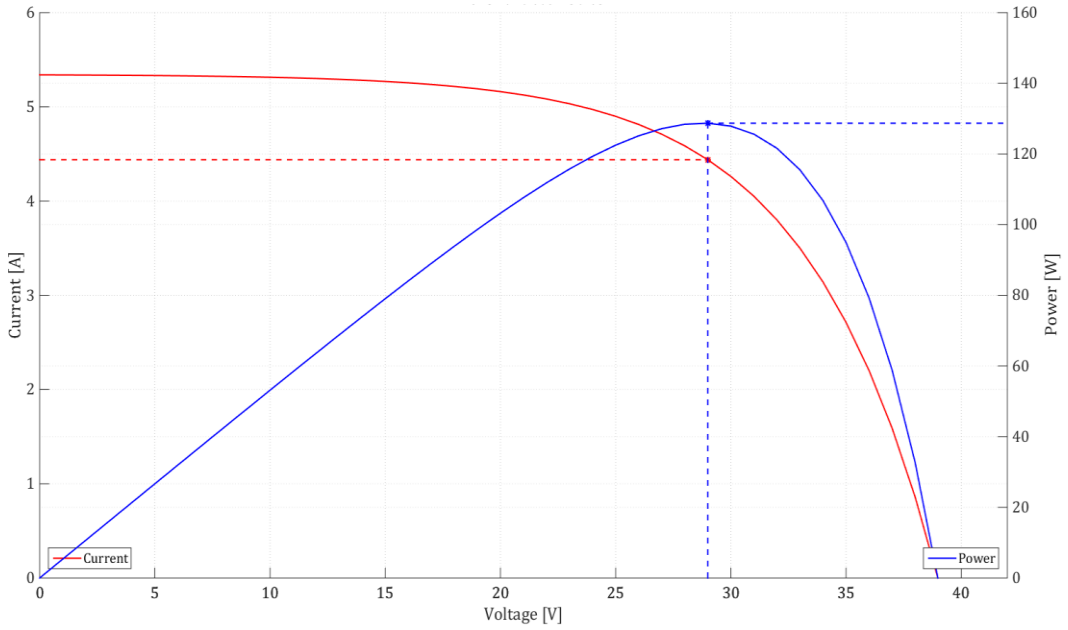

Figure 2.6: P-U and I-U Characteristics of a Solar PV Cell [12]

The power of the solar cell is the product of the current and voltage. It is the power that can be delivered to the external circuit. At a particular voltage and current point, the solar cell gives a maximum power. This point is termed the maximum power point (MPP) and is the most desirable point of operation. The point is shown at the intersection of the blue and red lines in Figure 2.6. In terms of efficiency, most commercial solar cell has an efficiency of 15-20 percent (%) and means a large area would be needed for higher power values. Therefore, it is important at all times the solar cell is giving out maximum power. With reference to Figure 2.2, the dc-dc converter part of the system incorporates maximum power point tracking (MPPT) system. The MPPT ensures that at all times the solar cell is operating at the maximum power point.

2.2.3 Solar PV Cell Operation

The operation of a PV solar cell centres on the action of solar irradiation and movement of holes/electrons in the p-n region and junction of the semiconductor material. The sun gives the cell solar radiation, G, which results in a current according to equation (2.3). The variation of solar irradiation causes different output currents from the cell and a shift in the maximum power point for the cell. An increase in irradiation causes an increase in the current and a decrease results in the decrease of the current. This is because the current produced is direct proportional to solar irradiation. The behaviour of the cell with different solar irradiance (G1, G2, G3 and G4) is shown in Figure 2.7.

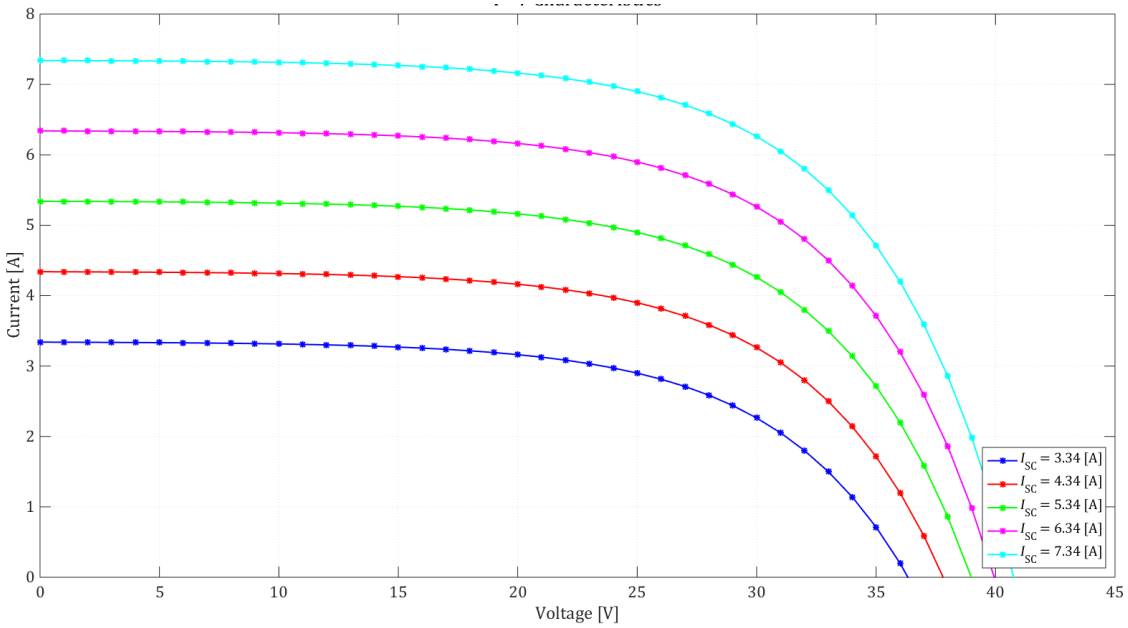

Figure 2.7: I-U Characteristics for Different radiation [6]

The characteristic I-U curves of Figure 2.7 show the change in current and voltage with varying solar irradiation. It can also be seen from Figure 2.7 that the change in irradiance causes a shift in the maximum power point of the cell.

Another parameter of interest is the solar cell temperature. The temperature increase has an impact on the voltage of the cell. As the temperature increases, the voltage reduces. This is mainly due to increasing internal carrier recombination rate as a result of higher carrier concentration with increasing temperature [22]. At a particular solar irradiation G, an increase in solar cell temperature results in a rapid decrease in power output.
The overall operation of a solar PV cell is affected by its efficiency, irradiance and temperature. These parameters cause changes to the power output of the cell and consequently the maximum power point (MPP).

2.3 Voltage Profile and Stability

Voltage profile can be defined as the numerical representation of the voltage level at a point, node or bus of an electric grid under different underlying operational conditions. For example, the voltage level at no load, light load, full load and overload operation conditions. For most power systems, it is important for the voltage profile of the grid to be within a specified limit. This is because some loads are sensitive to large changes and fluctuations in the voltage profile. In certain cases, large changes in the voltage profile may lead to wide system parameter changes and voltage instability may result. To maintain a good voltage profile, steady grid parameters and ensuring voltage stability are common goals of utility companies, transmission and distribution grid operators. Even in times of system upgrades, integration of new power generating units and operations, grid parameters must be maintained within stable operating conditions. Additionally, the changes in operating conditions may also affect power system loading and losses.

Voltage stability can be referred to a condition in which the power system or grid has the ability to maintain steady voltages at all buses after being subjected to an abnormal occurrence or condition different to the initial normal operating condition [15]. The grid must be able to restore the equilibrium operating conditions between the load demand and supply of the power system. If this does not happen and in turn the voltages at some buses or points in the power system rises or falls beyond the limit, then instability occurs.

2.3.1 Two Port Voltage Profile, Voltage Drop and Losses

The concept of voltage profile and stability of an electric grid can be derived and explained by considering a system that has a short transmission line (Z = R +jX), sending end voltage ($\overline{U_1}$), receiving end voltage ($\overline{U_1}$), and connection of a load (P,Q) at the receiving end in what is known as a two (2) port grid. The two port grid is used to derive the concepts of system behaviour in terms of voltage profile and voltage stability. Figure 2.8 shows a representation of a two port system.

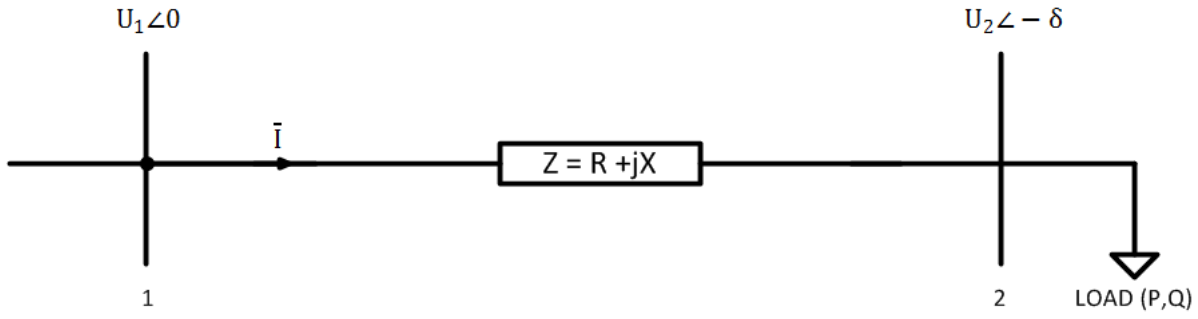

Figure 2.8: Two port Grid

From analysis of Figure 2.8, equation (2.4) is derived for the voltage relationship between bus 1 and bus 2;

$$\bar{U}_1 = \bar{U}_2 + \bar{I}Z \tag{2.4}$$

From equation (2.4), the magnitude of the voltage at the receiving end can be expressed as [23],

$$|U_2| = |U_1| - \left(\frac{RP + XQ}{|U_1|}\right) \tag{2.5}$$

The voltage magnitude level and profile ($|U_2|$) for a particular operating condition and loading at bus 2 can be expressed as in equation (2.5). The third term expresses the voltage drop. The voltage drop (ΔU) is a product of the line parameters (R and X), the load active and reactive power consumption at the receiving bus, bus 2. It is expressed as equation (2.6).

$$\text{Voltage drop: } \Delta U = \frac{RP + XQ}{|U_1|} \tag{2.6}$$

For a given grid with feeders at points A, B, C and D, and with feeder distances of a, b, c and d kilometres from the sending end voltage, the voltage profile is shown in Figure 2.9. The figure shows feeder voltage profile at distances from the sending end voltage which is the desired voltage level and profile. The distances are in increasing order with distance a kilometres closer to and distance d kilometres far away from the sending end point.

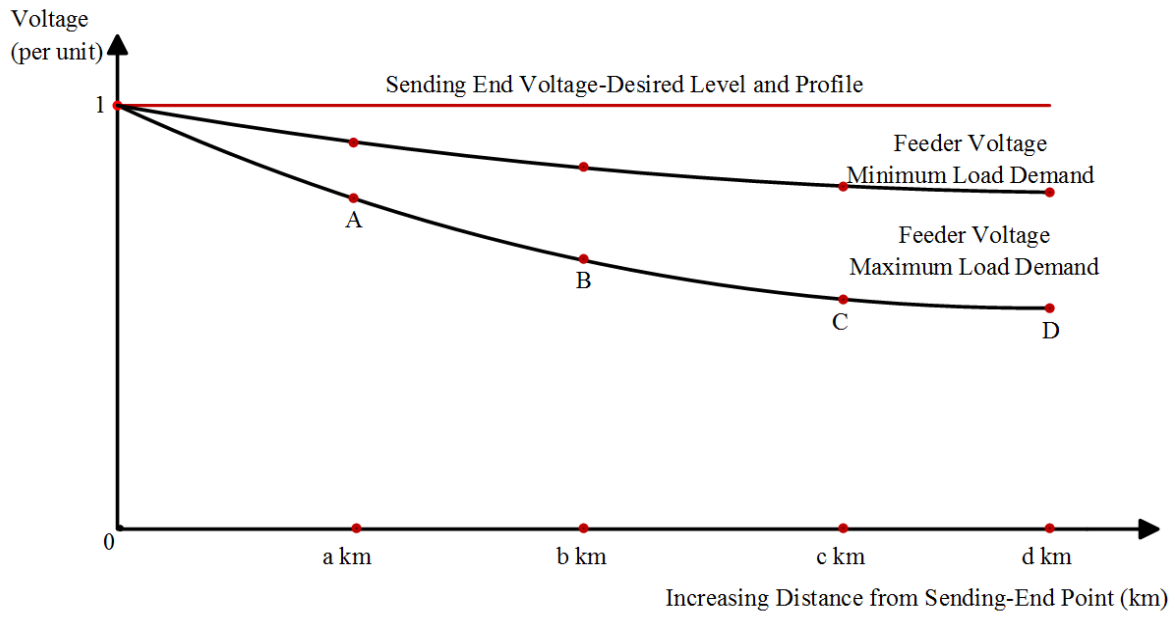

Figure 2.9: Feeder Voltage Level Profile [12]

The voltage profile and level reduces with increase in the distance from the sending end voltage as shown in Figure 2.9. This is due to an increase in line parameters (R and X) shown by equation (2.5) and (2.6) that causes the voltage level and profile to reduce.

The active and reactive losses of the line can be expressed by equations (2.7) and (2.8) [23].

$$P_{LOSS} = \quad |I|^2 R = \frac{P^2 + Q^2}{|U_2|^2} R \tag{2.7}$$

$$Q_{LOSS} = \quad |I|^2 X = \frac{P^2 + Q^2}{|U_2|^2} X \tag{2.8}$$

2.3.2 Integration of Solar PV Power

The two port grid in Figure 2.8 integrated with a solar PV power at the load bus results in Figure 2.10 shown below. The two port grid is modified (Figure 2.10) to include a solar PV generator at bus 2 injecting active power into the bus and zero (0) reactive power or with a power factor of 1.

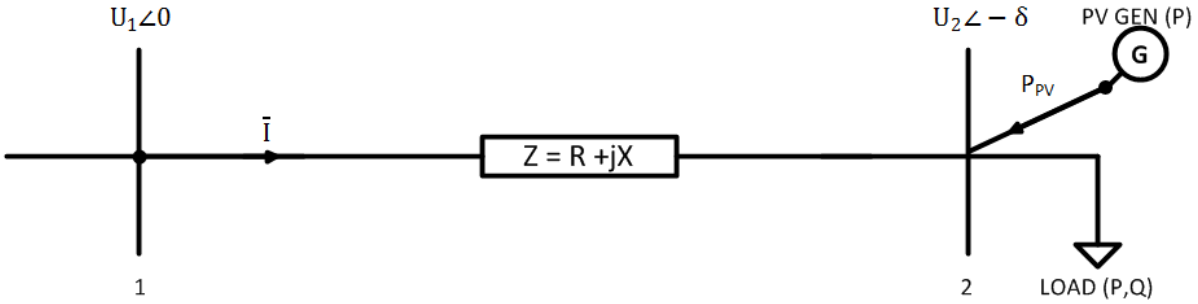

Figure 2.10: Two port Grid with Solar PV Power

The solar PV generator is added at bus 2 and is generating power (P_{PV}) that is injected into bus 2. When the inverter side is operating at a power factor of 1, the reactive power is zero (0). The two port equations for voltage profile, voltage drop and lines are modified to include solar PV power integrated as shown in Figure 2.11. They are modified to include solar PV power and results in equations (2.9), (2.10), (2.11) and (2.12).

$$|U_2| = \quad |U_1| - \left(\frac{R(P - P_{PV}) + XQ}{|U_1|}\right) \tag{2.9}$$

$$\text{Voltage drop: } \Delta U = \quad \frac{R(P - P_{PV}) + XQ}{|U_1|} \tag{2.10}$$

$$P_{LOSS} = \quad I^2 R = \frac{(P - P_{PV})^2 + Q^2}{|U_2|^2} R \tag{2.11}$$

$$Q_{LOSS} = \quad I^2 X = \frac{(P - P_{PV})^2 + Q^2}{|U_2|^2} X \tag{2.12}$$

With solar photovoltaics integrated, Figure 2.11 shows the feeder (A, B, C and D) voltage profile and level with increase in feeder distance from sending end point (a, b, c and d kilometres). It shows the voltage level and profile at maximum and minimum load demand with photovoltaics integrated.

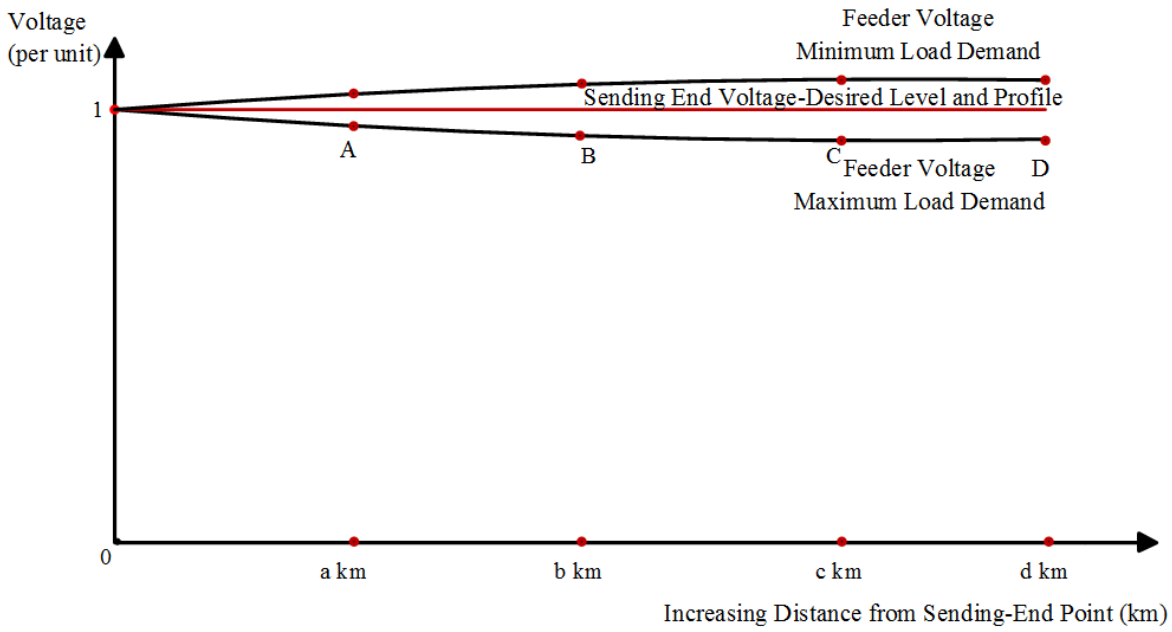

Figure 2.11: Feeder Voltage Level and Profile with Photovoltaics Integrated [12]

Figure 2.11 shows the expected results that could occur along the feeders A, B, C and D with photovoltaics integrated. At maximum load demand, the voltage profile increases but is less than the desired voltage profile for the sending end, while at minimum load demand, the voltage profile is likely to be more than the sending end voltage and could cause system voltage violations.

By analysis and comparison of the above equations for the voltage profile and voltage drop, for the case of solar PV power and without, it can be seen that the integration of the solar PV power at bus 2 causes a reduction in the voltage drop along the line and an increase in the voltage level at bus 2. This is due to a reduction in active power being drawn from the main supply through bus 1. The reduction in the active power from the main causes a reduction in the active component of the line current and reduction in active power losses and consequently the total losses.

2.3.3 Voltage Stability

The concept of voltage stability for the two port grid as shown in Figure 2.10 can be understood by assuming that the short transmission line is inductive (neglecting R) or lossless. In the grid of Figure 2.10, the resistive part is neglected and the impedance is approximated to the inductive reactance (X).

The active and reactive power transmitted from bus 1 to bus 2 can be given by equation (2.13) and (2.14) [15]:

$$P = \frac{|U_1||U_2|}{X} sin\,\delta \tag{2.13}$$

$$Q = -\frac{|U_2|^2}{X} + \frac{|U_1||U_2|}{X} cos\,\delta \tag{2.14}$$

According to equation (2.13) and (2.14), the active power and reactive power depends on the voltages at bus 1 and bus 2, the load angle (δ) and line reactance (X). Equation (2.14) can be written and expressed in terms of its cosine term. It is re-written as and shown in equation (2.15).

$$Q + \frac{|U_2|^2}{X} = \frac{|U_1||U_2|}{X} cos\,\delta \tag{2.15}$$

Using the trigonometry identity of $\sin^2 a + \cos^2 a = 1$, equations (2.13) and (2.15) can be combined. A simplified version of the combination using the latter trigonometric identity is given results in equation (2.16).

$$\left(Q + \frac{|U_2|^2}{X}\right)^2 + P^2 = \left(\frac{|U_1||U_2|}{X}\right)^2 \tag{2.16}$$

From equation (2.16), equations for the P-U and Q-U curves for the two port grid can be derived. The equations that will be derived when plotted will illustrate the behaviour of voltage at bus two with changes in the active and reactive power of the load. Using equation (2.16), an expression for the voltage at bus 2 is derived and given by equation (2.17). The equation shows the dependence of the voltage at bus 2 on the sending end voltage, the line reactance, active and reactive power of the load at bus 2.

$$|U_2| = \sqrt{\frac{|U_1|^2}{2} - QX \pm \sqrt{\frac{|U_1|^2}{4} - X^2P^2 - XQ|U_1|^2}} \tag{2.17}$$

By keeping the reactive power at the load constant with variation of the voltage and the active power gives the P-U curve for bus 2. Similarly, by varying the reactive power and voltage with the load power being kept constant a Q-U curve can be plotted. The P-U curve shows how much the voltage at the load bus 2 will be for different values of the power with Q being kept constant. The Q-U curve shows how much of the reactive power support is needed in order to be at a certain operating voltage provided that the load is maintained (P is constant). Figure 2.12 shows the P-U curve and Figure 2.13 shows the Q-U curve for the two port grid.

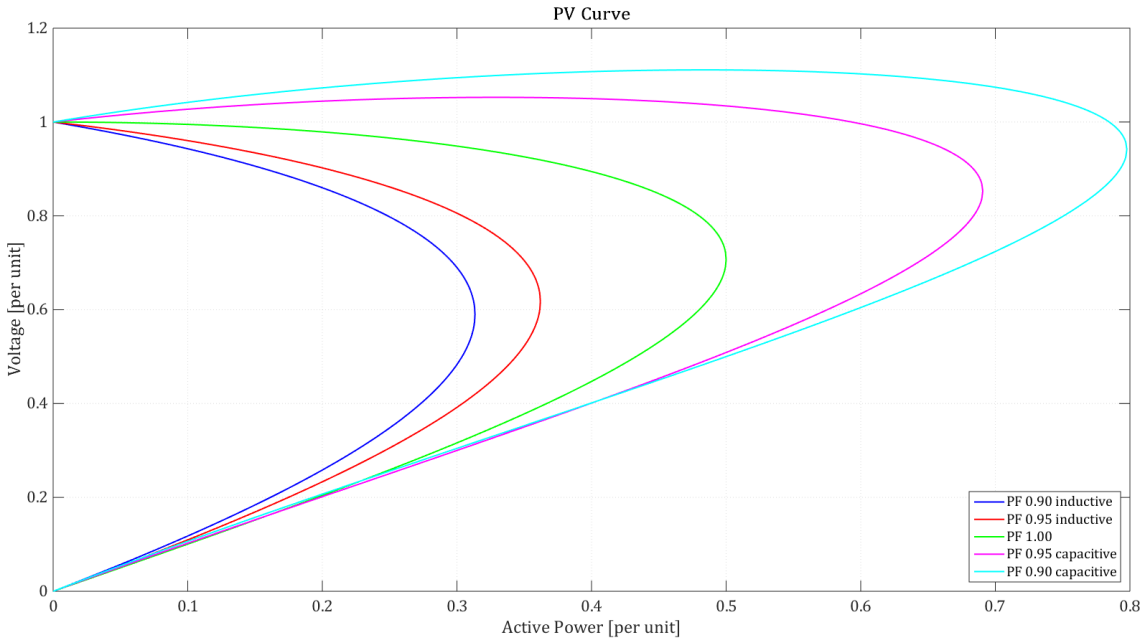

Figure 2.12: P-U Curves [15]

The P-U curves above show the behaviour of the voltage in relation to active power that can be consumed at the bus by the load with a constant reactive power (Q). There is a maximum power and a corresponding voltage level. These are the limits for the curve and it is critical to operate at this point. The upper part of the curve above the critical voltage is the stable operating region and the lower part of the curve below the critical voltage is the unstable operating region [14].

$$|U_2| = \sqrt{\frac{|U_1|^2}{2} - QX \pm \sqrt{\frac{|U_1|^2}{4} - X^2(P - P_{PV})^2 - XQ|U_1|^2}} \tag{2.18}$$

With integration of solar PV power at bus 2 as shown in Figure 2.10 and illustrated in equation (2.18), the P-U curve would be shifted outwards. This would increase the maximum power which the load can consume. Analysis of equation (2.18) shows an increase in the critical voltage. But this does not show an increase in the stability of the grid. This is because, in reality, operation at the maximum power and critical voltage is avoided at all cost. Furthermore, operation below the critical voltage is also avoided even when theoretically it is possible according to equation (2.17). According to equation (2.17), any power operation, P, has possibility of operation at two voltage points. One voltage is above the critical voltage and one is below the critical voltage [15].

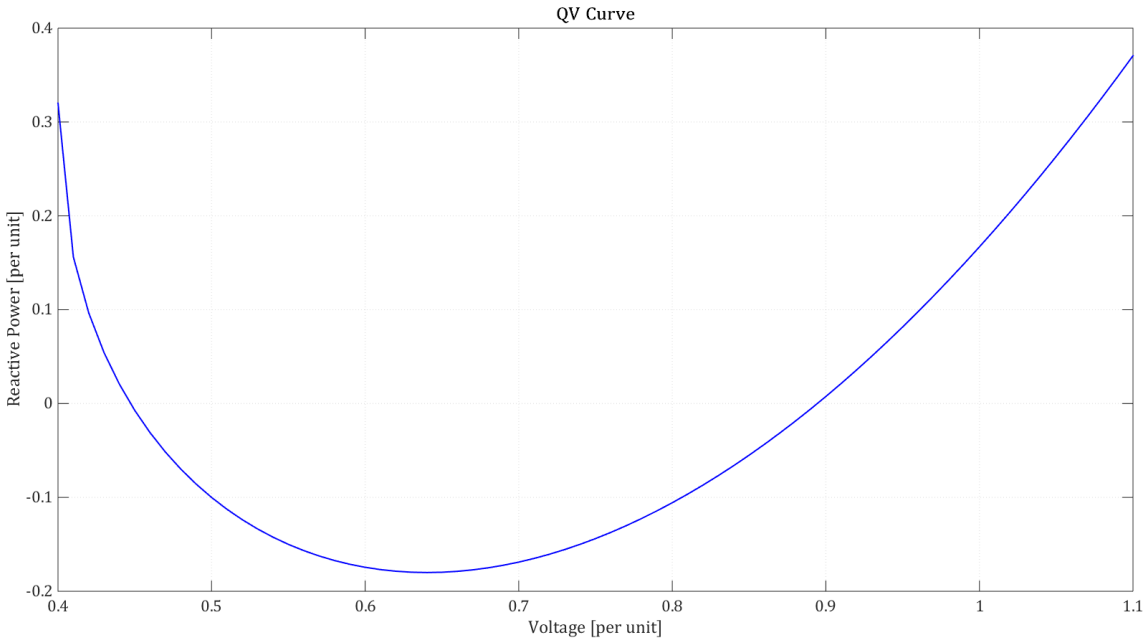

Figure 2.13: Q-U Curve [14]

Figure 2.13 shows the relationship between voltage and reactive power support needed at the receiving bus (bus 2) for a constant active power (P). The curve has a minimum point. This point that can be found by differentiating the reactive power with respect to voltage and equating to zero (dQ/dU=0). This is the voltage stability limit of the system. The points on the curve to the right of the minimum point are voltage stable or the stable operating region while the points to the left of the minimum point are voltage unstable or unstable operating region. With solar PV power integration, as shown by equation (2.18), the voltage at the receiving bus increases and reduces the reactive power demand from the sending end. This increases the available reactive power reserve in the grid and consequently could improve the voltage stability of the grid [14], [15].

3 Grid Modelling and System Studies

This chapter introduces grid modelling of the grids studied and the system studies performed. The grid voltage levels and characteristics of the grids under study are presented. It describes a brief process of data processing for the grids studied, software used and system studies. Models of grids built in Paladin designbase and NEPLAN for analysis are presented.

3.1 Distribution Grid Areas

The distribution grids to study are areas from two municipality energy companies in Sweden. These grids are from Mölndal energy and Orust energy. The distribution grids are radial, meshed and combination of both types. These areas have potential for solar PV power installation.

3.1.1 Mölndal Energy Grid Areas

This area is a medium to low voltage distribution grid. It is a 10/0.4 kV distribution grid. A total of two areas were chosen for the analysis of solar PV power integration. One area has a radial distribution grid type and the other area has a meshed distribution grid type. These areas are purely residential housing with houses of semi-detached, detached and terraced types. The characteristic of the loads in this area is entirely residential loads. Figure 3.1 shows the area for the radial distribution grid from Mölndal energy (captured on google maps [30]).

Figure 3.1: Mölndal Grid Area-1

The area is fed from a transformer rated at 500 kVA, 10/0.4 kV. The area has a total of forty (40) housing units. It is bounded by boråsvägen road, rådavägen road and rådasjön water body. In this area, the available roof area has been measured and roof tops solar PV power installation will be considered.

Figure 3.2 below shows the area for the meshed distribution grid under study from Mölndal energy (captured on google maps [30]).

Figure 3.2: Mölndal Grid Area-2

The area is called Solängen and has a total of one hundred and five (105) housing units that are taken into consideration in the study. It is also a purely residential area. The area is fed from a transformer rated at 800 kVA, 10/0.4 kV. Additionally, in this area, roof top areas have been measured and solar PV installations on the roofs are considered.

In both areas (area 1 and 2), the power distribution grids are entirely by cable grid feeders.

3.1.2 Orust Energy Grid Areas

Orust energy provides power and energy to the municipality of Orust in the Västra Götaland County of Western Sweden. The municipality covers areas of Ellös, Henån, Hällevissstrand, Mollösund, Svanvik, Varekil and Svanesund. The majority of the loads in this area are residential which accounts for ninety percent (90%) and large industries which accounts for ten percent (10%). In ninety percent of residential loads, ninety-five percent (95%) are houses

and five percent (5%) are apartments. In the study, the distribution grid to be studied is a 130/10 kV grid. The loads were aggregated at the 10 kV distribution substations.

The area is fed by two transformers rated at 16 MVA 130/10 kV (Bua substation) and 10 MVA 130/10 kV (Edshultshall substation). It has a switching substation at Slätthult. Some areas of Orust Municipality that Orust energy supplies power to and are part of the study have been shown in Figure A.1 to Figure A.4 in appendix A. The areas show the residential houses and industries in aerial view as captured from google maps.

3.2 Data Processing and Software

The software PVSyst [32], Paladin designbase 4.0 from Power Analytics Company of the United States of America [28] and NEPLAN V554 from NEPLAN AG in Switzerland [29] were used in the study of the impacts of solar PV power integration. During modelling, Paladin designbase was used as base software for data processing because of its capability to calculate missing cable or overhead lines parameters from basic data given by the utility companies (Mölndal and Orust Energy). After establishment of base grid and complete grid data, the grid was further modelled in NEPLAN with capability for load flow with load profiles and static voltage stability analysis. In the complete analysis and results formulation, both were used to complement each other.

The grid data for the distribution grids from Mölndal and Orust energy were given in its raw state with connectivity diagrams by the utility companies. The cables and lines parameters for the grid were given in terms of resistance, inductance and charging capacitance. This data was processed by calculating the positive, negative and zero sequence for the resistance, inductive reactance and charging susceptance using Paladin designbase. These complete grid information using Paladin designbase was used for modelling of the grid in NEPLAN software. The total energy and power consumption for the areas were given by the utility companies.

PVSyst, software that is dedicated entirely to solar PV design and analysis, was used to model the required PV systems and production of results for integration to the built grids. By using the roof top areas calculated ([30], [31]) for the residential houses in Mölndal and the solar irradiation data for the areas, solar PV power potential was designed, calculated and its parameters used in Paladin designbase and NEPLAN for analysis. Appendix B show samples of data given by the energy utility companies (Table B.1, Table B.2 and Table B.3), available roof top areas for Mölndal grids houses and solar PV power potential (kWp) as designed in PVSyst (Table B.4 and Table B.5). Orust energy provided the parameters for solar PV power plant and location of where they intend to construct (300 kW PV plant before 2017 at Sörbo and 1 MW PV plant after 2017 at Månsemyr) and integrate to the grid. This was used as additional (in addition to 0%, 30%, 60% and 90% penetration) study scenarios of PV impact to their grid.

3.3 Grid Models

The models for the processed data given by Orust and Mölndal energy were built in the software environment of Paladin and NEPLAN. These models were the normal cases for the studies to be performed before integration of photovoltaics.

3.3.1 Mölndal Energy Grid Models

The grid models for Mölndal energy built in the software environment were two. The first model represented the area shown in Figure 3.1, which is a radial distribution grid and the second model represented the area shown in Figure 3.2, which is a meshed distribution grid. In each of the models, the residential houses in the two areas are represented as electrical loads in the grid. The grid model built for area 1 has a total of 56 buses and 40 loads representing the houses in the area. Figure 3.3 and Figure 3.4 show the models as built in the software environment.

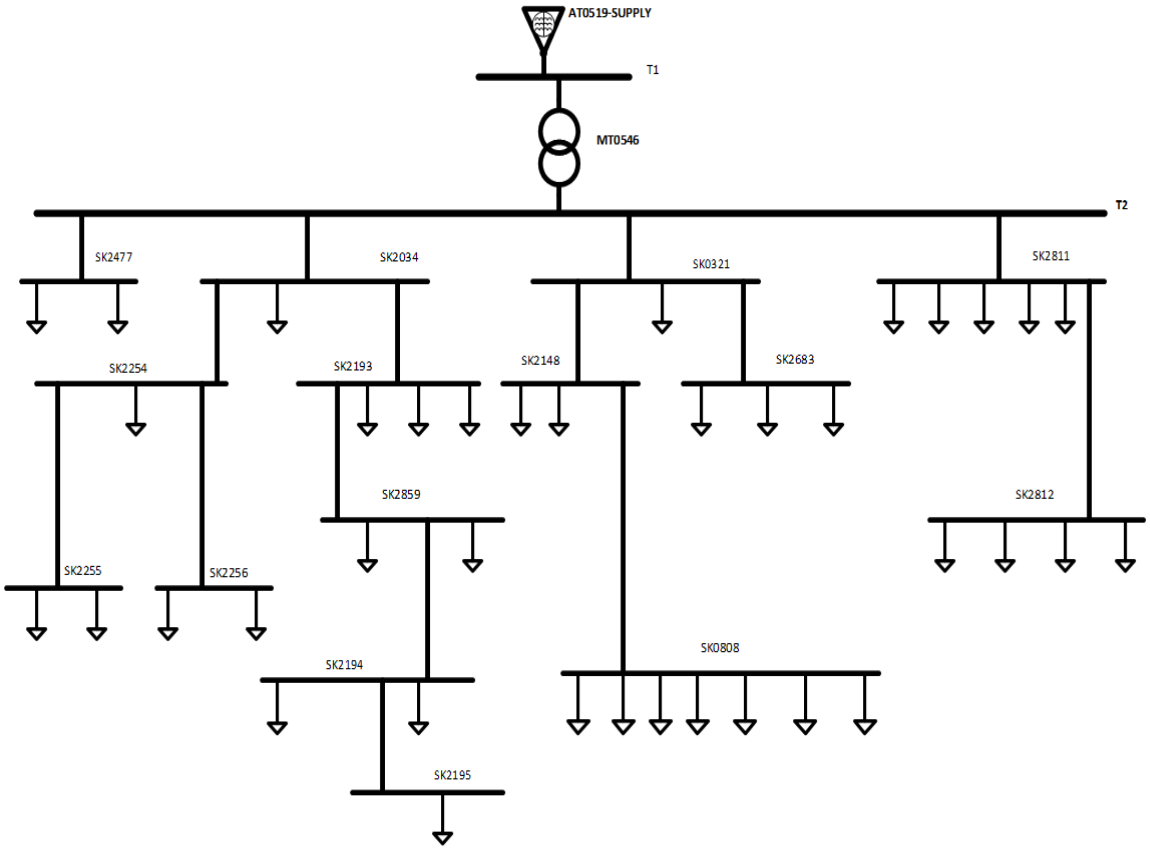

Figure 3.3: Mölndal Area 1 Grid Model (Paladin designbase)

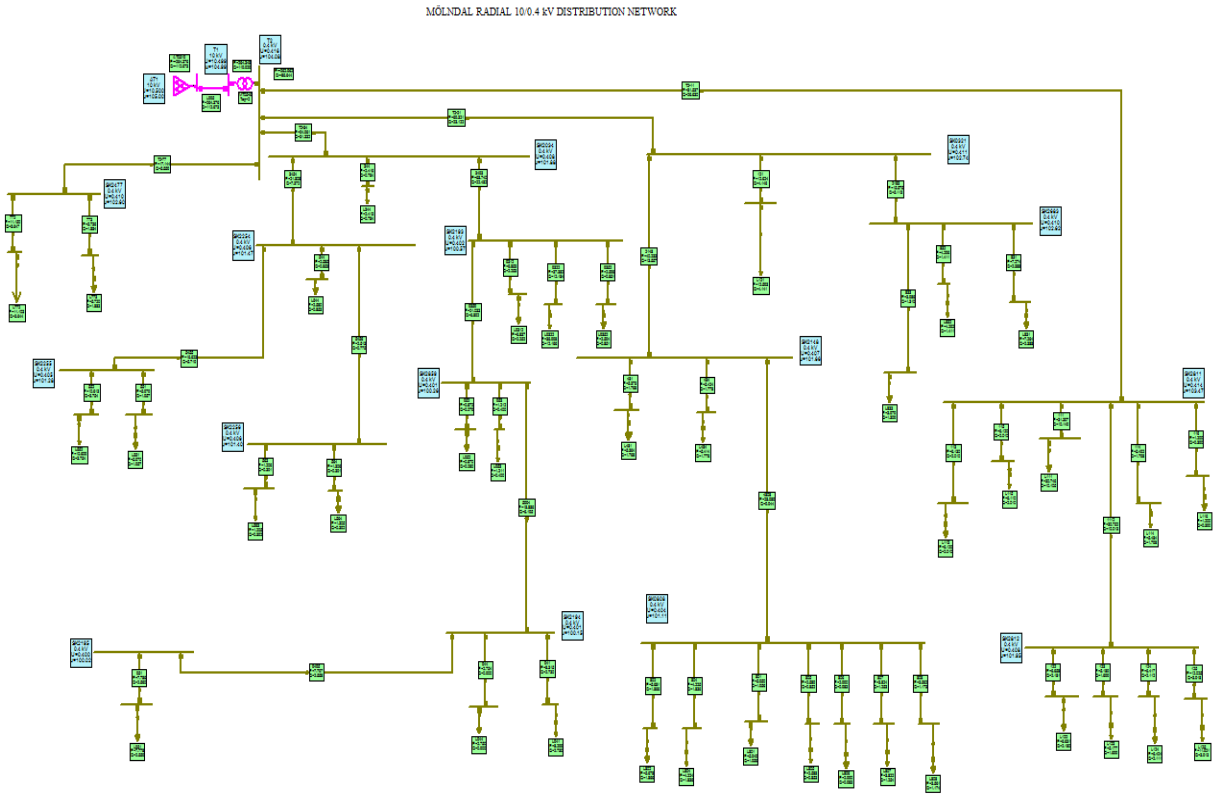

Figure 3.4: Mölndal Area 1 Grid Model (NEPLAN)

These are the normal cases to be used for further studies for area 1 in Mölndal. The buses represent the transformer and grid substations. The transformer substation step down the supply voltage of 10 kV to 400 V. The voltage level of 400 V is distributed in the area through grid substations. The grid substations receives incoming power at 400 V, supply houses within its perimeter and re-distribute to other grid substations. The area has a total active power consumption of 245 kW at peak time. The residential houses are modelled using ZIP load model in the software. That is a combination of constant impedance (Z), constant current (I) and constant power (P) load characteristics. According to [11], when nothing has been given of the load composition or characteristics of a residential area, a 70% and 30% combination of constant power and impedance load can be assigned to the load model for analysis and planning purposes. This was used for modelling of residential loads for analysis in combination with power and energy values obtained from the utility company for power consumption of the area.

Furthermore, Figure 3.5 and Figure 3.6 show the grid model built in the software environment for area 2 in Mölndal. Additionally, figure A.9 to figure A.12 in appendix A represents the grids as completely modelled in Paladin Designbase and NEPLAN.

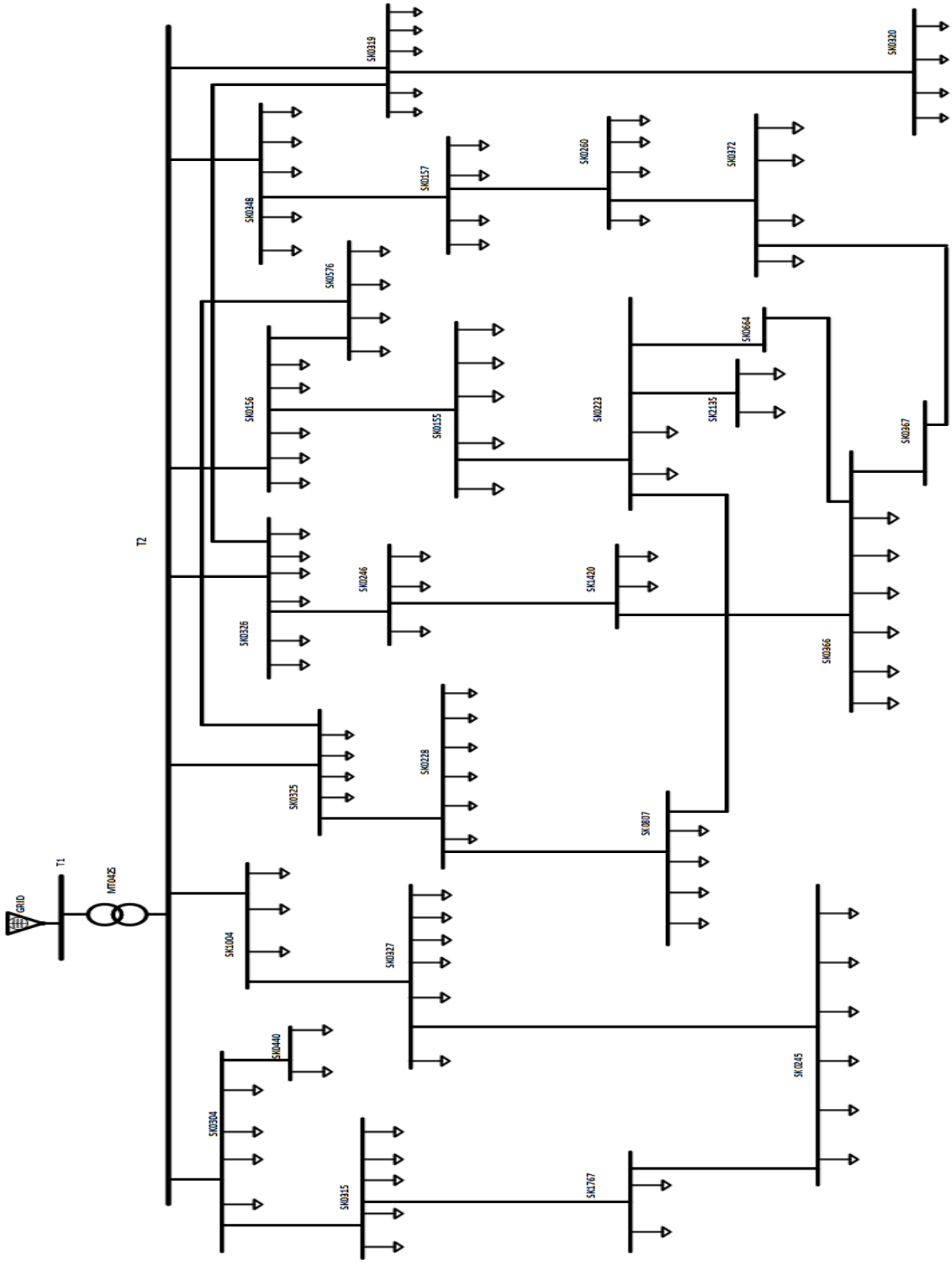

Figure 3.5: Mölndal Area 2 Grid Model (Paladin Designbase)

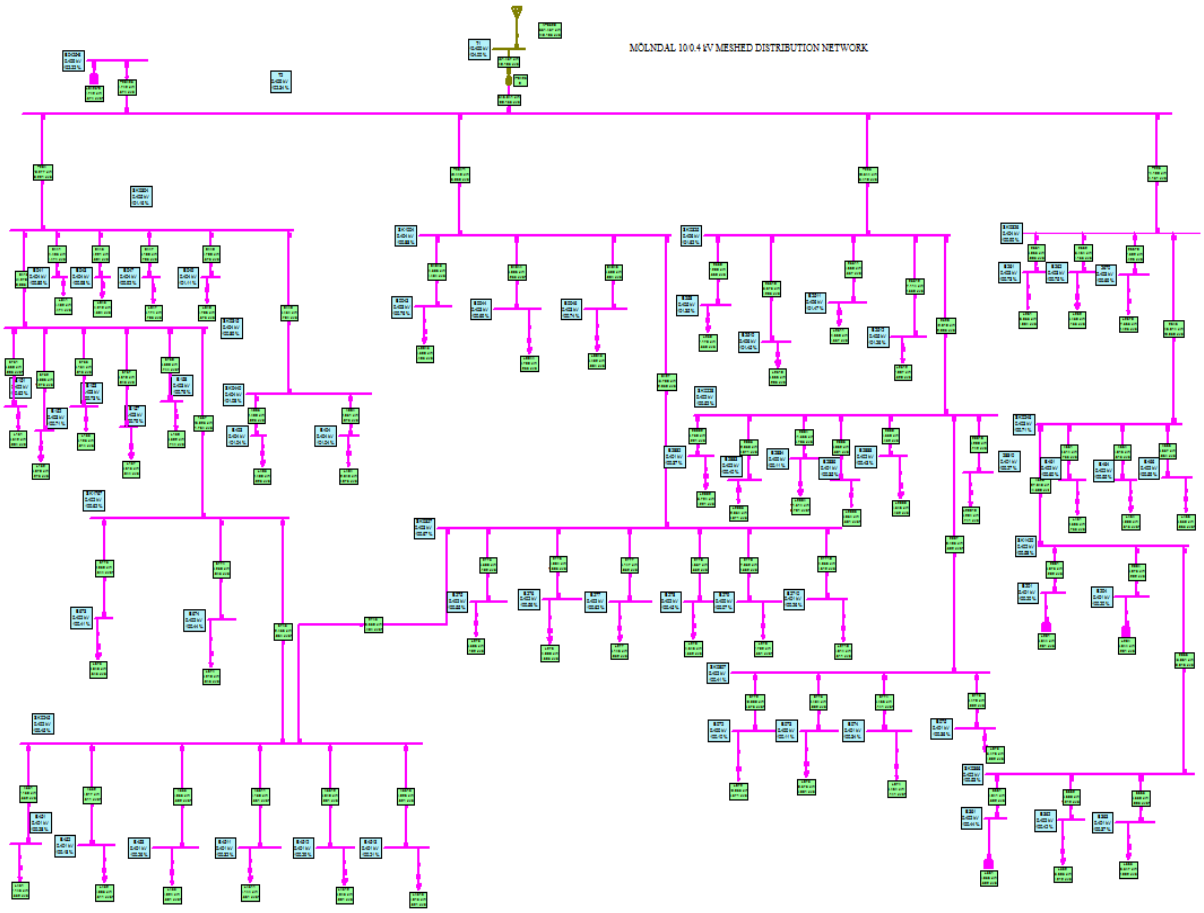

Figure 3.6: Mölndal Area 2 Grid Model (NEPLAN)

The area grid model has a total of hundred and five (105) loads representing the housing units in the area. The area is fed with power at 10 kV through the transformer substation and stepped down to 400 V. The power is supplied to the houses through the grid substations. This model formed the normal case for area 2 which is a meshed distribution grid type. It has a total of one hundred and thirty-four (134) buses in total representing the transformer and grid substations.

3.3.2 Orust Energy Grid Model

The grid model for Orust energy area was built in the software environment. It is a 130/10 kV grid with two main power substations (at S1 and S2), switching substation (at S3) and transformer substations. Figure A.13 in appendix A shows part of an as built circuit diagram with S1, S2 and S3 areas. The area grid model has a total of one hundred and sixty-six (166) buses. The aggregated loads at the transformer substations totals one hundred and fifty-eight (158) loads that were modelled as a combination of residential and industrial loads (90% and 10%). The built implemented model is shown in appendix A as figures from Figure A.5 to Figure A.8. The entire figures are a collection of the 130/10 kV distribution grid for Orust energy.

3.4 System Studies

The system studies that were used for the study of the impacts of Solar PV power integration to an existing grid on voltage level, voltage profile, line losses, loading and voltage stability are; Solar PV Power production analysis, load/power flow analysis, load/power analysis flow with load profiles and steady state voltage stability.

3.4.1 System Study Methodology

The methodology of the studies conducted was through theoretical knowledge and system simulation of the distribution grids under study. For system simulation studies, only steady state analysis was done.

In theory, understanding of underlying principles of voltage level, profile, line loading, system losses and steady state voltage stability was done for a simple two port system. An extension of theoretical principles was done with photovoltaics integrated to a simple two port system. Similar studies in other parts of the world and Sweden were looked at to get an insight into likely issues that other scholars have looked at [1] [7].

Consequently, with theoretical understanding done, a method was developed for modelling and simulating the distribution grids in the software environment. The software used was industrial power system software. These are NEPLAN and Paladin designbase. In addition to the power system simulation software, software for solar power feasibility study, design, economic and technical analysis was used. This software is called PVSyt. It was used to understand and simulate almost real system that can be installed in the areas under study. Normalised power output with actual climatic conditions of the areas for the distribution grids were used as input for Paladin designbase and NEPLAN modelled photovoltaics systems.

The method adopted was to compare two cases of simulations. In one case, the grids are presented without any photovoltaics integrated. This was the normal case for the distribution grids. In the second case, photovoltaics were integrated to the grids to determine the impact of its integration. In addition, different penetration levels were considered. The cases with photovoltaics were compared with the normal. Figure 3.7 shows the methodology of studying the systems that was adopted.

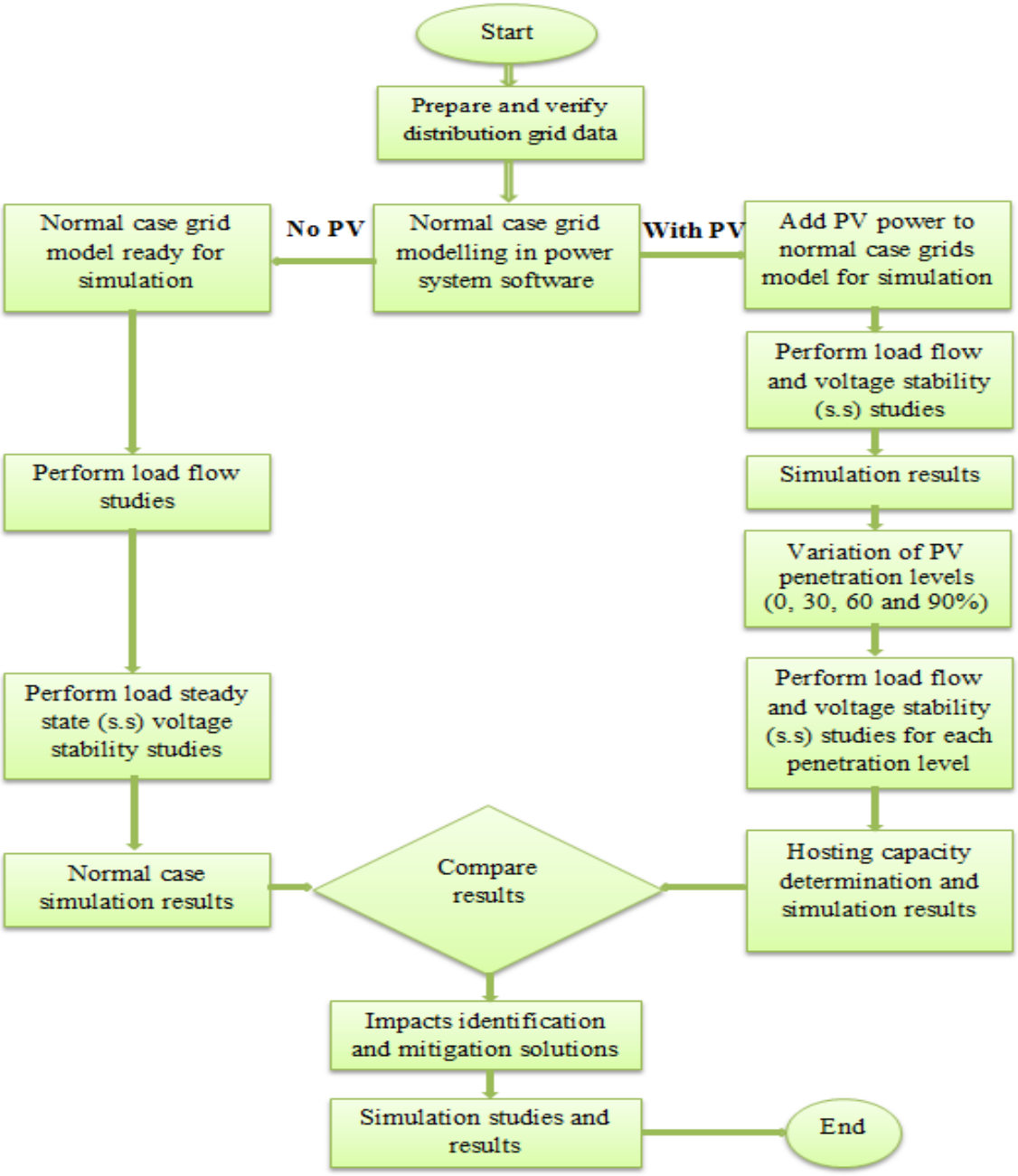

Figure 3.7: System Studies Methodology Flow Chart

As shown in Figure 3.7, the comparison of the two cases yielded results that were compared. In these studies, the normal case was considered at maximum load demand of the grids under study. For the cases with photovoltaics, both scenarios of maximum and minimum load demand for the grids were considered. In this process, the hosting capacity of the distribution grids was determined.

3.4.2 Power/Load Flow Studies

The process of power flow studies is a concept that shows/outlines the flow of power in a grid from one bus to another bus and/or power flow into a bus or leaving the bus. With

reference to Figure 2.8 in Chapter 2, which shows a two port or bus grid, power was flowing from bus 1 to bus 2. The power could be seen to enter and leave bus 2. The main aim of a power flow study is to determine power system electrical quantities with some quantities known while others unknown. These quantities are voltage magnitude ($|U|$), voltage or load angle (δ), active power (P), reactive power (Q) and apparent power (S). During the process of power flow, line loadings, voltage drops and losses are also determined.

To determine unknown electrical quantities to a grid, a load flow analysis needs to be done either manually or with an aid of power system simulation software. One way of determining the voltages (U) and currents (I) at the bus is through the use of bus admittance ($Y = -y$) matrix method [23]. This method and circuit analysis yields equations (3.1) and (3.2).

$$I_{BUS} = Y_{BUS}\, U_{BUS} \tag{3.1}$$

Therefore, $U_{BUS} = Y_{BUS}^{-1}\, I_{BUS}$ (3.2)

Equation (3.1) for a three bus grid yields,

$$\begin{pmatrix} I_1 \\ I_2 \\ I_3 \end{pmatrix} = \begin{pmatrix} Y_{11} & Y_{12} & Y_{13} \\ Y_{21} & Y_{22} & Y_{23} \\ Y_{31} & Y_{32} & Y_{33} \end{pmatrix} \begin{pmatrix} U_1 \\ U_2 \\ U_3 \end{pmatrix} \tag{3.3}$$

The resultant individual equations from equation (3.3) for currents and voltages are non-linear equations. To solve these non-linear equations, methods of solving non-linear equations and by estimation are used. These are Gauss-Seidel Method, Newton-Raphson and Fast Decoupled methods [23]. These are iteration methods that reduce an error to the first estimated value of the unknown parameter until it is very small. In addition, the power flow into a named bus (i) can be expressed by equation (3.4) [23] .

$$P_i - jQ_i = U_i^* \left[U_i \sum_{j=0}^{n} y_{ij} \; - \sum_{j=1}^{n} y_{ij}\, U_j \right] \; where\; i \neq j \tag{3.4}$$

Using Gauss-Seidel Method and Newton-Raphson, the equations for power (Q and P) and voltage can be written for a three bus grid .These equations are non-linear and use of iteration methods is done to estimate unknown values at the buses. The power system simulation software, Paladin Design base and NEPLAN, has the power flow capabilities with the iteration methods mentioned.

3.4.3 Power/Load Flow Studies with Load Profiles

Power/load flow with load profiles is load flow study that is an extension of the conventional power/load flow but with an added function of performing the analysis on time based. This analysis is able to determine the bus voltage and power consumption (active and reactive) of a load against a period of time. Power flow studies do not take time into consideration and

therefore gives the results of simulation on an instant based scenario. For the thesis study, power flow with load profiles analysis is very important. This is because output from a solar PV is not a constant output but varies depending on the time of the day and the climatic conditions prevailing at that time [6]. Additionally, the consumption of active and reactive power for residential and industrial loads equally varies with time.

In this analysis, the load profile over a period of time (twenty-four (24) hour period) was defined and solar PV power output over the same period of time was defined. A single time load flow calculation was then performed to determine the interaction of the two. The load flow, bus voltages, losses and maximum loads over time (twenty-four (24) hour period) were determined in this way.

3.4.4 Steady State Voltage Stability

Voltage stability analysis can be either dynamic or steady state. Dynamic voltage stability takes into account the time simulation of the grid under study. Dynamic voltage stability analysis gives a time sequence of events leading to an instability situation. This gives a much detailed analysis of the collapse that can be used for protection coordination and control. Static or steady state voltage analysis does not take time into account. It gives a state of stability, point of start of instability, nature of problem and some key factors likely to contribute to the phenomena of voltage stability. The static voltage stability is associated with Q-U curves, P-U curves, Q-U sensitivity analysis and Q-U modal analysis [14] [15] [16].

A P-U curve gives the relational variation of the voltage at a bus to active power consumed by a load. Figure 2.12 in Chapter 2 showed a P-U curve, which is a plot of power against voltage. It also shows the critical voltage and maximum power beyond and below which instability is very likely to occur. A Q-U curve, similarly to a P-U curve, gives a relational variation of bus voltage to reactive power support needed at a bus. Figure 2.13 in Chapter 2 showed a Q-U curve plot of reactive power against voltage. It is from a Q-U curve that Q-U sensitivity and modal analysis are determined from. Q-U sensitivity analysis takes into account the rate of change of reactive power consumption with respect to the voltage. Q-U modal analysis considers the eigenvalues of the buses under consideration, gives if the bus is voltage stable or not and gives the degree of voltage stability depending on the value of the eigenvalue that results from the analysis [14].

The concept of Q-U sensitivity can be explained by considering the following expression of incremental changes in power flow, voltage magnitude and angle of a bus [14]:

$$\begin{pmatrix} \Delta P \\ \Delta Q \end{pmatrix} = \begin{pmatrix} J_{P\delta} & J_{PU} \\ J_{Q\delta} & J_{QU} \end{pmatrix} \begin{pmatrix} \Delta\delta \\ \Delta U \end{pmatrix} \quad (3.5)$$

Where; ΔP is the incremental change of the bus active power.

ΔQ is the incremental reactive power change at the bus.

$\Delta\delta$ is the incremental angle change at the bus.

ΔU is the voltage incremental change at the bus.

The Jacobian matrix (J-2 x 2) represents the sensitivities between the power flow and the change in the bus voltages at the bus. The slope of a Q-U curve for a given operating point is given by the Q-U sensitivity. A positive Q-U sensitivity indicates a stable operation and a negative one indicates an unstable operation. A smaller positive Q-U sensitivity is indicates a more stable system while the opposite is a less stable system [14]. In a situation that the stability of the system changes from a more stable operation to a less stable operation, the magnitude of the sensitivity increases. At the point of stability limit, in theory, the sensitivity is taken to be infinity. For a typical Q-U curve, points on the left hand side of the stability limit have negative sensitivities values and are in the unstable region of operation. The points on the right hand side of the stability limit have positive sensitivities values and are in the stable region of operation.

The concept of Q-U modal analysis emanates from equation (3.5). It considers the elements of the inverse of the Jacobian matrix (J^{-1}) and the Jacobian matrix (J). The Jacobian matrix can be expressed by equation (3.6) [14].

$$J = \psi \Lambda \varphi \tag{3.6}$$

The inverse of the Jacobian matrix is:

$$J^{-1} = \psi \Lambda^{-1} \varphi \tag{3.7}$$

In equation (3.6), ψ and φ are the right and left hand eigenvector matrices. The symbol Λ, represents the diagonal matrix of the Jacobian with eigenvalues along its diagonal. The voltage and reactive power at the bus can be expressed in terms of the incremental changes and the eigenvectors in equation (3.4). Combining of equation (3.6), (3.7) and incremental change of voltage yields to equation (3.8) [14].

$$\Delta U = \psi \Lambda^{-1} \varphi \Delta Q \tag{3.8}$$

In equation (3.8), a positive eigenvalue entails a stable system and a negative eigenvalue entails an unstable system. A larger positive value of the eigenvalue gives a more stable system and a small value gives a less stable system. A very small value close to zero (0) gives the critical operating point of the system [14].

In this system study for voltage stability, the static stability of the distribution grids under study will be determined and the impacts of adding solar PV power to the grids determined with use of NEPLAN software.

3.4.5 Solar PV Power Production Analysis

The production analysis of solar PV power of a system was done using PVSyst software. The software was used to design typical systems for the areas and a study of the solar PV system to be used for integration in the areas of interest. The software has meteorological information of the areas on the globe and with exact geographical area definition of the areas

under study, a production profile for the designed PV system is obtained. This is because the production of power/energy is depended on the climatic conditions of a geographical area which is different for different areas [6]. A typical system model was designed with reference to the available aerial area available for roof top and power level for ground mounting system. Typical PV power systems for Mölndal and Orust areas were simulated in PVSyst software. The results were obtained and are shown in Table B.6, Table B.7 and Table B.8 in appendix B. These results were used to plot normalised power against a twenty-four hours period for a day in June. The plots for normalised power production for the day chosen for the areas are shown in Figure 3.8, Figure 3.9 and Figure 3.10.

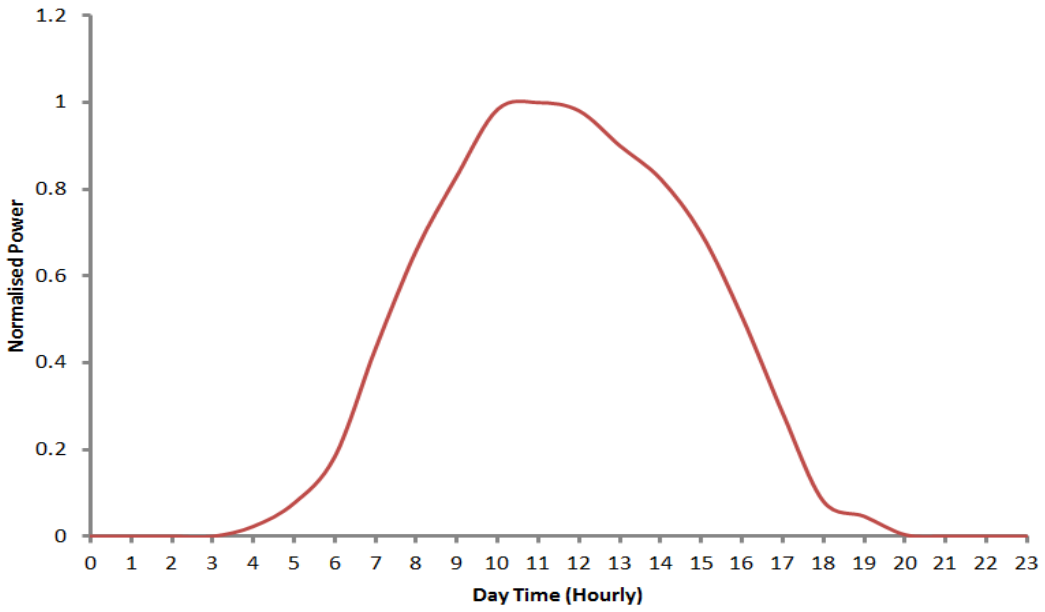

Figure 3.8: Solar PV Production-Mölndal Area 1

The figure above (Figure 3.8) is a graph showing production from a typical designed solar PV power from Mölndal area 1. The power production is normalised to indicate likely production pattern of a PV plant in the area. To plot this curve, a designed system was simulated and its output power obtained for twenty-four hours. The maximum power output in this period was used as a denominator for all the other results to obtain per unit normalised output. This was plotted as shown in Figure 3.8. This is the characteristic curve for power production for PV systems in this area and the systems will differ in power output magnitude due to difference in potential of the roof tops as indicated in Table B.4.

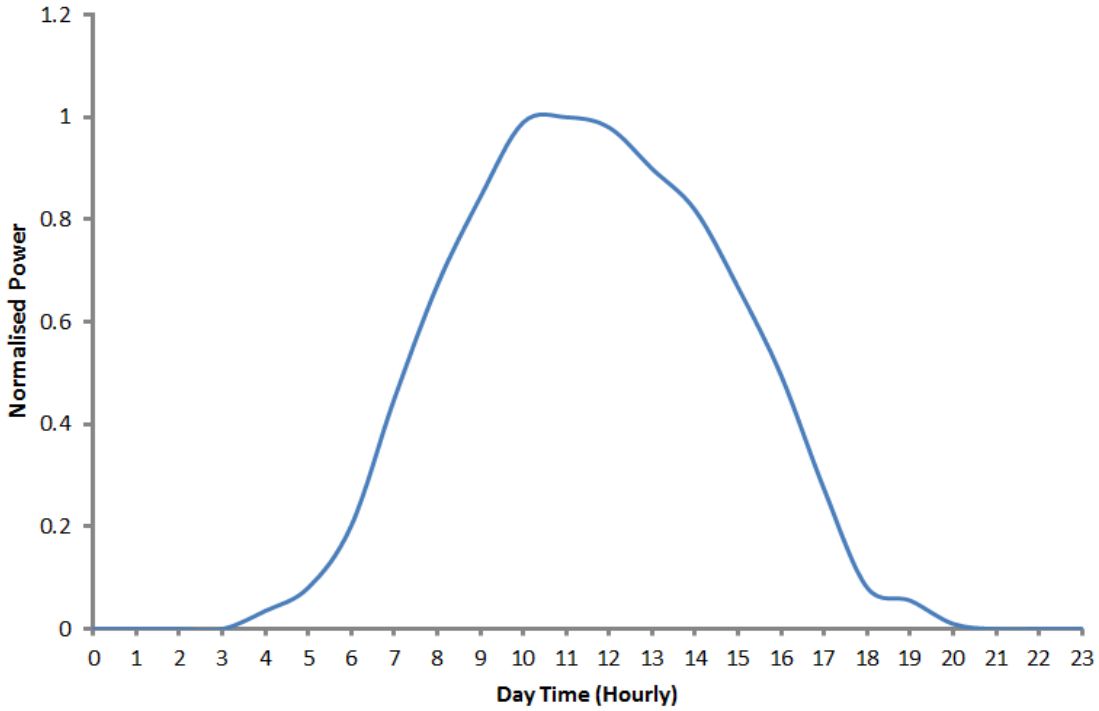

Figure 3.9: Solar PV Production-Mölndal Area 2

Similarly to Figure 3.8, Figure 3.9 show normalised power production for twenty-four hours (1 day). The graph is characteristic of solar PV systems in Mölndal area 2 and will differ in power production due to different in roof to potential.

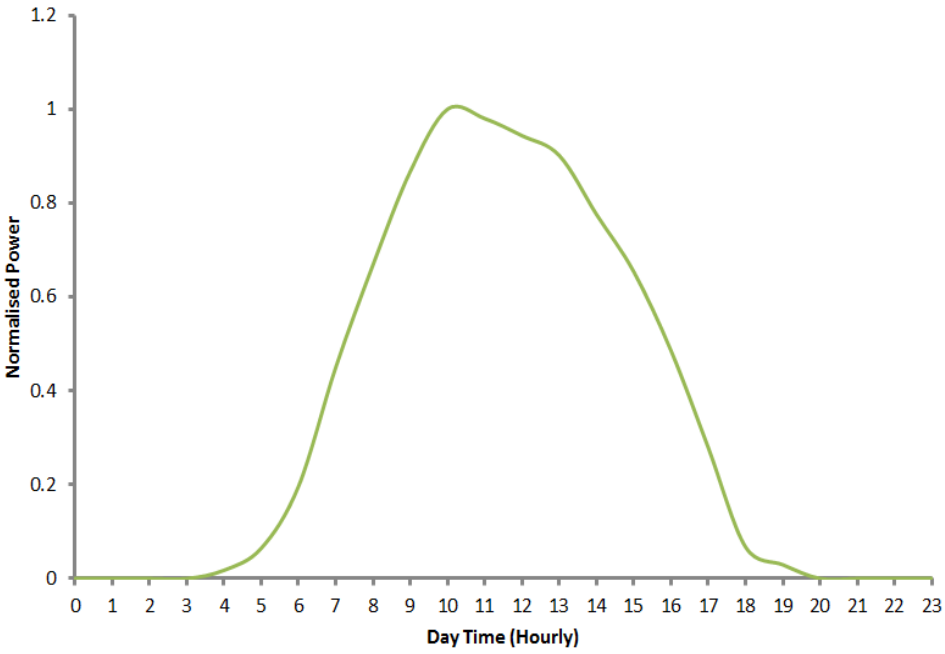

Figure 3.10: Solar PV Production-Orust

The solar PV power characteristic curve for Orust area is shown in Figure 3.10. This is a normalised power production graph. In Orust, the solar PV power system is higher in value than the roof top systems in Mölndal area. The power range is from 300 kW to 7.67 MW (4% to 90% penetration). The power production will follow this curve with difference in power output magnitudes.

The characteristic solar PV power shown in Figure 3.8, Figure 3.9 and Figure 3.10 was simulated on a clear sky solar day that gives the most power that can be produced by a PV plant or system. This solar day picked has a variability index (VI) of less than two (2) and clearness index (CI) of greater than or equal to half (0.5). The other types that can be used to simulate the conditions for solar production are high (VI >10) moderate (5≤ VI <10), mild (2≤ VI <5) and overcast (VI <2, CI ≥0.5) [24] [25].

The characteristic graphs were used as input information for the system to be integrated in Paladin designbase and NEPLAN software. The average production for the month of June was used to determine impact of a particular penetration level and the profiles (Figure 3.8, Figure 3.9 and Figure 3.10) were used for simulation with load profiles. The areas of interest are Mölndal (area 1 and 2) and Orust area. For Mölndal areas, the PV systems are roof top mounted on roofs of residential houses. For Orust, the PV systems are ground mounted and for the Utility company (Orust energy).

Solar PV power was integrated at the load bus for Mölndal area 1 and 2. These are rooftop systems that the customers might install in future. For Orust grid, solar PV power plant was integrated at Sörbo and Månsemyr. These were coupled to the substation in these areas. The integration considered a power factor of 1 for the plants. This means active power production only and no reactive power capability. In paladin designbase, there is a solar PV plant that was used for integration and in NEPLAN a disperse generator is used for renewable generation. Figure 3.11 shows how the integration was done in the software environment.

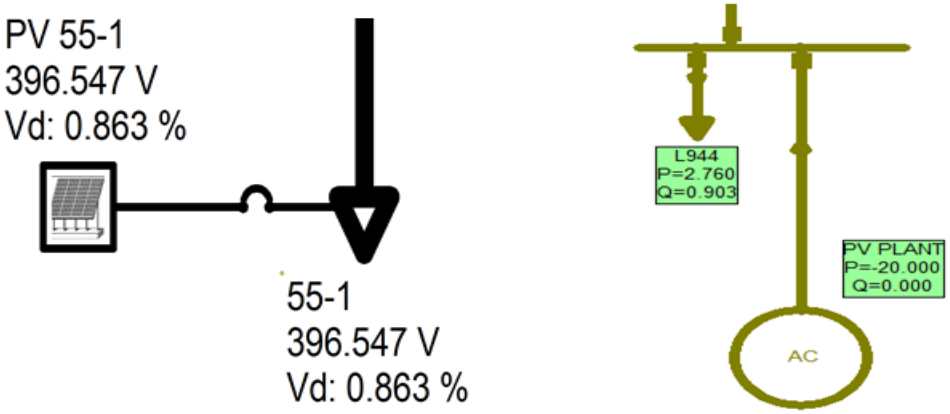

Figure 3.11: Paladin designbase and NEPLAN Photovoltaics Integration

3.5 Hosting Capacity

The increased rate of renewable energy systems addition to conventional electric power system grids and demands has potential to cause system parameters to be or not to be altered beyond or below the operational limits set by international, national and system operations standards. This has led to a term that has become common with renewable energy integration called “hosting capacity” of a grid. Hosting capacity can be defined as the measure of how much renewable energy can be added to an existing grid or power system just enough to cause operation within operating regulations [2], [12]. When applied to Solar PV power integration, which is a renewable energy resource, hosting capacity is the amount of Solar PV power that can be added to a transmission and/or distribution grid enough not to cause power system operational violations of set limits. This is the maximum penetration level, equation (1.1), which can be allowed in a power system just to be within acceptable system operational limits. Parameter operational limits of interest (voltage, loading or system losses) are used in determining the hosting capacity of a grid. The system parameter that has been frequently used in determining the hosting capacity of a grid is the bus/system voltage [2], [3], [10], [12]. However, balance has to be established with other system parameters and ensured that they are also within acceptable operating limits or margins. In the study, bus/system voltages, loading and system losses were used in determining the hosting capacity of grids.

In line with determining the impacts of integrating Solar PV power for the grids of Mölndal and Orust energy, the hosting capacity of the grids need to be determined. While studying the impacts of a different penetration level of 0%, 30%, 60% and 90%, the hosting capacity was determined.

According to [12], there are two known theoretical methods of determining the hosting capacity namely deterministic approach and statistical/probability approach. The third approach that can be employed is by software simulation and monitoring of system parameters to determine just when a system violation is recorded.

The probability and statistical approach to hosting capacity is based on stochastic processes and probability theory. In this approach, parameters like active power, reactive power and voltage are considered as random variables and the correlation among them need to be determined statistically. On the other hand, parameters for transmission lines and cables (R, X and Z) are considered to be deterministic in nature [1]. The association of the system parameters with renewable energy integration is used to determine the probabilistic chance of an over or under voltage for a particular value of a renewable energy source. If the chance is high and causing operation beyond or above limit, then that is the hosting capacity of the grid. This approach involves a long and detailed process to determining the hosting capacity and is not used for this study.

The deterministic approach takes into account the system operational limits. For example, on a 400 V distribution grid, the allowed rapid voltage changes limits from the nominal system voltage are ± 5% according to the standard EN50160. Using the limits, the hosting capacity

can be determined with simple analytical estimation of the voltage drop of a system as shown by equation (2.5) and (2.6). The voltage drop equation is re-written as equation (3.9) [12].

$$|\Delta U| = \left(\frac{R(P - P_{PV}) + XQ}{|U_1|}\right) \tag{3.9}$$

From equation (3.9), the solar PV power at the bus can be estimated using equation (3.10).

$$P_{PV} = P + \left(\frac{XQ}{R}\right) - \left(\frac{|U_1||\Delta U|}{R}\right) \tag{3.10}$$

This is an equation that can be used in general to estimate the hosting capacity at the bus which depends on the voltage before integration, the acceptable voltage rise, reactive power and the line parameters. For a low R/X ratio at the point of coupling, more PV power can be integrated to the grid. From equation (3.10), the theoretical maximum hosting capacity can be estimated when the bus voltage is as given in equation (3.11).

$$|U_1| = \frac{QX}{|\Delta U|} \tag{3.11}$$

To determine the hosting capacity at a feeder, bus or entire grid, the yearly average power consumption P, the minimum reactive power recorded, equivalent impedance parameters at that point, maximum allowed voltage rise (with safety margin) and the maximum voltage recorded at the point of coupling are considered.

In terms of steady state software simulations, three simulations were done and are:

1. No PV penetrations to obtain bus voltages (Base conditions for the grid)
2. Maximum PV power generation with maximum load consumption (minimum range)
3. Maximum PV power generation with minimum load consumption (maximum range)

Voltage levels and other parameters (loading and losses) are also observed. From results of the three simulations, the hosting capacity of the grid under study was determined. Deterministic approach to hosting capacity gives an estimate value and in combination with results from simulations, an estimate near to the exact hosting capacity can be determined. This approach was shorter than probability approach and hence used in this study.

4 Results and Discussions

This chapter presents the simulation results for the distribution grids from Orust and Mölndal energy utility companies. The results as obtained from the simulation softwares are presented for the base (normal) cases and with integration of Solar PV power. These results are for voltage level, voltage profile, system losses, line loading and steady state voltage stability. Discussions of the results obtained by comparison of base cases and with Solar PV power are presented.

4.1 Normal Cases

The normal cases of the grids were simulated in Paladin designbase and NEPLAN using load flow analysis function. The distribution grid of Mölndal for area 1 has a maximum power consumption of 257.76 kW and 85.39 kVar and Mölndal area 2 has a maximum power consumption of 543.02 kW and 178.61 kVar. In addition, the distribution grid of Orust has a maximum power consumption of 8.525 MW and 3.512 MVar.

4.1.1 Voltage Level, Profile and Drop

As stated in the methodology, the distribution grids were simulated without any photovoltaics power integrated. Table 4.1 shows base results for selected grid substation feeders and loads in Mölndal and Orust Area.

Table 4.1: Normal Bus Voltage Level and Drop

Area	Substation	Load	Voltage Level (kV)	Voltage Drop (%)
Mölndal 1	SK2812	12-5	0.4	0.01
Mölndal 2	SK0807	07-5	0.396	1.08
Orust	35010	L35010	10.06	-0.64

The results in Table 4.1 indicate the base case for the substations and loads of interest. The voltage level and voltage drop for the substations have been shown. These will be compared with the results that will be obtained with photovoltaics integrated to the grids. For voltage drop, a decrease in voltage drop is represented by a small percentage towards negative sign.

In addition to Table 4.1, the base voltage profile for selected buses in Mölndal and Orust areas for a period of twenty-four (24) hours. These voltage profiles are shown in Figure 4.1 and Figure 4.2.

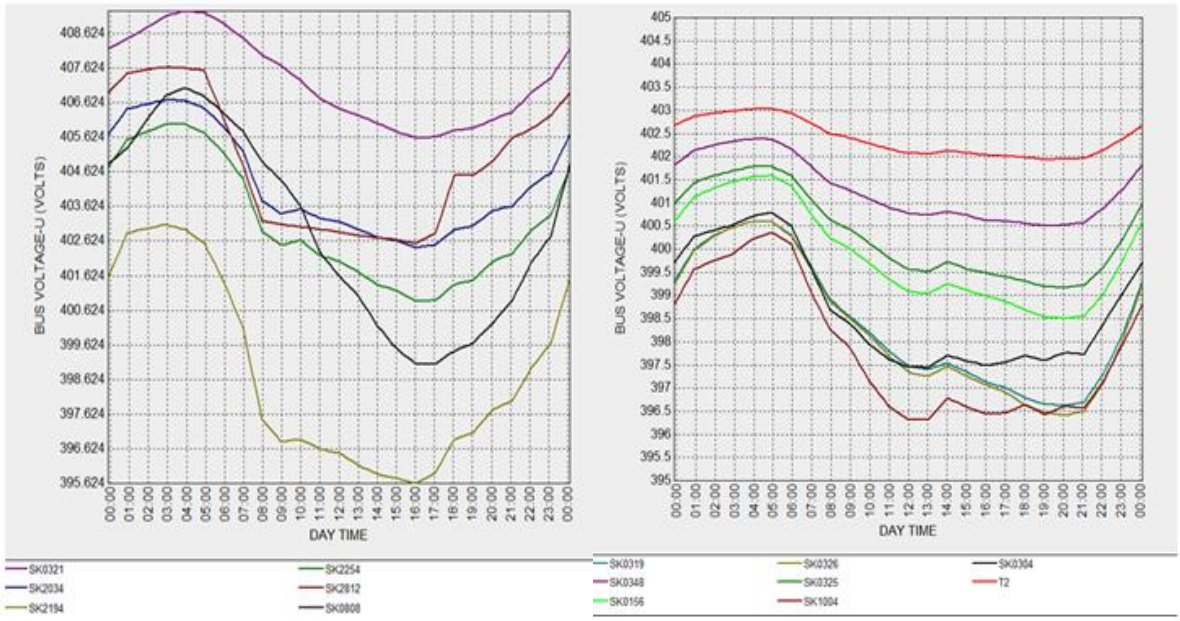

(a) Bus Voltage Profile-Mölndal area 1 *(b) Bus Voltage Profile-Mölndal Area 2*

Figure 4.1: Normal Mölndal Area Bus Voltage Profile

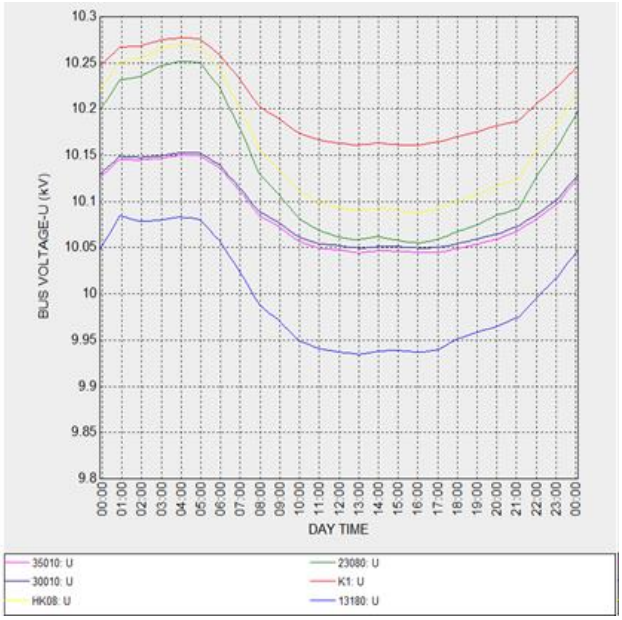

Figure 4.2: Normal Orust Bus Voltage Profile

The voltage profiles shown in Figure 4.1 and Figure 4.2 are a function of time. They show behaviour of a feeder bus over a period of one day or twenty-four (24) hours. These are compared to cases with PV power. Furthermore, it is important to track the behaviour of the bus feeders that are far away from the sending end bus feeder. Figure 4.3 shows the trend of

feeders that are at distances away from the sending end voltage. Figure C.5 and Figure C.10 in appendix C shows a diagram of these feeders.

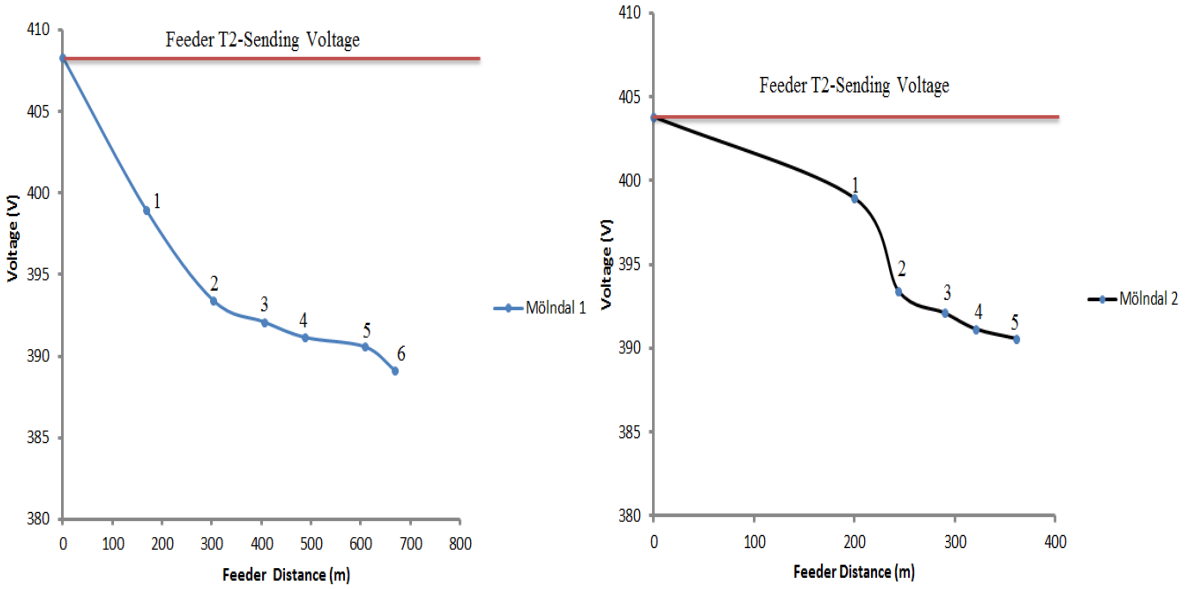

Figure 4.3: Normal Voltage Profile along Feeders for Mölndal Areas

The voltage profiles along feeders shown in Figure 4.3 are the normal case for Mölndal area 1 and 2. Mölndal area 1 is a radial grid and Mölndal area 2 is a meshed grid. Orust area is a combination of both radial and meshed grid type hence it was not plotted. To determine the characteristics of the grid voltages for the areas under study, scatter plots were plotted for the normal cases. Figure 4.4 and Figure 4.5 show the voltage scatter plots.

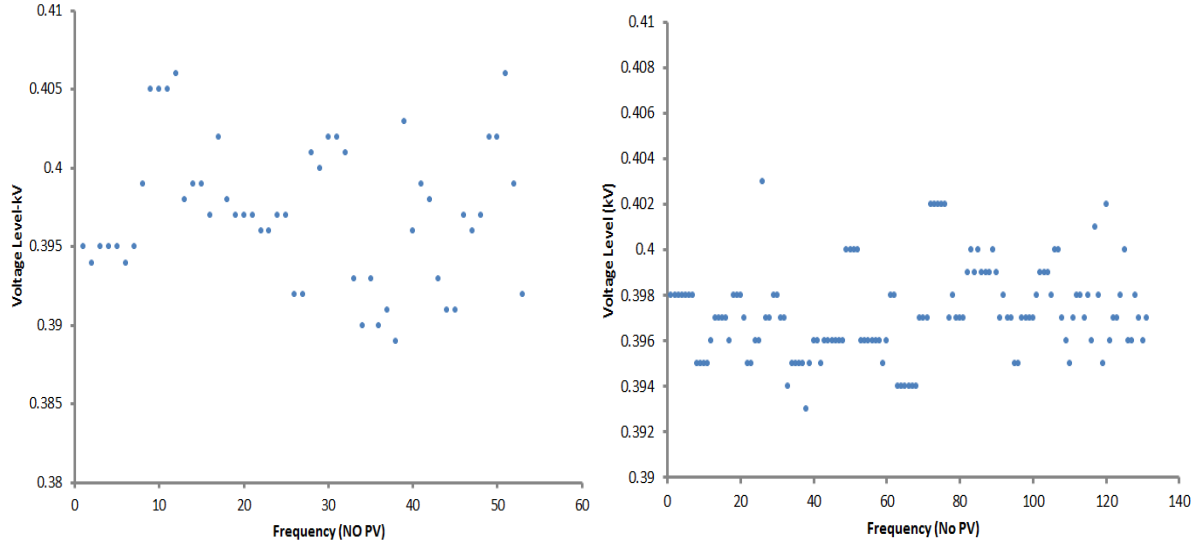

(a) Mölndal Area 1 Voltage Scatter Plot *(b) Mölndal Area 2 Voltage Scatter Plot*

Figure 4.4: Mölndal Area Grids Voltage Scatter Plots

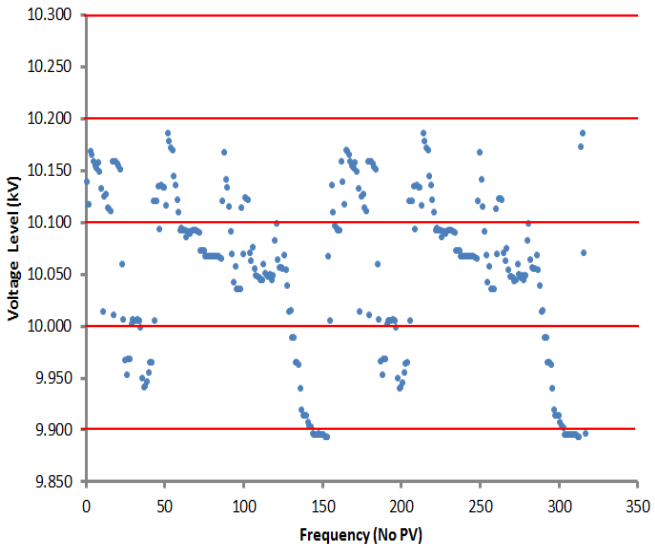

Figure 4.5: Orust Area Grid Voltage Scatter Plot

The voltage Scatter plots for the areas in Figure 4.4 and Figure 4.5 will help in attempting to determine the overall impact of photovoltaics to the entire grids. The frequency on the x-axis represents the number of buses at a particular voltage level on the y-axis. In addition, monitoring of grid voltages to determine if voltage violations occur was aided by use of a scatter plot.

4.1.2 Line Loading

From the simulated normal case for the areas, the feeder line loading for selected buses and loads were obtained. In addition, the feeder line loading of additional feeders over a period of twenty-four hours was obtained. Table 4.2 shows the line loadings for selected feeders for Mölndal and Orust areas for the normal case.

Table 4.2: Selected Feeders Line Loadings-Normal Case

Area	Feeder/Cable/Line To	Line Loading (%)
Mölndal Area 1	Substation SK2812	26.86
Mölndal Area 1	Load 12-5	28.75
Mölndal Area 2	Substation SK0807	12.20
Mölndal Area 2	Load 07-5	13.25
Orust Area	Substation 35010	1.57

A line has a limit to which it cannot be loaded beyond that point. Therefore, the line loading for the feeders shown in Table 4.2 are monitored.

In addition, more feeders are selected for the grids and their loading monitored over a period of one day. Figure 4.6 and Figure 4.7 shows the loadings of these selected feeders over a day.

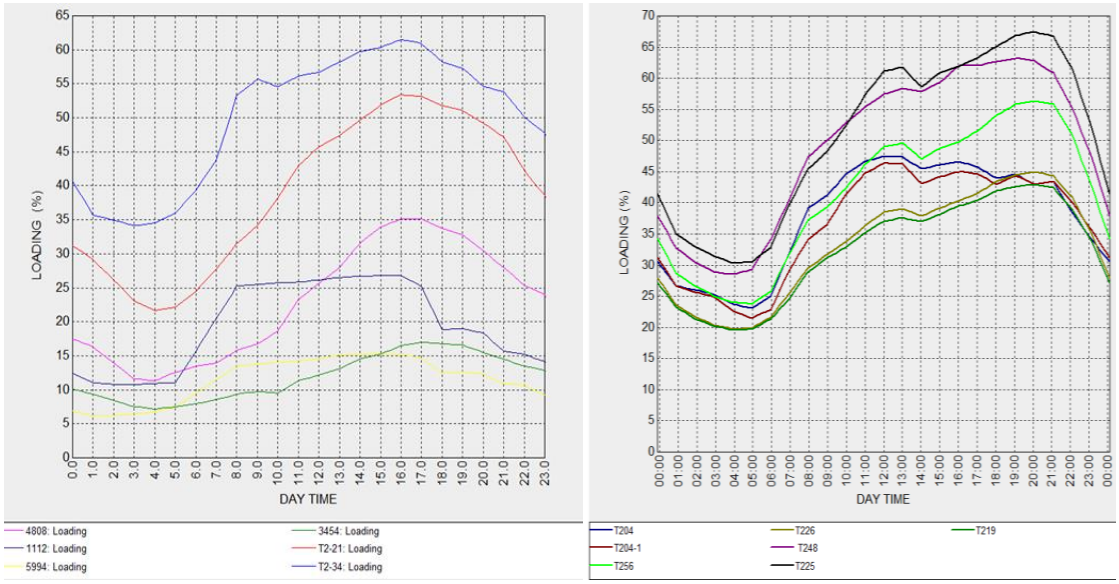

(a) Mölndal Area 1 Line Loadings *(b) Mölndal Area 2 Line Loadings*

Figure 4.6: Mölndal Area Line Loadings

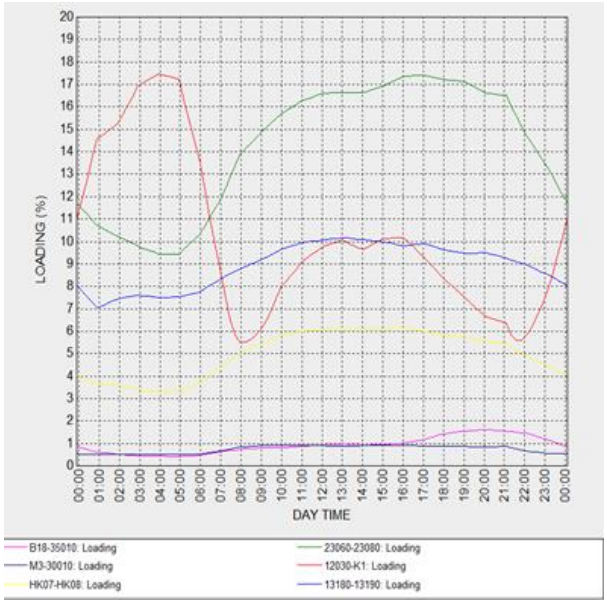

Figure 4.7: Orust Area Line Loadings

The loadings shown in Figure 4.6 and Figure 4.7 for feeders are monitored for the normal cases and when photovoltaics are not integrated to the grids. The loadings show high values during day for most feeders and less value during night times.

4.1.3 Losses

In terms of losses for the normal cases, the grids were simulated at maximum load demand. The total losses for Mölndal area 1 are 8.62 kW and 1.44 kVar at maximum load demand. Mölndal area 2 has 11.86 kW and 14.97 kVar at maximum demand and Orust area has 0.13 MW and 1.272 MVar power losses. In addition to power losses, energy losses were also considered for the grids. These losses are 0.136 MWh for Mölndal area 1, 0.177 MWh for Mölndal area 2 and 2.28 MWh for Orust area distribution grid. These are monitored in attempting to determine the impacts of PV power.

4.1.4 Steady State Voltage Stability

The distribution grids for Mölndal and Orust areas were analysed for steady state voltage stability. NEPLAN was used for this study. For the distribution grid for Mölndal area, Table 4.3 and Table 4.4 shows the results obtained for normal case.

Table 4.3: Base Bus Sensitivity Values (%U/MVar) for Mölndal Area 1

Bus	SK0808	SK2812	SK2254	SK2194	SK2034	SK0321
Sensitivity	15.4368	16.5818	15.6411	22.6006	9.5686	8.2183

Table 4.4: Normal Grid Eigenvalues for Mölndal Area 1

Value No.	1	2	3	4	5	6	7	8	9	10
Eigenvalue	0.003	0.005	0.011	0.012	0.024	0.042	0.048	0.053	0.064	0.070

According to results obtained in Table 4.3 and Table 4.4 for the normal case, the distribution grid for Mölndal area 1 is voltage stable. In addition to the modal analysis and sensitivity value results for the normal case, Q-U and P-U curves were plotted for selected grid substation bus. For Mölndal area 1, grid substation bus SK0321 was selected. Figure 4.8 show the plots. The bus sensitivity values are expressed in percentage voltage per reactive power (%U/Var) for the buses. For the eigenvalues, one hundred (100) values were specified in the software (NEPLAN). However, the grid was able to give fifteen (15) stored values. All the values were positive, an indication of stability. At this point, it was decided to use ten (10) stored eigenvalues for all the grids under study to determining the steady state stability of the grids and comparison of these values for scenarios with solar PV installed. For Mölndal area 1, Mölndal area 2 and Orust area grids, ten (10) eigenvalues were selected for modal analysis method for determining steady state voltage stability.

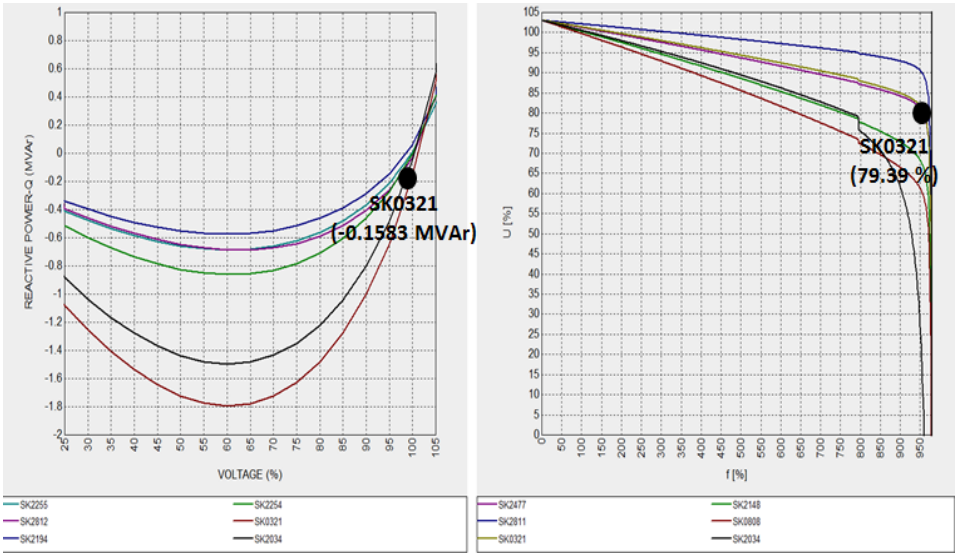

Figure 4.8: Q-U and P-U Curves for Mölndal Area 1 Grid-Normal Case

For P-U curves, it should be noted that the x-axis for power was plotted as a function of f which is in percent (%) by the software (NEPLAN). This is not frequency but a symbol representing percentage scaling up of loads connected to a bus. This was software generated by NEPLAN and where the bus load power scaled up is expressed in terms of f which is in percent (%). The function f in percent (%) is set equally for buses in the parameter settings for steady state voltage stability of NEPLAN but it has different power values for the buses and loads. The parameter of interest in this curve is the critical voltage or voltage collapse point that is compared with other different case scenarios.

The normal distribution grid for Mölndal area 2 was simulated. The results for bus sensitivity value, Eigen values, and Q-U curves were obtained. Table 4.5 and Table 4.6 show the sensitivity values (%U/MVar) of buses. These are base sensitivity values for the grid in area 2. Sensitivity is expressed in percentage voltage (%U) per reactive power (MVar or kVar).

Table 4.5: Normal Bus Sensitivity Values (%U/MVar)-Mölndal Area 2

Bus	SK0319	SK0348	SK0156	SK0326	SK0325	SK1004	SK0304
Sensitivity	4.9537	2.3964	3.6967	4.6266	3.0231	6.5788	6.6366

Table 4.6: Normal Grid Eigenvalues for Mölndal Area 2

Value No.	1	2	3	4	5	6	7	8	9	10
Eigenvalue	0.004	0.007	0.014	0.021	0.026	0.035	0.038	0.039	0.056	0.068

The results obtained in Table 4.5 and Table 4.6 indicates that the grid for Mölndal area 2 is voltage stable.

In addition, Q-U curves for some selected buses are shown in Figure 4.9. The bus for grid substation T2 and SK0155 were selected for monitoring of the reactive power at the bus.

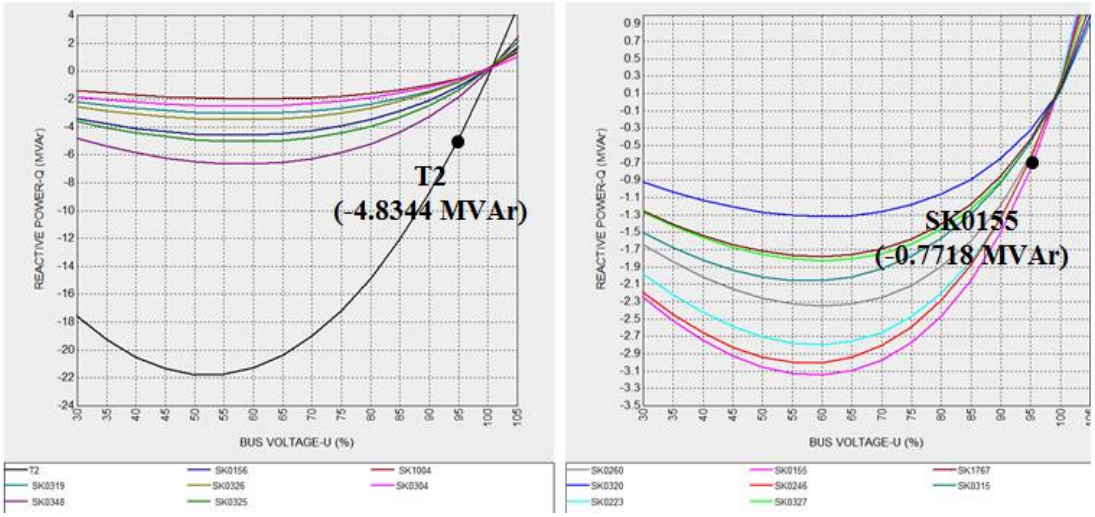

Figure 4.9: Normal Q-U Curves for Mölndal Area 2 Grid

Similarly to results obtained for Mölndal area distribution grids, results for Orust area grid were obtained for steady state voltage stability for the normal case. Table 4.7 and Table 4.8 show steady state voltage stability obtained for Orust area grid.

Table 4.7: Normal Grid Eigenvalues for Orust Area

Value No.	1	2	3	4	5	6	7	8	9	10
Eigenvalue	0.010	0.021	0.042	0.086	0.247	0.299	0.316	0.401	0.451	0.651

Table 4.8: Normal Bus Sensitivity Values (%U/MVar)-Orust Area

Bus	13180	K1	HK08	23080	30010	35010
Sensitivity	1.5997	0.5888	1.1302	1.1276	0.5694	0.6568

According to the results obtained for Orust area grid for voltage stability, the normal case is voltage stable. In addition to this, Q-U and P-U curves were obtained for the analysis. In these curves, substation K1 was selected for monitoring purposes of voltage collapse point and reactive power support of the bus. The curves are shown in Figure 4.10.

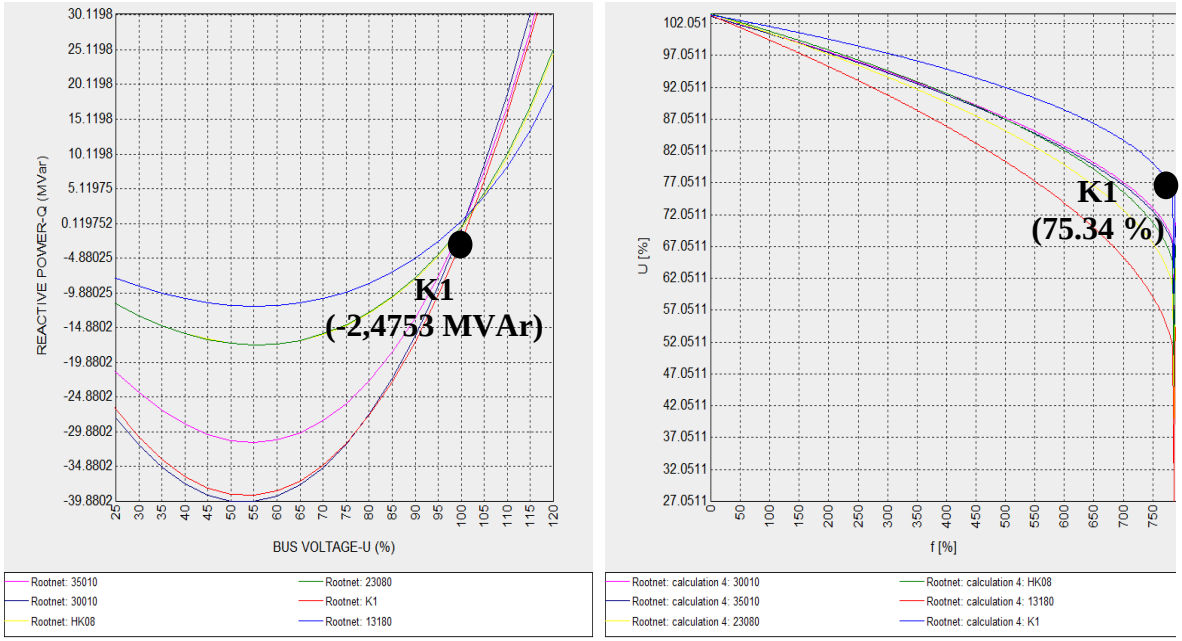

Figure 4.10: Base Q-U and P-U Curves of Selected buses-Orust

The voltage collapse point for K1 was 75.34 percent (%) for the normal case. The reactive power support at this bus was -2.4753 MVAr. These are shown in Figure 4.10.

4.2 Impacts of PV and Scenario Integration to an Existing Grid

The impacts of Solar PV power integration were determined using a penetration level of solar PV power for a selected grid substation. Additionally, 30% penetration level was used for the distribution grids. For Mölndal area distribution grids, the power levels of 77.33 kW and 162.91 kW were used while 2.56 MW was used for Orust area distribution grid. Table 4.9 shows all the integration power levels for the distribution grids. The table shows the active power that was integrated to the distribution grids to determine the impacts at different penetration levels.

Table 4.9: Solar PV Power Penetration Levels

Penetration Level	Mölndal Area 1	Mölndal Area 2	Orust Area
0 %	0 kW	0 kW	0 kW
4 %	N/A	N/A	300 kW
15 %	N/A	N/A	1.30 MW
30 %	77.33 kW	162.91 kW	2.56 MW
60 %	154.66 kW	325.81 kW	5.12MW
90 %	231.98 kW	488.71 kW	7.67 MW

The solar PV penetration levels for the areas in Mölndal were distributed to the loads based on the solar PV power potential of a house as a fraction of the total area potential to the penetration level. This is shown in equation (4.1).

$$Integrated\ PV\ =\ \left(\frac{PV\ Potential\ per\ load}{Total\ PV\ potential}\right) \times (Watthour\ \ penetration\ level) \quad (4.1)$$

For Mölndal area 1 and 2 grids, rooftop systems were considered representing the desire of households to installing these systems. For Orust grid, solar PV power plant was integrated at Sörbo and Månsemyr. These were coupled to the substation in these areas. For photovoltaics integration, a power factor of 1 was considered for the plants. This means active power production only and no reactive power capability. Figure 4.11 and Figure 4.12 show samples of a part of the grid with rooftop solar PV integrated to the load (households). The ground mounted system is not shown in this case. This is because of its similarity to the rooftop system integration in NEPLAN shown in Figure 4.12.

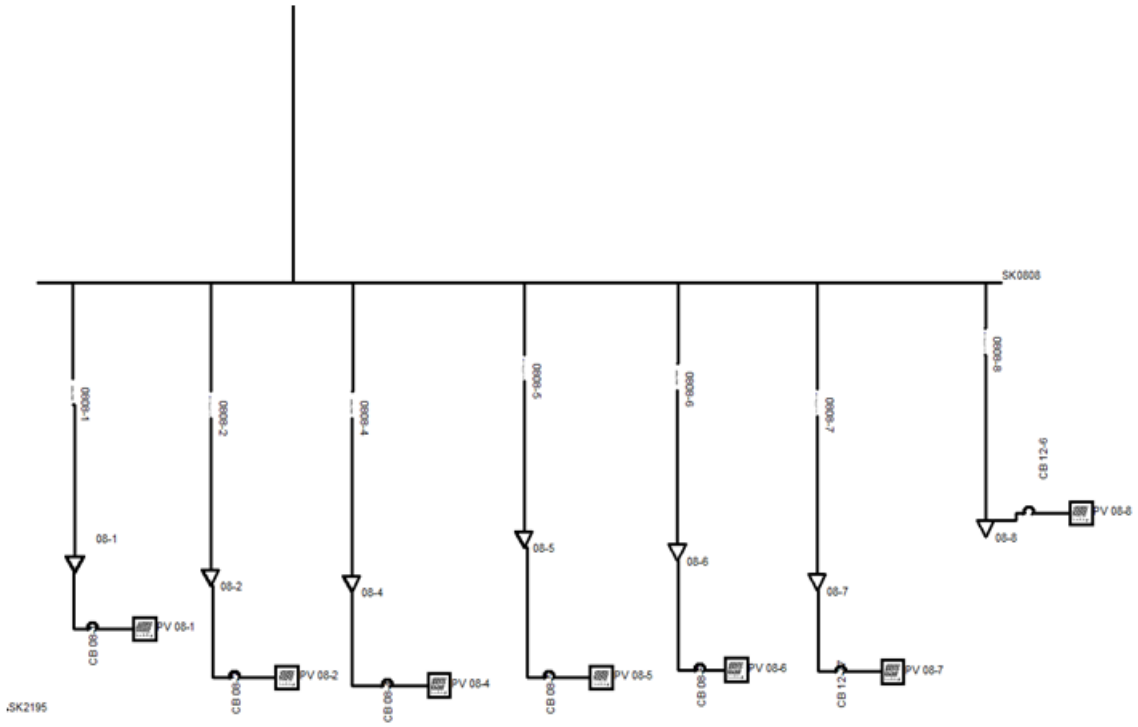

Figure 4.11: Rooftop Solar PV Integration-Paladin designbase

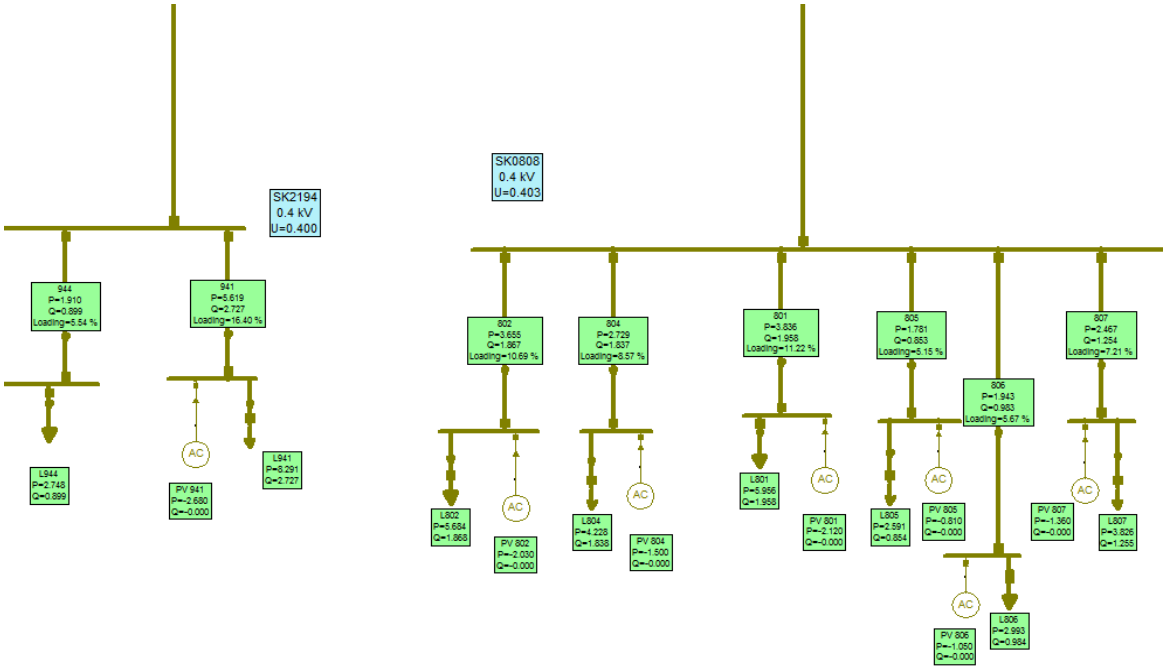

Figure 4.12: Rooftop Solar PV Integration-NEPLAN

4.2.1 Impacts on Voltage Level, Profile and Drop

With photovoltaics integrated to the grids, the impacts on voltage level, voltage profile and voltage drop were studied. For selected buses, the results were obtained. Table 4.10 shows the results obtained after integration.

Table 4.10: Bus Voltage Level and Drop with Photovoltaics

Area	Substation	Load	Voltage Level (kV)	Voltage Drop (%)
Mölndal 1	SK2812	12-5	0.402	-0.58
Mölndal 2	SK0807	07-5	0.397	1.01
Orust	35010	L35010	10.07	-0.71

Comparing the results obtained in Table 4.10 to the results in Table 4.1, it was seen that voltage level of the bus in all the areas increase with integration of photovoltaics while a reduction in voltage drop was obtained.

Additionally, Figure 4.13 and Figure 4.14 show the voltage profile of selected buses over a period of twenty-four hours at a penetration level of 30%.

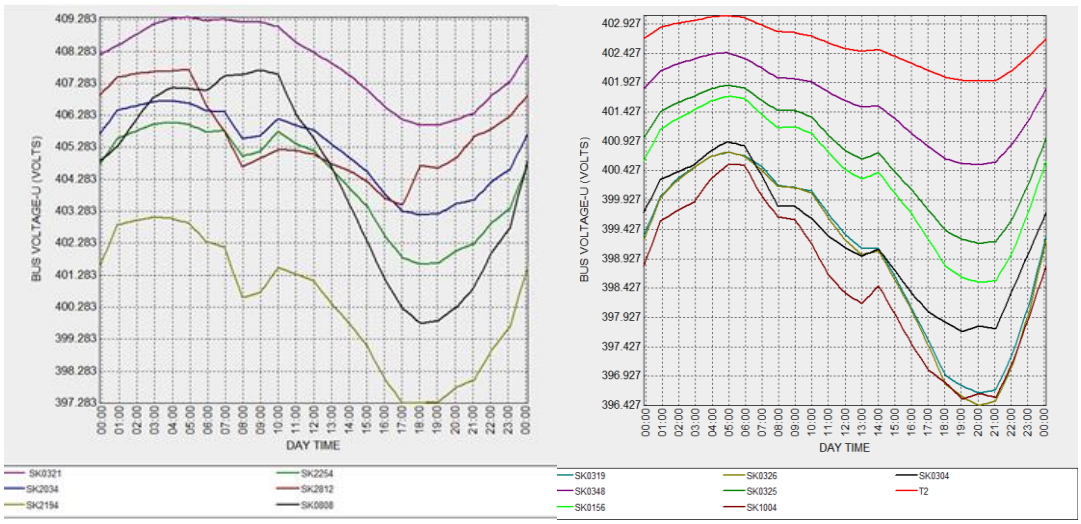

(a) Voltage Profile for Mölndal Area 1 *(b) Voltage Profile for Mölndal Area 2*

Figure 4.13: Voltage Profile at 30 % Penetration Level-Mölndal Area

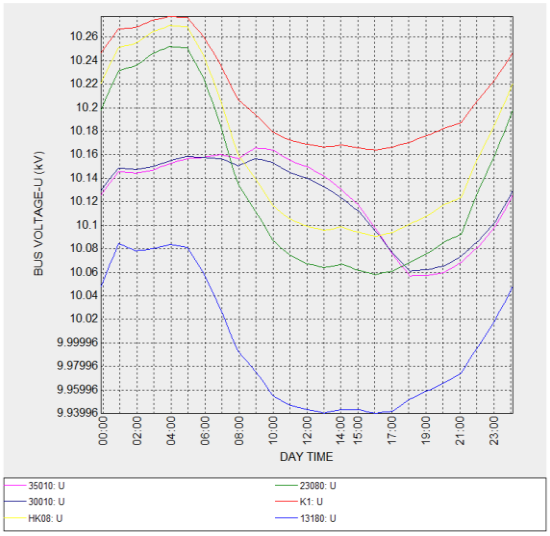

Figure 4.14: Voltage Profile at 30 % Penetration Level-Orust

The voltage profiles in Figure 4.13 and Figure 4.14 show an increase in voltage during the day time and when the PV plants are at maximum power production. When compared to normal case results, integration of photovoltaics causes an increase in voltage profile for selected buses. Additional plots for the voltage profile along feeders with increase in distance from the sending end feeder. Figure 4.15 shows the plots for voltage profile without and with photovoltaics. The feeders taken are shown in Figure C.5 and Figure C.10 of appendix C with the length away from the sending end bus at main substation feeder T2.

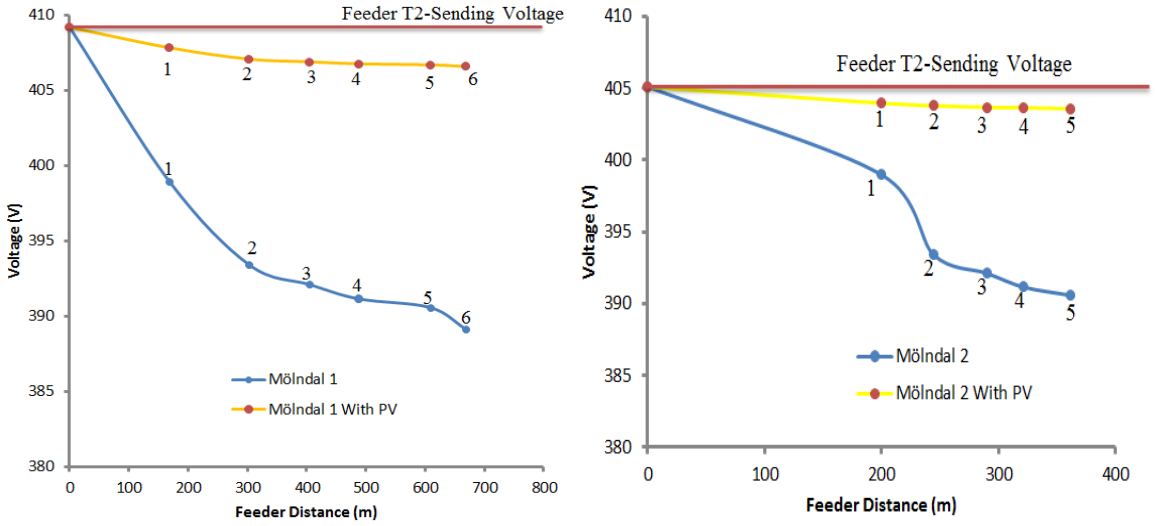

Figure 4.15: Voltage Profile along Feeders for Mölndal Areas

The voltage profiles shown in Figure 4.15 are at the same penetration level for the two areas in Mölndal. In both areas, integration of PV increases the voltage profile along the feeders.

The impact of PV on the entire grid voltage level and profile was investigated. It was done with use of penetration levels of 0%, 30%, 60% and 90%. Figure 4.16, Figure 4.17 and Figure 4.18 show the grids voltage level scatter plots at 0 and 60% penetration level. Figure D.5 Figure D.10 and Figure D.17 in appendix D show scatter plots for the penetration levels.

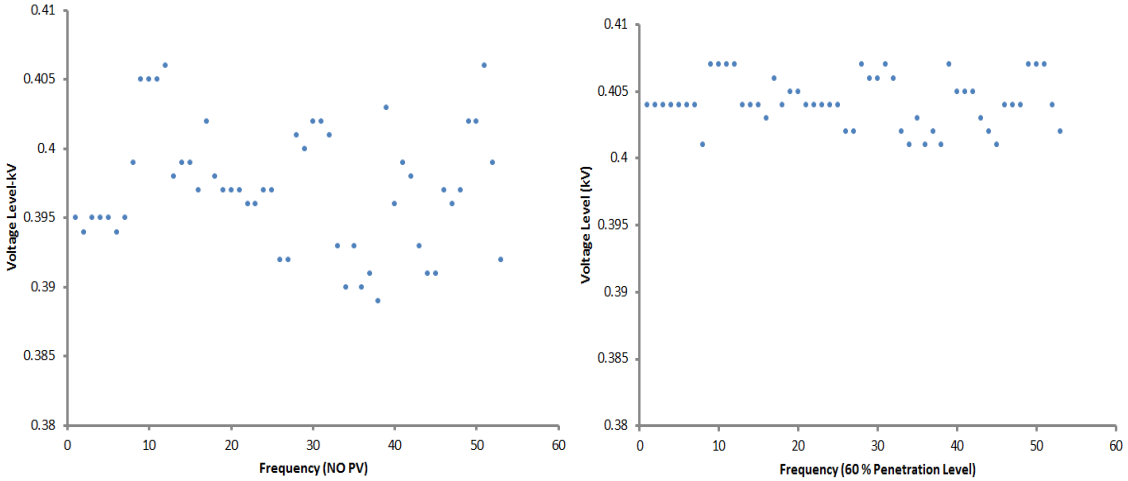

Figure 4.16: Voltage Level Scatter Plots at 0 and 60% Penetration-Mölndal Area 1

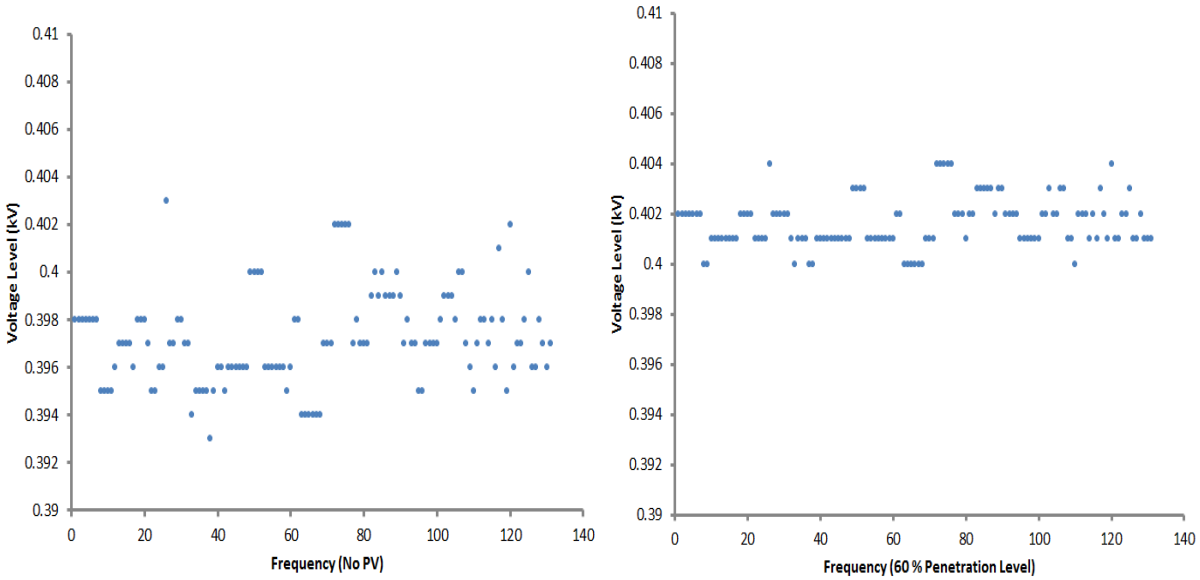

Figure 4.17: Voltage Level Scatter Plots (0, 30, 60 and 90 % Penetration)-Mölndal Area 2

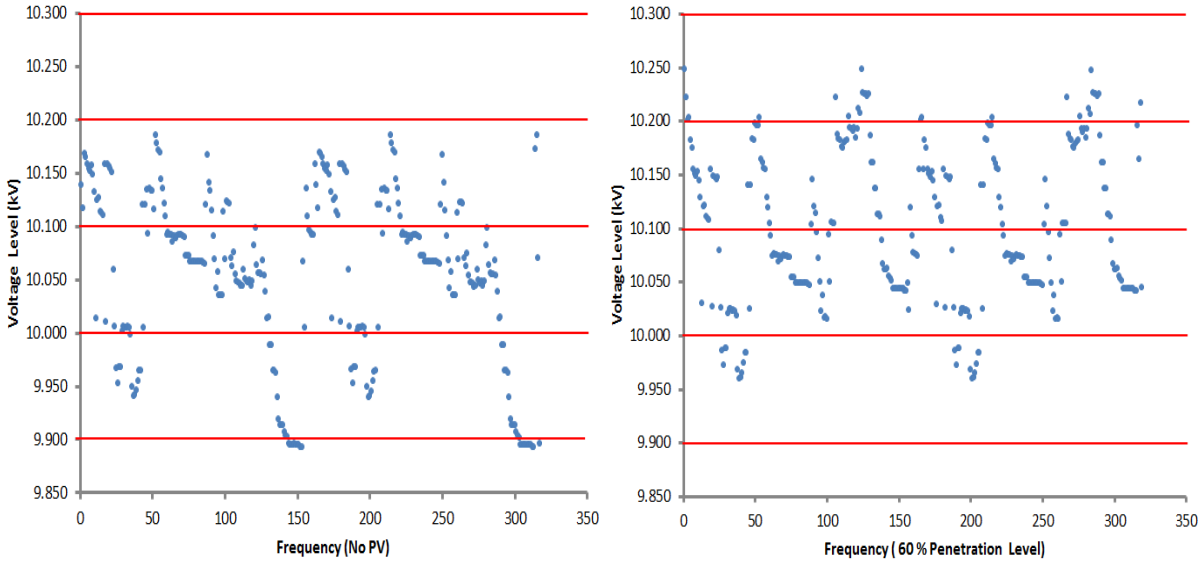

Figure 4.18: Voltage Level Scatter Plots at 0 and 60 % Penetration-Orust

It can be seen from the grids scatter plots figures for the areas that an increase in penetration caused an increase in grids voltage levels. This was also obtained for selected feeders as it was shown in Figure 4.15.

To add to the results obtained for impacts on voltage level and profile, voltage drop results for selected buses in the areas were obtained. These results are shown in Table 4.11, Table 4.12 and Table 4.13.

Table 4.11: Voltage Level and Drop for Substation 35010 and 30010-Orust

Voltage Drop (%) at	4% Penetration	15% Penetration	30% Penetration	60% Penetration	90% Penetration
35010	-0.83	-1.12	-1.58	-2.49	-3.36
30010	-0.79	-1.09	-1.47	-2.22	-2.93

Table 4.12: Voltage Drops for Selected Buses-Mölndal Area 1

Voltage drop at (%)	0% Penetration	30% Penetration	60% Penetration	90% Penetration
SK0808	1.1	-0.03	-1.13	-2.18
SK2812	0.19	-0.00	-1.07	-1.68
SK2254	0.69	-0.20	-1.08	-1.93
SK2194	2.21	0.87	-0.43	-1.69
SK2034	0.26	-0.50	-1.24	-1.96
SK0321	-0.65	-1.18	-1.70	-2.21

Table 4.13: Voltage Drops for Selected Buses-Mölndal Area 2

Voltage drop at (%)	0% Penetration	30% Penetration	60% Penetration	90% Penetration
SK0319	0.45	-0.01	-0.51	-1.01
SK0348	-0.55	-0.74	-0.96	-1.20
SK0156	-0.01	-0.34	-0.70	-1.07
SK0326	0.50	0.02	-0.48	-0.99
SK0325	-0.19	-0.48	-0.80	-1.13
SK1004	0.42	-0.04	-0.53	-1.02
SK0304	0.38	-0.05	-0.52	-0.99

According to the results shown in Table 4.11, Table 4.12 and Table 4.13, integration of photovoltaics and the increase in penetration level cause a reduction in the voltage drop at the buses and feeders.

4.2.2 Impacts on Line Loading

The results for simulated grids with photovoltaics integrated are presented. Table 4.14 shows results of selected lines from the grids.

Table 4.14: Selected Feeders Line Loading with PV Integrated

Area	Feeder/Cable/Line To	Line Loading (%)
Mölndal Area 1	Substation SK2812	18.92
Mölndal Area 1	Load 12-5	9.94
Mölndal Area 2	Substation SK0807	10.28
Mölndal Area 2	Load 07-5	4.46
Orust Area	Substation 35010	10.3

According to results in Table 4.14, integration of PV in Mölndal area 1 and 2 grids caused a reduction in line and feeder loadings. For Orust area, the loading for line feeder to substation 35010 increased with integration of photovoltaics. In addition, more feeders were selected from the areas and 30% penetration of PV integrated to the grids. Figure 4.19 and Figure 4.20 shows the results obtained over a period of twenty-four hours.

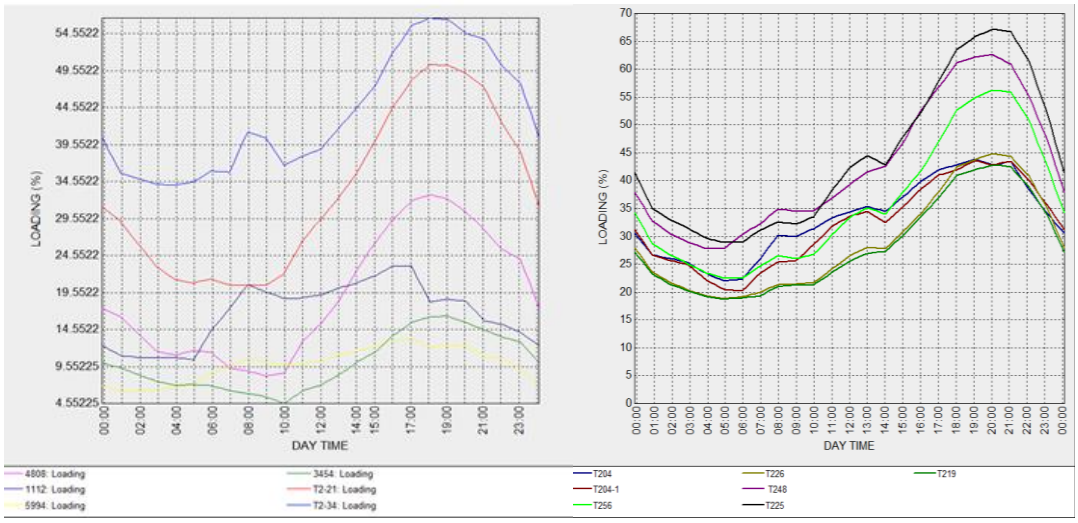

(a) Mölndal Area 1 Loadings *(b) Mölndal Area 2 Loadings*

Figure 4.19: Mölndal Area Line Loadings at 30% Penetration Level

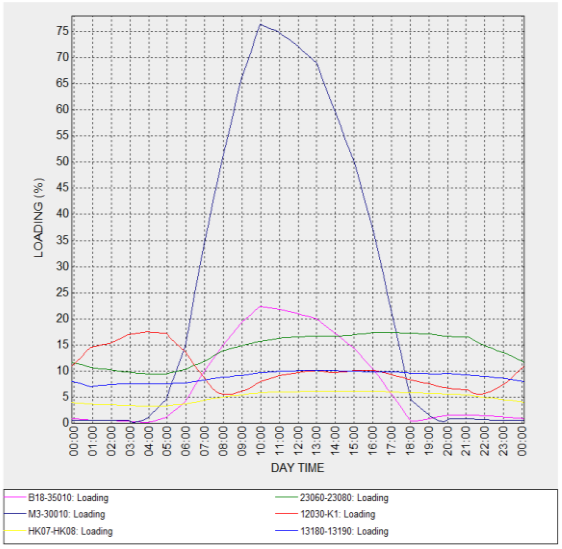

Figure 4.20: Orust Area Loadings at 30% Penetration Level

For a period of twenty-four (24) hours for selected lines, integration of 30% penetration level in Mölndal area caused a reduction in loadings. For the feeders to the substation where PV was coupled in Orust area, integration of 30% penetration level caused an increase in line loading. Furthermore, line loading of the lines with all penetration levels was simulated. Table 4.15, Table 4.16 and Table 4.17 shows obtained results for selected feeders and lines to substation bus.

Table 4.15: Line Loading for Selected Buses-Mölndal Area 1

Feeder Loading (%)	0% Penetration	30% Penetration	60% Penetration	90% Penetration
SK0808 Feeder	35	24	15	11
SK2812 Feeder	27	20	13	9
SK2254 Feeder	17	12	7	6
SK2194 Feeder	15	11	7	5
SK2034 Feeder	64	46	30	20
SK0321 Feeder	55	38	23	17

Table 4.16: Line Loading for Selected Buses-Mölndal Area 2

Feeder Loading (%)	0% Penetration	30% Penetration	60% Penetration	90% Penetration
SK0319	37	31	18	12
SK0348	45	36	22	14
SK0156	51	43	25	16
SK0326	39	33	19	13
SK0325	70	51	34	23
SK1004	37	31	18	12
SK0304	60	38	29	19

Table 4.17: Line Loading for Feeders to Substation 35010 and 30010

Feeder Loading (%)	4% Penetration	15% Penetration	30% Penetration	60% Penetration	90% Penetration
35010	1.57	10.3	21.26	44.36	66.65
30010	1	38.54	76.45	152.57	227.39

Similarly to results obtained for simulation over a period of twenty-four hours with photovoltaics integrated, integration of different penetration levels in Table 4.15, Table 4.16 and Table 4.17 showed similar trends for the grids. For Mölndal area, the loading decreased with increase in penetration levels while for Orust area it increased with increase in penetration level.

4.2.3 Impacts on Losses

With PV integrated at 30% for Mölndal area 1, the active and reactive power losses at this level were 0.00534 MW and 0 MVar. Losses of 0.00694 MW and 0.01152 MVar for Mölndal area 2 was obtained. Orust area grid lost 0.13 MW and 1.27 MVar. To begin with, Figure 4.21 shows power and energy losses for Mölndal Area.

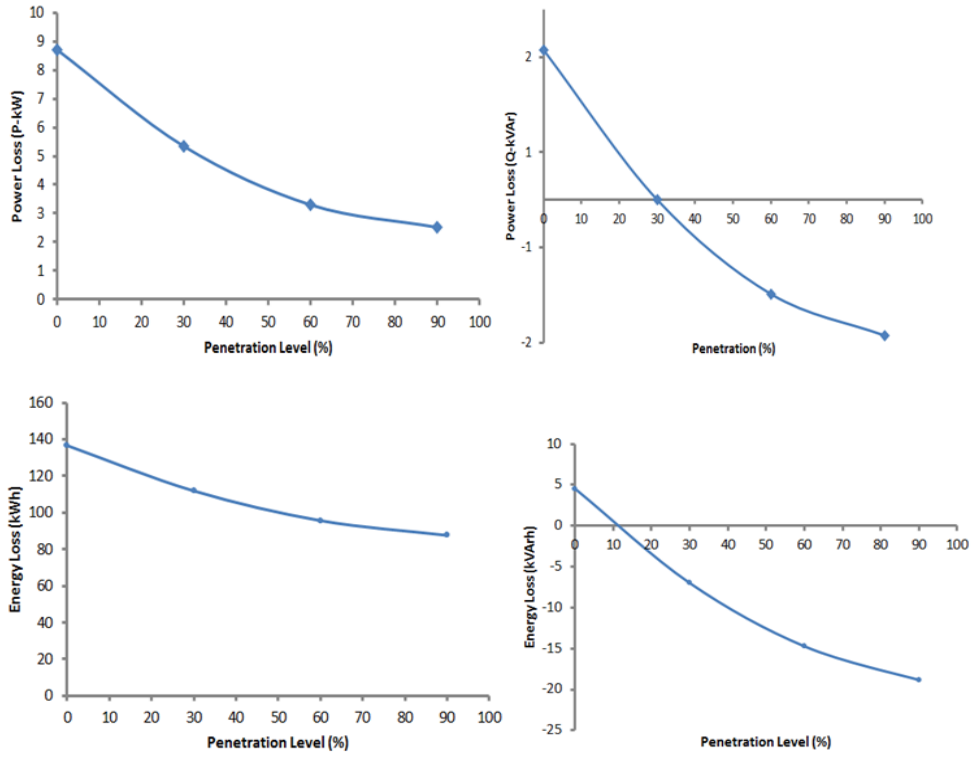

Figure 4.21: Grid Total Power and Energy Losses-Mölndal Area 1

The power and energy loss for Mölndal area 1 grid decreased with an increase in photovoltaics penetration level. This trend is shown Figure 4.21. At penetration levels of 0%, 30%, 60% and 90%, the power and energy loss were decreasing in value.

In addition, the losses for Mölndal area 2 and Orust area were also plotted. The power and energy losses for Mölndal area 2 are shown in Figure 4.22. To sum it all, the losses of Orust are shown in Figure 4.23.

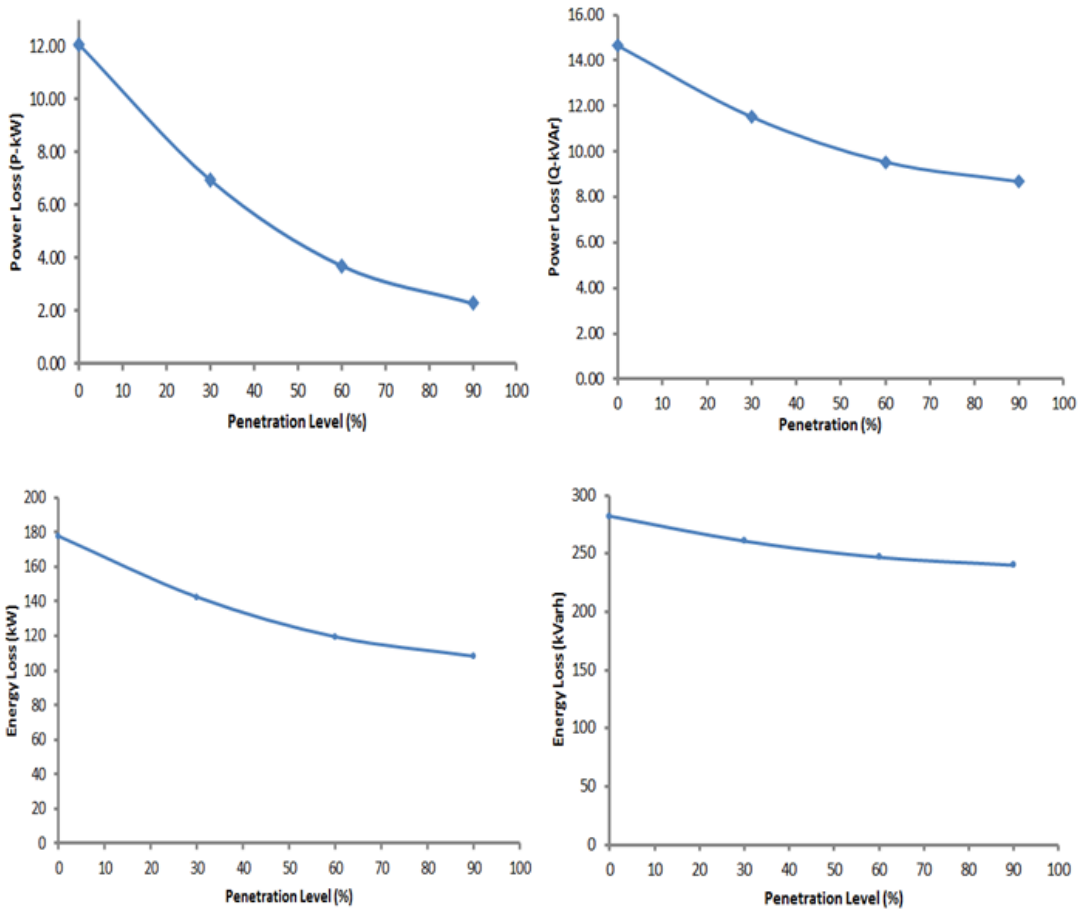

Figure 4.22: Grid Total Power and Energy Losses-Mölndal Area 2

Observation of the plots for power and energy loss for Mölndal area 2 shown in Figure 4.22 revealed a similar trend to results obtained for Mölndal area 1 grid. Both results for power and energy loss decreased with increase in PV penetration levels.

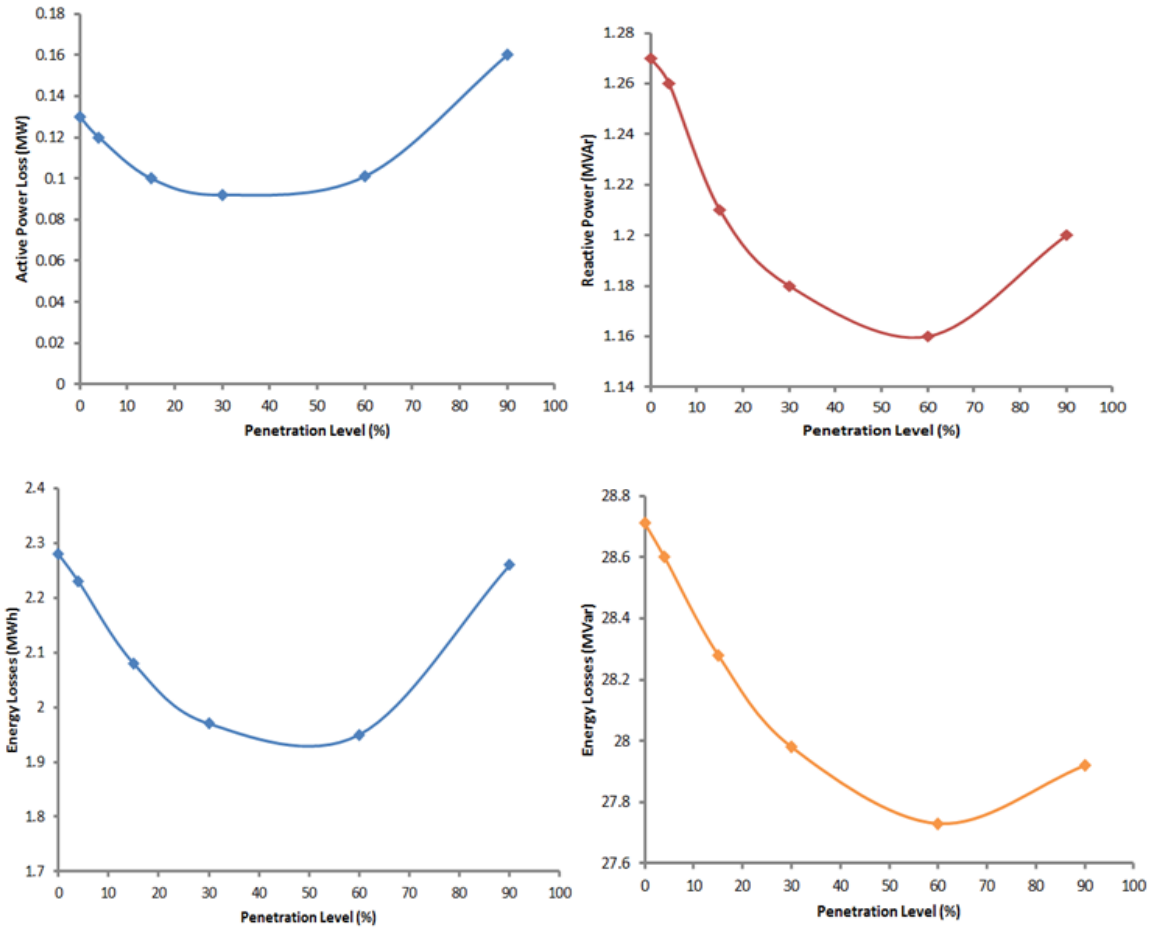

Figure 4.23: Total Power and Energy Losses at 0, 30, 60 and 90 % Penetration Levels-Orust

Figure 4.23 show plots obtained for losses with increase in penetration level for Orust area grid. According to the plots, power and energy loss for Orust area grid decreases with PV integration. For active power and energy loss, this is up to 45% and 50% penetration. For reactive power and energy loss, this is true up to 60% penetration level. After the latter penetration levels for active and reactive power and energy, the losses start to increase with increase in penetration levels. The losses were simulated at maximum load demand for the grids.

4.2.4 Impacts on Steady State Voltage Stability

With solar PV power penetration levels integrated to the grid, the steady state voltage analysis simulations were performed for the grids to the areas. These are sensitivity analysis, modal analysis, P-U and Q-U curves.

To begin with, Table 4.18 and Table 4.19 present the grid sensitivity and modal analysis results for Mölndal area 1. In addition to this, Figure 4.24 shows the Q-U and P-U curves for selected buses for the grid. For the purpose of monitoring reactive power support and voltage collapse point, bus SK0321 is shown in bold.

Table 4.18: Sensitivity Results (%U/MVar) of selected Buses-Mölndal Area 1

Substation Bus	NO PV	30% PV Penetration	60% PV Penetration	90% PV Penetration
SK0808	15.4368	15.2816	15.1323	14.9911
SK2812	16.5818	16.4910	16.4026	16.3164
SK2254	15.6411	15.5184	16.3999	16.2865
SK2194	22.6006	22.3367	22.0843	21.8447
SK2034	9.5686	9.5050	9.4444	9.3869
SK0321	8.2183	8.1813	8.1455	8.1112

Table 4.19: Eigenvalues at Different Penetrations –Mölndal Area 1

Mölndal Area 1				
Eigenvalue Number	Eigenvalue (NO PV)	30% PV Penetration	60% PV Penetration	90% PV Penetration
1	0.003	0.003	0.003	0.003
2	0.005	0.005	0.006	0.006
3	0.011	0.011	0.011	0.011
4	0.012	0.012	0.012	0.012
5	0.024	0.024	0.025	0.025
6	0.042	0.043	0.043	0.043
7	0.048	0.048	0.049	0.049
8	0.053	0.053	0.053	0.053
9	0.064	0.065	0.066	0.066
10	0.07	0.071	0.072	0.073

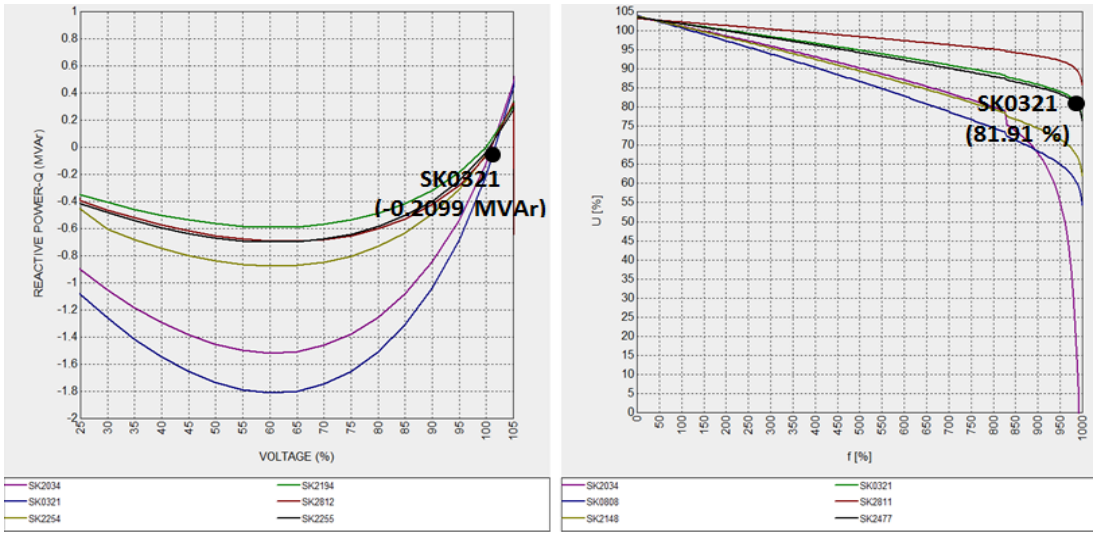

Figure 4.24: Q-U and P-U curves at 30% PV Penetration-Mölndal Area 1

Solar PV integration to the distribution grid of Mölndal area 1 resulted in positive value results for sensitivity and modal analysis (eigenvalues). The P-U and Q-U curves results shown in Figure 4.24 outline an increase in the critical voltage for the bus at substation SK0321 and an increase in reactive power support for the bus. Results of the P-U and Q-U curves for 60% and 90% penetration levels shown in Figure D.3 and Figure D.4 (appendix D) show the similar trends as 30% penetration level results shown in Figure 4.24.

Similarly to Mölndal area 1 grid, modal and sensitivity analysis with plots of Q-U curves were performed for Mölndal grid area 2. The sensitivity analysis results for selected buses and modal analysis results for the grid are presented in Table 4.20 and Table 4.21. In addition, Figure 4.25 shows the Q-U curves for selected substation buses for the area.

Table 4.20: Sensitivity Results (%U/MVar) of selected Buses-Mölndal Area 2

Solar PV Power Penetration/Bus	NO PV	30 % Penetration	60 % Penetration	90 % Penetration
SK0319	4.9537	4.9303	4.9074	4.8854
SK0348	2.3964	2.3913	2.3863	2.3814
SK0156	3.6967	3.6840	3.6716	3.6594
SK0326	4.6266	4.6043	4.5824	4.5616
SK0325	3.0231	3.0139	3.0049	2.9962
SK1004	6.5788	6.5452	6.5124	6.4803
SK0304	6.6366	6.6088	6.5815	6.5548

Table 4.21: Eigenvalues at Different Penetrations-Mölndal Area 2

Mölndal Area 2				
Eigenvalue Number	Eigenvalue (NO PV)	30% Penetration	60% Penetration	90% Penetration
1	0.004	0.004	0.004	0.004
2	0.007	0.007	0.007	0.007
3	0.014	0.014	0.014	0.014
4	0.021	0.021	0.021	0.021
5	0.026	0.026	0.026	0.026
6	0.035	0.035	0.035	0.035
7	0.038	0.039	0.033	0.038
8	0.039	0.039	0.039	0.039
9	0.056	0.056	0.056	0.057
10	0.068	0.068	0.069	0.068

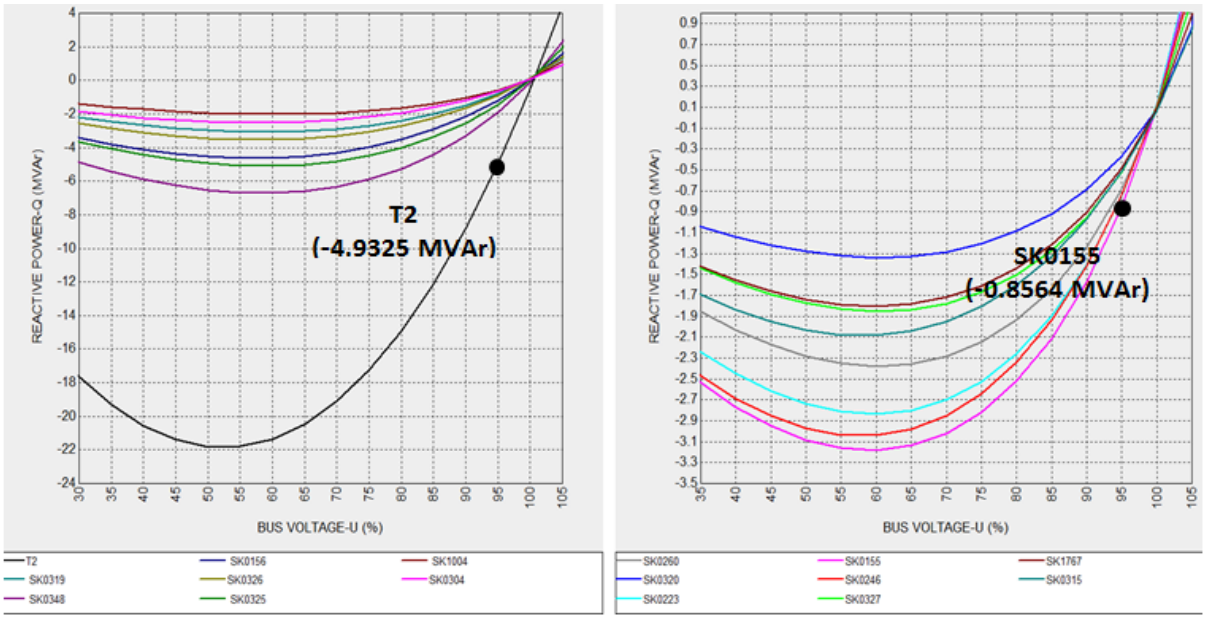

Figure 4.25: Q-U curves at 30% PV Penetration Level-Mölndal Area 2

The results in Table 4.20 and Table 4.21 show a decrease in sensitivity values for the selected buses with increase in penetration levels. While the stored eigenvalues slightly increased with increase in penetration levels.

The bus T2 and SK0155 show an increase in reactive reserve for the bus with increase in penetration level of 30%. The trend is same with penetrations of sixty percent (60%) and ninety percent (90%) shown in Figure D.8 and Figure D.9 in appendix D.

For Orust area grid, steady state voltage stability was analysed. That is sensitivity, Q-U curves, P-U curves and modal analysis was performed. Table 4.22 shows obtained sensitivity value results and Table 4.23 shows obtained modal analysis results.

Table 4.22: Sensitivity Results (%U/MVar) of selected Buses-Orust

Solar PV Power Penetration/Bus	NO PV	4% Penetration	15% Penetration	30% Penetration	60% Penetration	90% Penetration
Bus 13180 Sensitivity	1.5997	1.5996	1.5991	1.5986	1.5979	1.5976
Bus K1 Sensitivity	0.5888	0.5888	0.5886	0.5884	0.5882	0.5880
Bus HK08 Sensitivity	1.1302	1.13	1.1297	1.1294	1.0989	1.1288
Bus 23080 Sensitivity	1.1276	1.1275	1.1272	1.1268	1.1264	1.1262
Bus 30010 Sensitivity	0.5694	0.5688	0.5666	0.5640	0.5592	0.5549
Bus 35010 Sensitivity	0.6568	0.6555	0.6531	0.6496	0.6431	0.6373

Table 4.23: Eigenvalues at Different Penetrations-Orust

Solar PV Power Integration						
Eigenvalue Number	Eigenvalue (NO PV)	4% Penetration	15% Penetration	30% Penetration	60% Penetration	90% Penetration
1	0.01	0.01	0.01	0.01	0.01	0.01
2	0.021	0.021	0.021	0.021	0.021	0.021
3	0.042	0.042	0.042	0.042	0.042	0.042
4	0.086	0.086	0.087	0.087	0.088	0.088
5	0.247	0.247	0.247	0.247	0.248	0.248
6	0.299	0.299	0.301	0.302	0.305	0.307
7	0.316	0.316	0.316	0.316	0.317	0.317
8	0.401	0.401	0.402	0.402	0.402	0.402
9	0.451	0.451	0.453	0.455	0.458	0.462
10	0.651	0.651	0.654	0.657	0.662	0.668

In addition to sensitivity and modal analysis results, P-U and Q-U curves were plotted. These are shown in Figure 4.26. Substation bus K1 was used for voltage collapse and bus reactive power support monitoring with PV penetration level.

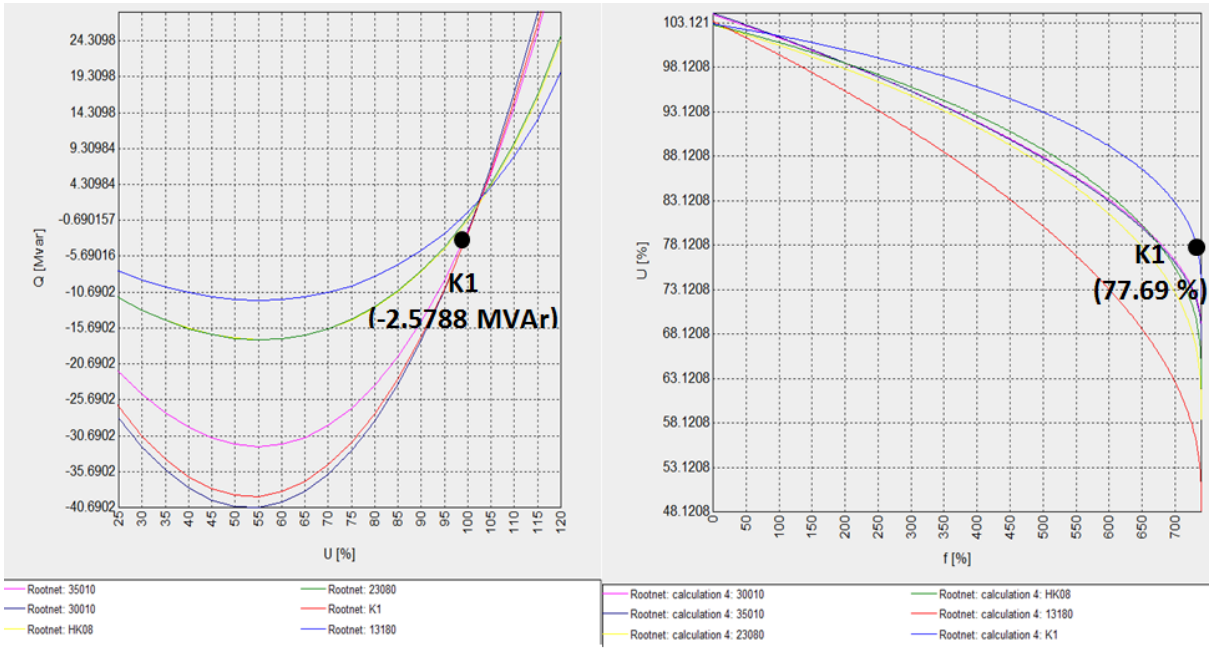

Figure 4.26: Q-U and P-U curves at 30% PV Penetration-Orust

The bus sensitivity results obtained in Table 4.22 show that with increase in the solar power penetration level the sensitivity value decreases. But the decrease in sensitivity value was marginal penetration levels lower than 30% penetrations. These are penetration levels of 4% and 15% that showed least marginal decrease in sensitivity value.

Bus Q-U and P-U curves were plotted for selected buses in order to observe the shift in the graphs. Figure 4.26, Figure D.15 and Figure D.16 (appendix D) presents plots of Q-U and P-U curves at 30%, 60% and 90% penetration level. The P-U and Q-U curves for bus K1 showed an increase in critical voltage and reactive power reserve for the bus with increase in penetration level as compared to the normal case.

4.3 Discussions

Having obtained the results of the simulations for the integration of solar PV power to the distribution grids from Möndal and Orust energy utility companies, their impacts on the system are discussed in the proceeding paragraphs

4.3.1 Voltage Level, Profile and Drop

To begin with, the impacts on the distribution grid for area 1 in Mölndal are discussed. This low voltage distribution grid is a radial grid with unidirectional power flow (substation to load) or one path route supply to the customer [11]. For feeders, the further it is from the main substation the lower its voltage level as compared to the sending voltage level. The results obtained for voltage level, voltage profile and voltage drop results with solar PV power integrated to the grid resulted in an increase in voltage level/profile and a reduction in voltage drop. Further analysis of the results from the time simulation of load/power showed similar trends. With time simulation, the integration of solar PV power resulted in voltage boost for buses during the time of high load demand and consumption. For the simulated day, the increase in voltage level and voltage profile did not result in any system violation (i.e. above ± 5%). The voltage level, profile and voltage drop results for the radial grid for Mölndal area grids correlated with expected theoretical impact discussed in Section 2.3.1 of Chapter 2.

Secondly, the results obtained for Mölndal area 2 was similar to the results for area 1 but with some minor differences. Mölndal area 2, as earlier alluded to, is a meshed distribution and multi-directional power flow. The bus voltage levels are very close to each other as compared to a radial grid where bus voltage levels for the grid are not close to each other and depend on the distance from the main substation. The meshed grid can also be operated in radial. In this case the impacts are exactly similar to results for Mölndal area 1 grid. The results obtained for the voltage level, voltage profile and voltage drop showed an increase in voltage level, voltage profile and a decrease in voltage drops. However, as one can see from the scatter plots in Figure 4.17, an increase in PV penetration level caused a more flat voltage profile and levels for the bus and entire grid during time of high load demand. For the simulated day, there was no voltage violations recorded for the penetration levels simulated.

To end it all for this section, results obtained for Orust distribution grid showed similar results to Mölndal area. This distribution grid has a mixture of radial, loop and meshed type of distribution grid. In principle, the grid can be divided into three areas (S1, S2 and S3). These areas are shown in Figure A.13. Area S3 has a switching station while S1 and S2 have

130/10 kV Power substation. The areas for solar PV power planned installation are in area S3 which have been shown in the Figure A.13 (Sörbo and Månsemyr). The results obtained as seen in Section 4.2.1 for the voltage level, voltage profile and voltage drop showed an increase with increase in PV penetration levels for voltage level and profile while a decrease in voltage drop.

4.3.2 Line Loading

The integration of PV decreased the line loading for the cables in the grid for Mölndal area grids. As expected from theory, the increase in solar PV power penetration resulted in subsequent reduction in line loading for Mölndal area. This is because the integration of solar power provided power locally and reduced the flow for power from the source. However, for Orust area grid, the integration of PV resulted in an increase in line loading with increase in PV penetration to the line supplying the substation where PV was coupled. This is because, when the load demand for the substation is met, power needs to be transmitted to other substations in the area. At a penetration level of 60% and higher, feeder cable to substation 30010 had a line loading violation. Therefore, not more PV can be integrated beyond this level.

4.3.3 Losses

The results for power and energy losses were a mixture of positive and negative impacts for the areas. For the grids for Mölndal area 1 and 2, the integration of PV resulted in reduction of grid losses. The increase in penetration of PV resulted in corresponding decrease in grid losses for the areas. However, for Orust area grid, the results were a mixture. Integration of PV resulted in decrease in the grid power loss. The increase in PV penetration level resulted in both decrease and increase of grid losses as can be seen in Figure 4.23. For active power and energy loss, this is up to 45% and 50% penetration. For reactive power and energy loss, this is true up to 60% penetration level. After the latter penetration levels for active and reactive power and energy, the losses started to increase with increase in penetration levels. As a result, this indicates a limit to PV integration at a penetration level when the losses are minimized. In this case, the maximum penetration level can be dictated by the cost saving margin of the two active and reactive losses. The one that would translate into a higher cost saving would be the optimal penetration level for the grid.

4.3.4 Steady State Voltage Stability

The results obtained for the steady state voltage stability indicated an improvement in the stability and degree of stability for the grid. This was indicated by a decrease in the bus sensitivity value and an increase in grid stored eigenvalue results. For all the grids for Mölndal and Orust, integration of PV and increase in penetration levels improved the steady state voltage stability, increased the bus voltage collapse point and reactive power reserve for a bus. This is because, power was provided locally and the bus voltage level was increased.

4.3.5 Impacts Hypothetical Extrapolations

From the foregoing discussions of the impacts to the distribution grids, some hypothetical conditions were formulated that could guide utility companies with regards to solar PV power penetrations and load/area/ grid power demand at a particular point. From a power and energy point of view, and for installation of a rooftop solar PV power (Mölndal energy grid), the following hypotheses were formulated;

- If $P_{SOLAR\ PV\ POWER\ PRODUCTION} < P_{LOCAL\ LOAD\ DEMAND}$ (Beneficial to Utility Company)
- If $P_{SOLAR\ PV\ POWER\ PRODUCTION} = P_{LOCAL\ LOAD\ DEMAND}$ (Beneficial to both –Not True for entire grid)
- If $P_{SOLAR\ PV\ POWER\ PRODUCTION} > P_{LOCAL\ LOAD\ DEMAND}$ (Beneficial to Customer)

The above hypotheses could guide the utility company with regard to rooftop installations where power and energy loss are concerned. The second point when there is a perfect load matching, the benefit does not fall on the utility company as it results in loss of revenue if all the power consumed in an area is supplied by customers' rooftop PV systems. The highest benefit comes in when installed solar PV power is less than the load demand. The losses in the grid are reduced and translates to cost saving on the power/energy losses. The third hypothesis translates to benefits for the customer with solar PV power installed. This depends on the purchasing power of the grid connected to and the regulations that are in place in that area.

For utility installed solar PV power and area divided grid (Orust energy grid);

- If $P_{SOLAR\ PV\ POWER\ PRODUCTION} \leq P_{AREA\ LOAD\ DEMAND}$ (Low cost on grid Losses)
- If $P_{SOLAR\ PV\ POWER\ PRODUCTION} > P_{AREA\ LOAD\ DEMAND}$ (Higher Cost on grid Losses)

For utility area installed solar PV power, the costs are minimised when the production of solar PV power installed equal to area load demand. At the point when the production exceeds the area load demand, the losses start increasing and increase the grid operation costs.

The hypothetical conditions outlined above could guide utility companies for planning and implementation purpose of solar PV power integration together with equation (3.10) to determine how much can be allowed for normal steady state system operation.

4.4 Hosting Capacity Determination

Determination of the hosting capacity for the distribution grids was done with the guide presented in Section 3.5 under Chapter 3. That is, simulation of maximum solar PV power production for the simulated day (June) and minimum load demand. For this simulated day, 130 kW was the lowest consumption for Mölndal area 1, 237 kW for Mölndal area 2 and 4052 kW for Orust area grid. Steady state power flow in Paladin designbase was used for

these simulations. The grid parameters of voltage, power loss, line loading and power flow were used to determine the hosting capacity of the grids.

4.4.1 Mölndal Area 1 Grid Hosting Capacity

For Mölndal area 1 distribution grid, the grid substation SK2477 and its loads were monitored together with grid parameters for determination of hosting capacity.

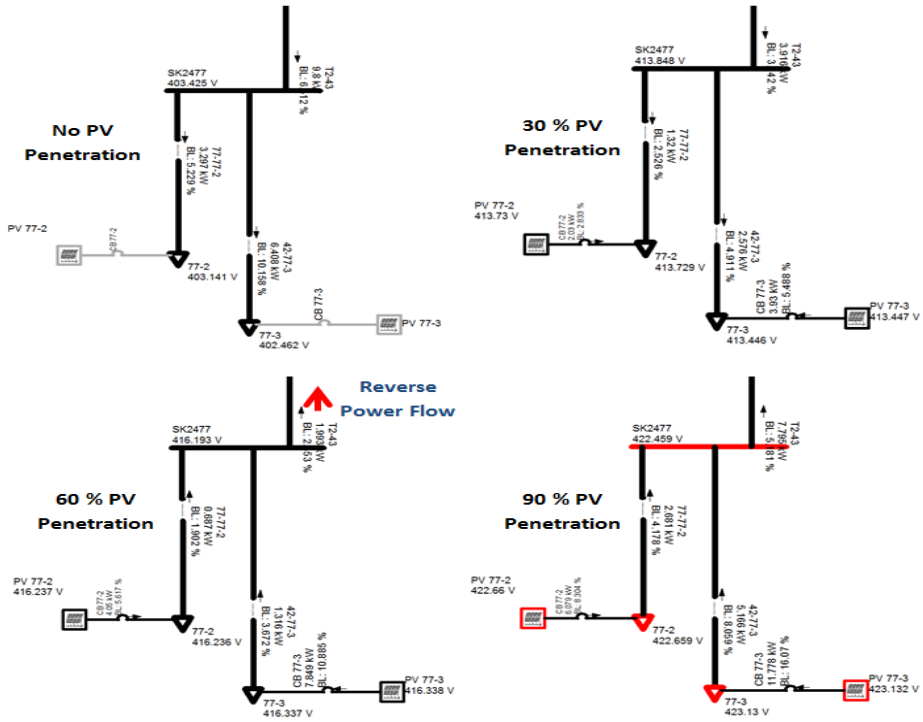

Figure 4.27: Grid Substation SK2477 at Different Penetration Levels

Figure 4.28 shows grid substation SK2477 at different Solar PV penetration levels in the grid. From this figure, at 60% and 90% penetration there were grid and system violations. In addition, scatter plots and power loss for the entire grid were plotted. These are shown in Figure 4.28 and Figure 4.29.

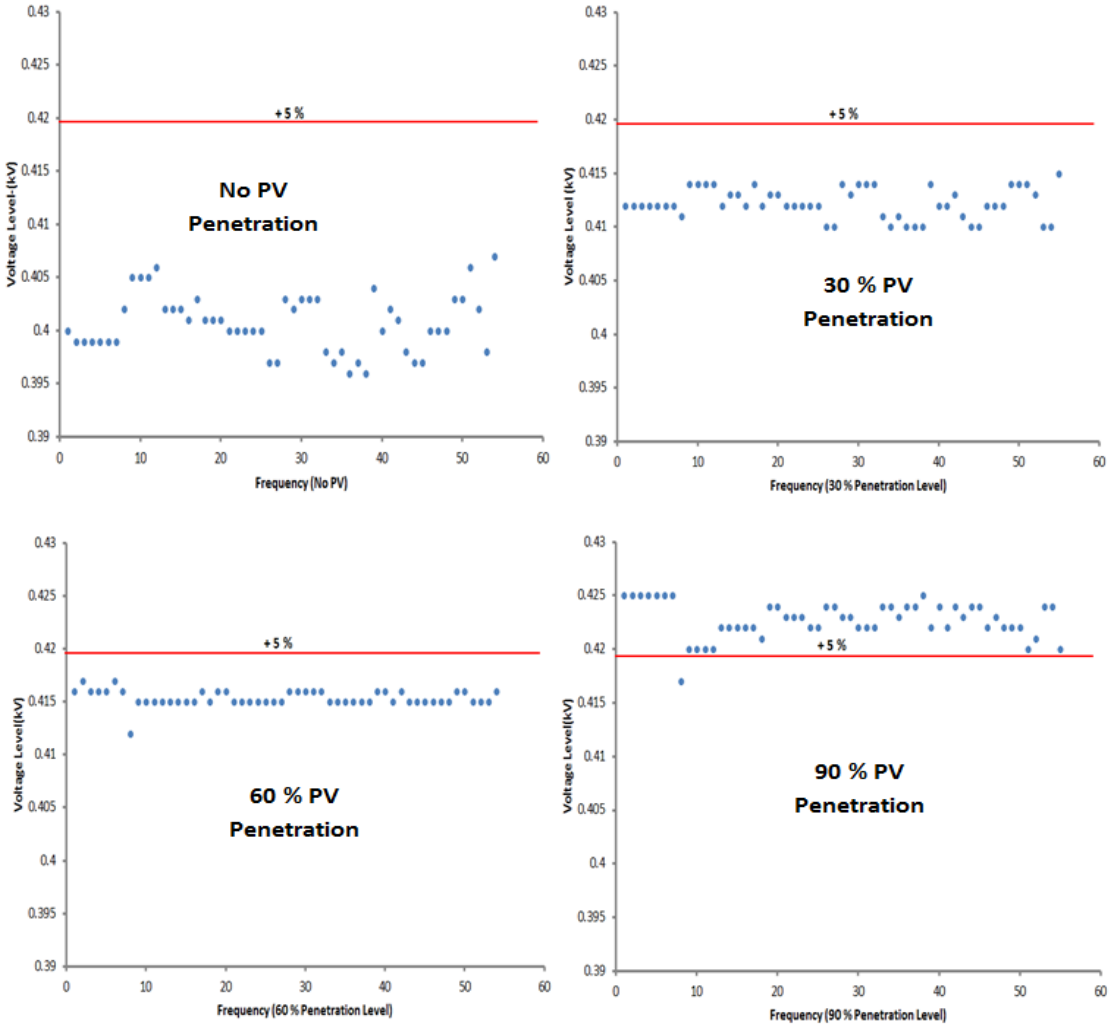

Figure 4.28: Mölndal Area 1 Grid Voltage Scatter Plots

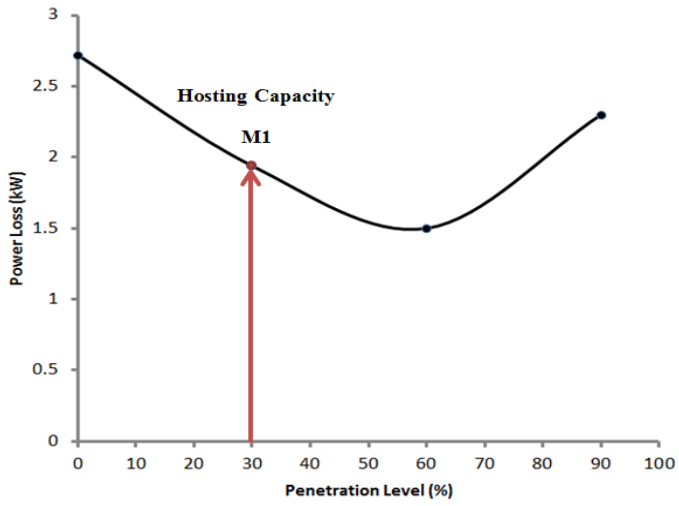

Figure 4.29: Mölndal Area 1 Grid Power Loss at Minimum Load Demand

According to the results obtained at minimum load consumption for the grid with maximum PV power production, the hosting capacity was determined. In terms of voltage level monitored for substation SK2477 and entire grid bus/loads voltages, at penetration level above 60% there were violations. At penetration level above 30%, there was reverse power flow. By considering line loading, losses, voltage level and profile, and reverse power flow for Mölndal area 1 grid (radial grid with unidirectional power flow), 30% penetration level was determined as the hosting capacity and is shown in Figure 4.29 as point M1.

4.4.2 Mölndal Area 2 Grid Hosting Capacity

In determination of the hosting capacity for Mölndal area grid 2, grid substation SK0807 and grid parameters were monitored. Additionally, the loads fed from substation SK0807, entire grid voltage level and power losses were monitored in order to determine the grid hosting capacity. Figure 4.30, Figure 4.31 and Figure 4.32 show the grid substation (SK0807) voltage level, grid voltage scatter plots and power loss plot at different penetration levels.

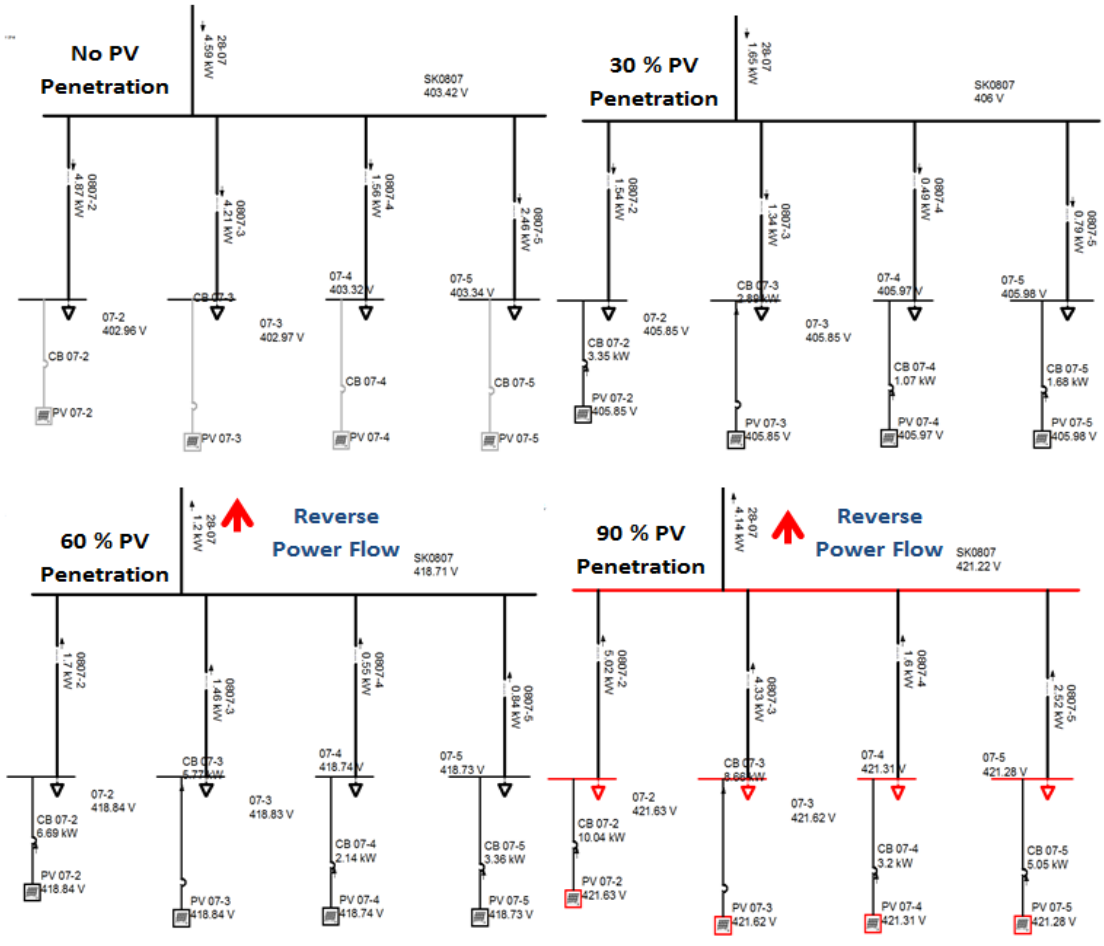

Figure 4.30: Grid Substation SK0807 at Different Penetration Levels

Figure 4.30 show the voltage levels at different solar PV power penetration levels for the loads and grid substation SK0807. At a penetration level of 90%, there was violation of bus voltage level. In terms of voltage level, the hosting capacity of the grid would be 60% penetration level. At 60% and 90% penetration, there was an indication of reverse power flow. However, this is not a challenge for a meshed distribution grid like Mölndal area 2. This is because there is multi-directional power flow in such a grid. It only becomes a challenge if and when a meshed grid is operated in radial (unidirectional power flow) [11].

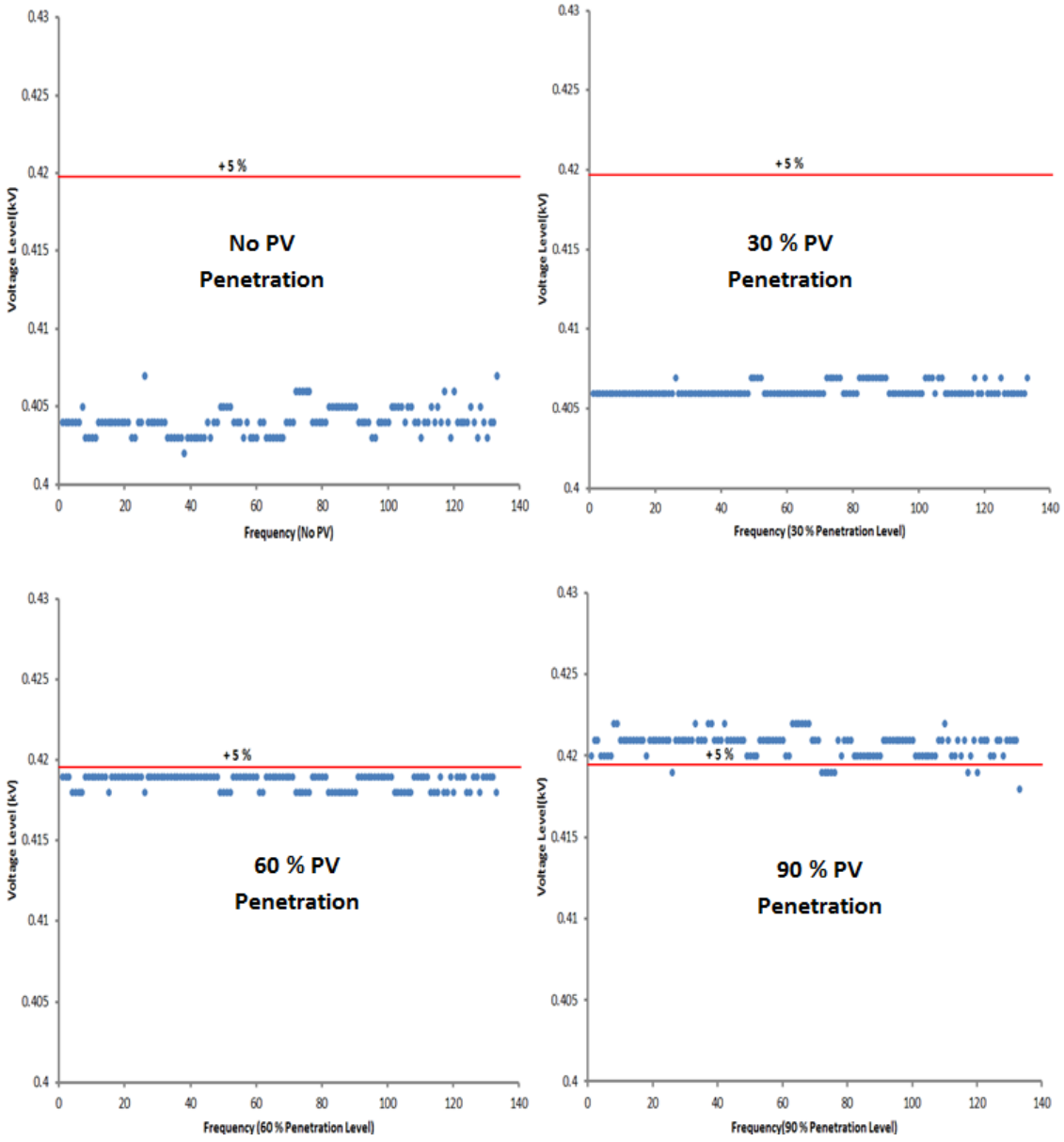

Figure 4.31: Mölndal Area 2 Grid Voltage Scatter Plots

In addition to grid substation SK0807 parameter results, Figure 4.31 shows voltage scatter plots for the entire grid at different substations. The plots indicate a hosting capacity of 60% penetration for the grid.

In addition to voltage level indication of a possible hosting capacity, Figure 4.32 was plotted. This figure presents the grid power loss at different penetration levels. According to Figure 4.32, the grid power loss decrease with increase in penetration level up to a particular level. At this level, the grid power loss starts to increase with increase in penetration level.

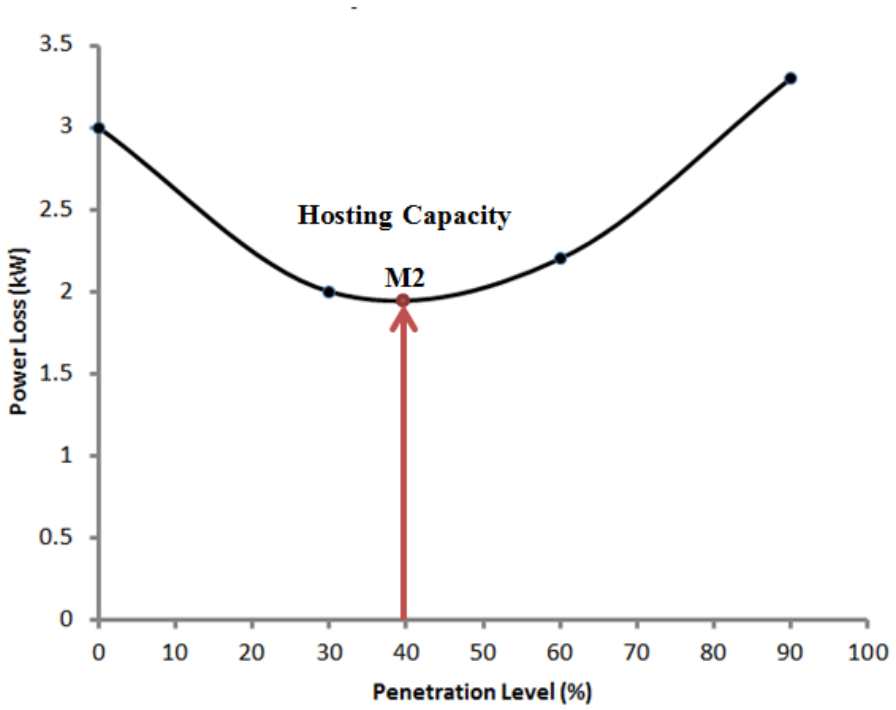

Figure 4.32: Mölndal Area 2 Grid Power Loss at Minimum Load Demand

In summary and considering the observations made from Figure 4.30, Figure 4.31 and Figure 4.32, the hosting capacity for Mölndal area grid 2 is 40% penetration. The hosting capacity for the grid is denoted by M2 in Figure 4.32. This penetration level satisfy the results conditions for voltage level, grid voltage scatter plot and grid power loss criteria for the grid.

4.4.3 Orust Area Grid Hosting Capacity

The hosting capacity for Orust area was determined similar to the method adopted for Mölndal areas distribution grids. An addition criterion of line loading was used to determine the hosting capacity. This was because in this area, the solar PV power is was to be owned by the utility company (Orust Energy) and not customer owned rooftop solar PV power in Mölndal. In addition, Solar PV power to be coupled/connected to substation within area of installation.

From simulations of the low grid load demand in Paladin designbase, the voltage level, line loading, grid voltage scatter plots and grid power loss were obtained. In these simulations, substation 30010 and 35010 were monitored in addition to the grid parameters (voltage and power loss). These represent substations where the solar PV power to be installed in Orust

area by Orust energy will be coupled (Månsemyr and Sörbo areas). Figure 4.33 shows the simulation results for these areas.

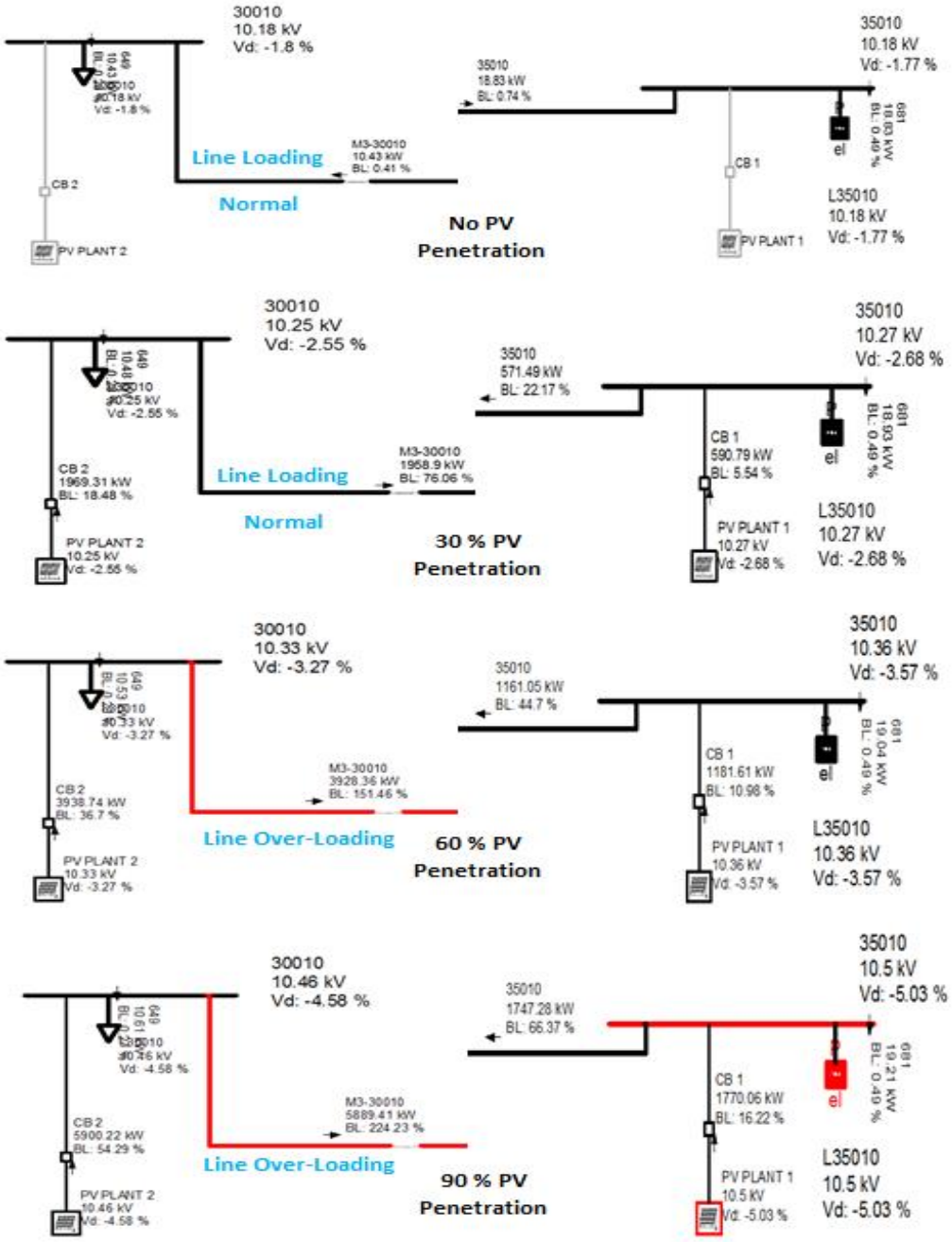

Figure 4.33: Substation 30010 and 35010 at Different Penetration Levels

Figure 4.33 presents the voltage levels and line loading at different solar PV penetration levels at Månsemyr (30010) and Sörbo (35010) area. From these results, the hosting capacity would be 30 percent in terms of line loading and 60 percent in terms of voltage level. There

was line loading violation for feeder cable to substation 30010 at 60 percent penetration and voltage level violation for substation 35010 at 90 percent penetration.

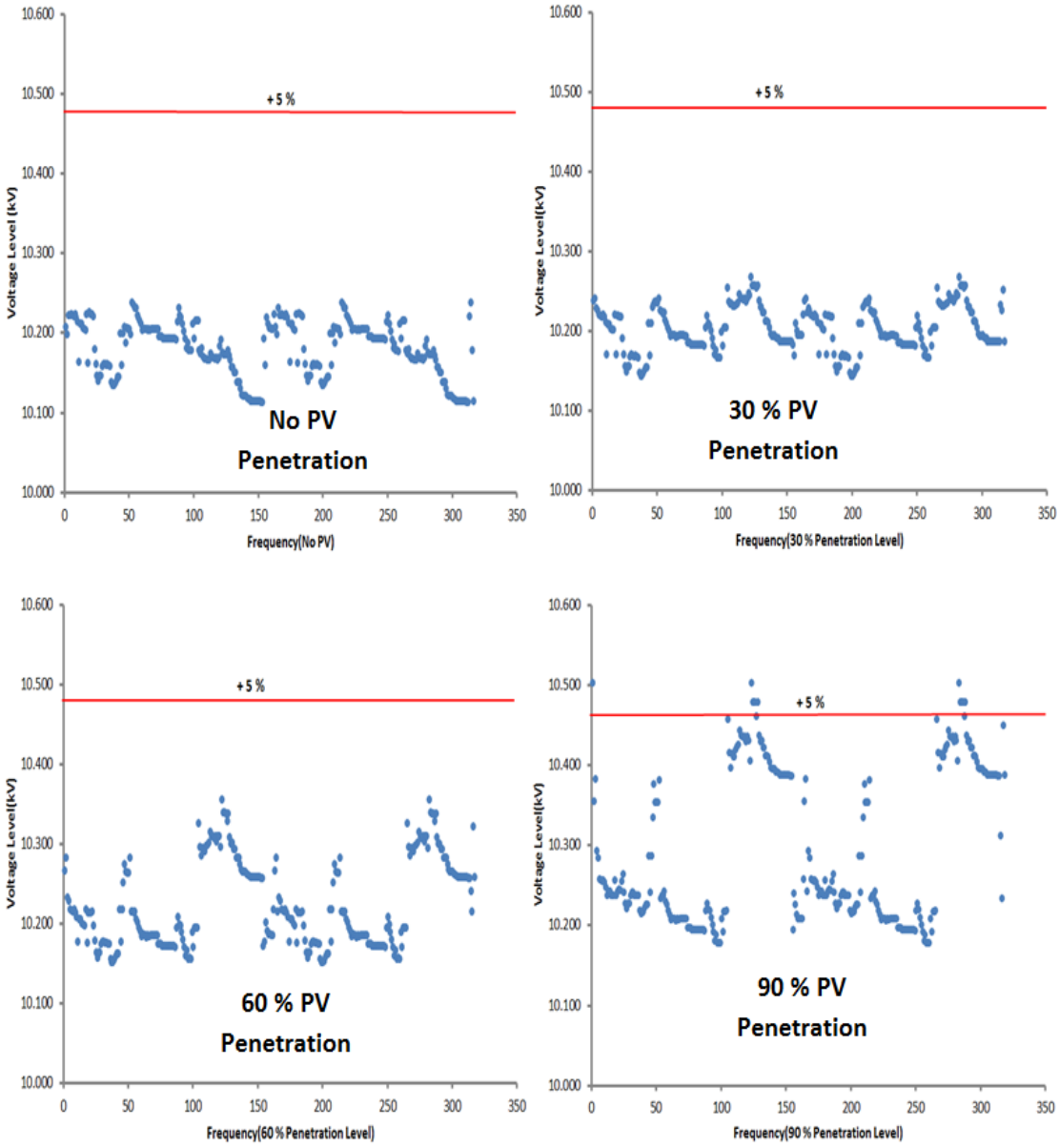

Figure 4.34: Orust Grid Voltage Scatter Plots

In addition to voltage violation at substation 35010 and line loading violation feeder cable to substation 30010, Figure 4.34 presents results of grid voltage levels in form scatter plots. From the scatter plots, there were grid voltage violations at 90% penetration. This was indication of a 60% penetration in terms of grid voltage levels at different solar PV power penetration levels.

In addition, grid power loss at different penetration levels were obtained and plotted. The grid power loss against penetration levels are shown in Figure 4.35.

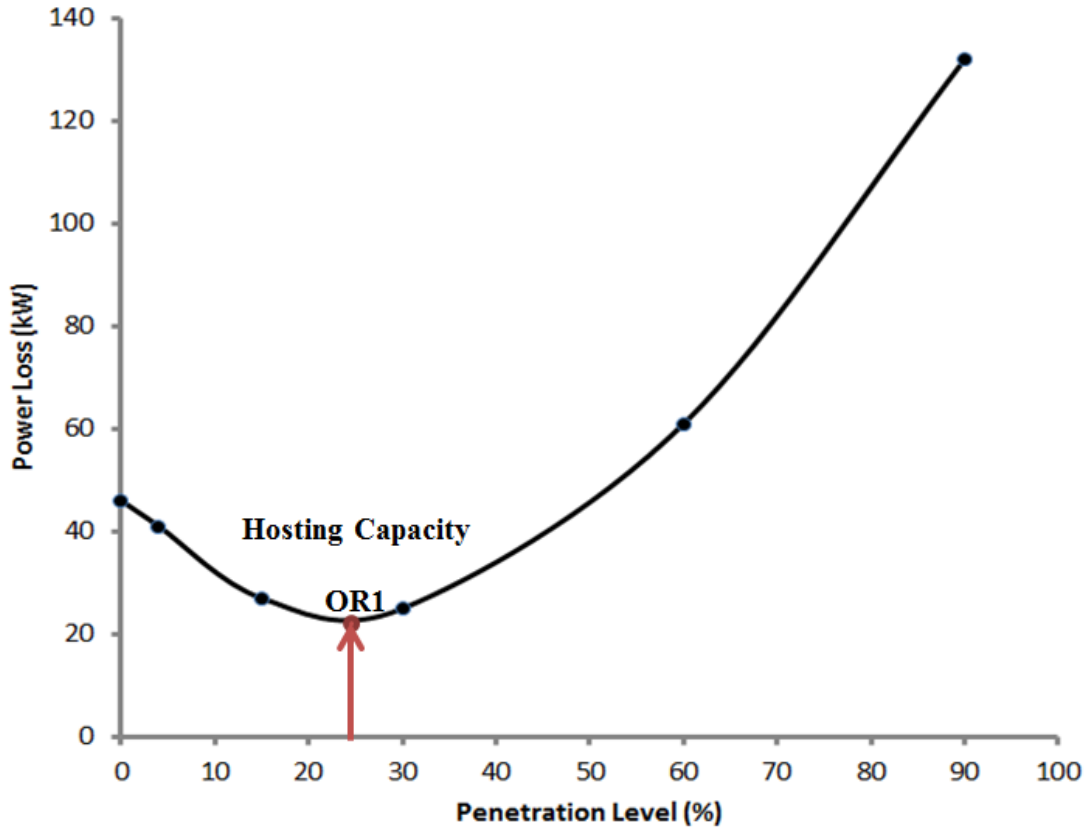

Figure 4.35: Orust Grid Power Loss at Minimum Load Demand

By monitoring the voltage levels, line loading and grid power loss at different penetrations presented in Figure 4.33, Figure 4.34 and Figure 4.35, the grid hosting capacity that conforms to the parameters monitored was 25 percent penetration. This point is shown in Figure 4.35 as OR1. At this point, the violations are avoided and the grid has minimal grid power loss. Therefore, this was the hosting capacity for Orust distribution grid.

4.5 Impacts Mitigation and Hosting Capacity Increase Solutions

From the scenario simulations conducted for the grids, these being system with no solar PV penetration, with solar PV penetration at maximum production/maximum load demand and with solar PV penetration at maximum production/minimum load demand, impacts to grid parameters were identified in Section 4.2 and the hosting capacity determined in Section 4.4.

4.5.1 Solutions at Maximum Load Demand

At maximum PV production and maximum load demand, the integration of solar PV power caused increase to the voltage level/profile, reduction to voltage drop, reduction in system losses and increase again at some penetration level, line loading changes (increase and decrease) and improvements to steady state voltage stability of the grids under study. At different penetration levels of 0%, 30%, 60% and 90% (4 and 15 % inclusive for Orust

energy), the only violation that was observed was overloading of the feeder cable for Orust distribution grid. The other grid system parameters were within acceptable limits. This entailed a steady state penetration level of 90% would be allowable for Mölndal energy grids at maximum load demand. While for Orust energy distribution grid, a steady state penetration level of 30% would be allowed.

4.5.1.1 Line Overloading

To solve the problem of overloading and increasing the penetration level for Orust energy distribution grid, an upgrade of the feeder cable would be needed. Additionally, distributing installation of solar PV plant as opposed to concentrating in the area planned by the utility company would solve the overloading problem and increase the maximum penetration level at maximum load demand. The solutions to overloading problem were implemented in the software environment of Paladin Designbase and Figure 4.36 shows the results obtained.

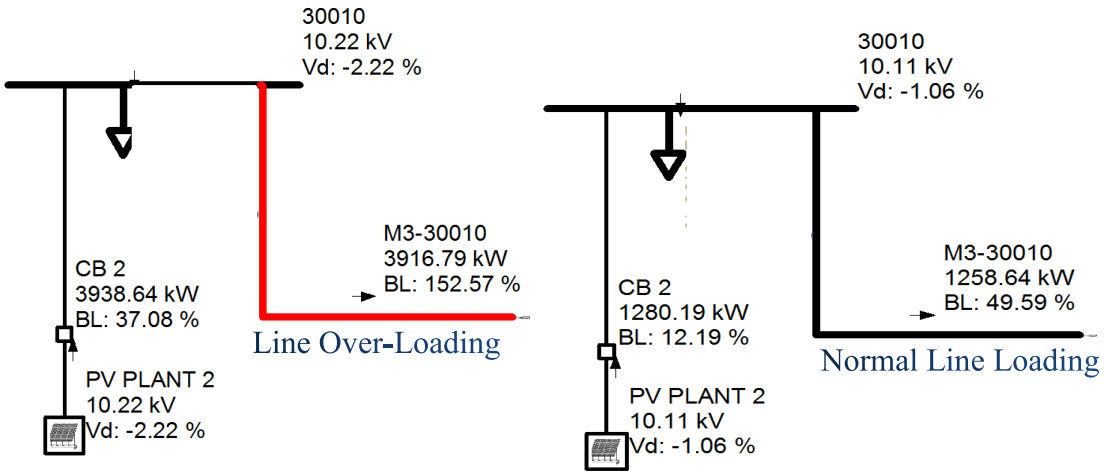

Figure 4.36: Line Over-Loading Solution at 60% Penetration Level-Orust

The proposed solution (feeder cable upgrade and distributing the solar PV plants share) to the impact of solar PV power integration observed for the distribution grid for Orust energy solved the problem, increased the penetration level above 60% and lowered the bus voltage level at substation 30010 from 10.22 kV to 10.11 kV.

4.5.2 Solutions at Minimum Load Demand

With reference to Section 4.4 (hosting capacity determination), this scenario condition was used to determine the hosting capacity. In [12], it is stated that there is/should be a strong correlation between minimum grid consumption and maximum penetration level (hosting capacity) that can be allowed in a grid. This presents the worst operational scenario of the distribution grids. As it was presented in Section 4.4, the minimum load demand/consumption with maximum PV production was used to determining the hosting capacity of the distribution grids. The interaction produced system parameter violations (voltage, line loading and reverse power flow) and different behaviour in system losses.

The system violations that resulted from the scenario condition simulations and resulted in determination of the hosting capacity when solved would result steady state operations within system limits and can allow more solar PV power to be added. This leads to an increase in the hosting capacity of the distribution grids.

In order to curb the problems that resulted in Section 4.4 and increase the hosting capacity of the distribution grids, the following solutions in isolation or combination with others have been proposed and these are [1], [2], [7] , [12];

Reactor Installation and Tap Changer Operation

The installation of a reactor and tap changer operation for the main transformer results in reactive power consumption at the bus and the voltage at the bus is controlled. These solutions were implemented for Mölndal area grids.

For Mölndal distribution grid area 1, to increase the hosting capacity and control the voltage level, a reactor was installed at grid substation SK2477 and results obtained from this simulation are shown in Table 4.24

Table 4.24: Results without and with Mitigation-Mölndal Area 1 Substation SK2477

Voltage Level with 90% PV	Without Mitigation	With Mitigation
SK2477 Bus	422.46 V	418.33 V
Load 77-2	422.66 V	418.54 V

Table 4.24 show results for two scenarios at 90% penetration level for grid substation SK2477 and its load 77-2. With installation of the reactor, the voltage level was controlled to be within normal operation limits (from 422.5 V to 418.3 V). Additionally, the PV plants could be set to consume reactive power and control the voltage level. However, this solution should only be used if there is really a need as it increases the losses of the grid due to the resistive component of the reactor and an increase in loading of the line due to reactive power consumption. Consequently, for this distribution grid, there is additional need of grid reconfiguration to handle reverse power flow problem that makes it have a low penetration level as compared to a meshed grid configuration that has multi-directional power flow.

For the meshed distribution grid of Mölndal energy area 2, a reactor was installed at grid substation SK0807 to control the voltage level and increase the hosting capacity. The solution was added at 90 percent penetration level for substation SK0807. Table 4.25 shows obtained results without and with a reactor added to the substation.

Table 4.25: Results with and without Mitigation-Mölndal Area 2 Substation SK0807

Voltage Level with 90% PV	Without Mitigation	With Mitigation
SK0807 Bus	421.22 V	418.51 V
Load 07-2	422.63 V	418.92 V
Load 07-3	422.62 V	418.91 V
Load 07-4	422.31 V	418.60 V
Load 07-5	422.28 V	418.57 V

The voltage level for the bus at grid substation SK0807 was controlled from 421.22 V to 418.5 V by installation of a reactor at the substation SK0807. In the process, the substation remained within operational limits with an integration of 90 percent penetration level at the substation.

Feeder Cable Upgrade and Distribution of Photovoltaics

For the distribution grid of Orust energy, at 60% and 90% penetration levels, the proposed solution of tap changer, feeder cable upgrade and distribution of the solar PV power plants were implemented in Paladin designbase. With distribution solar PV power plants for Orust energy distribution grid, there was no overloading of feeder cables to substation of common coupling. Additionally, Figure 4.37 shows the grid scatter voltage plots at 90% penetration levels. These shows for planned installation (concentrated) and proposed solution (distributed) to increasing the grid hosting capacity.

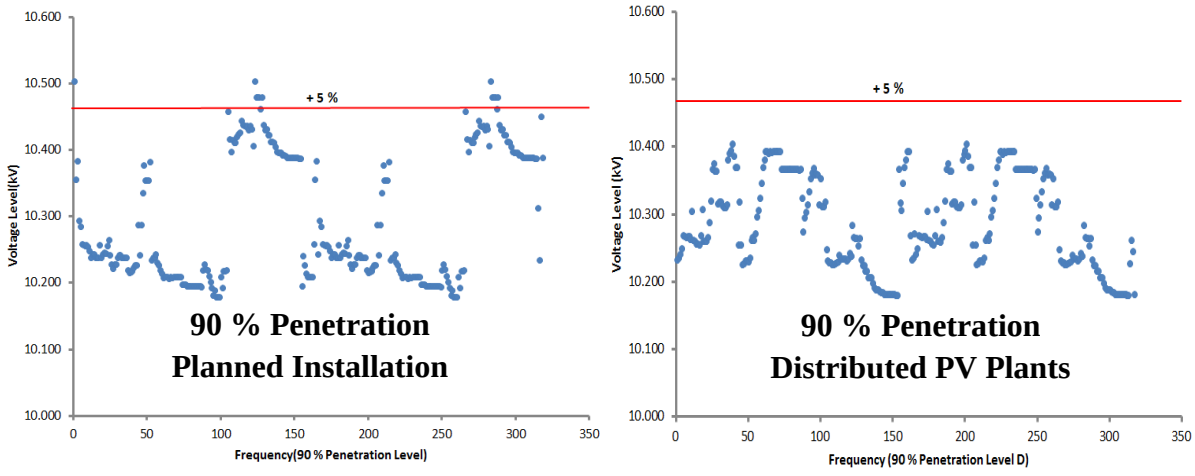

Figure 4.37: Orust Grid Voltage Scatter Plots at 90% Penetration

According to results obtained in Figure 4.37 for planned PV power installation for the grid and the proposed solution with distributed PV power plants, the grid voltage level was controlled within operational limits. With the proposed solutions implemented, the grid can operate at a penetration of 90% with voltage level consideration only. In addition to the voltage level scatter plots, the grid power loss was plotted for the planned installation and proposed solutions at all the penetration levels. Figure 4.40 shows the two plots of power loss.

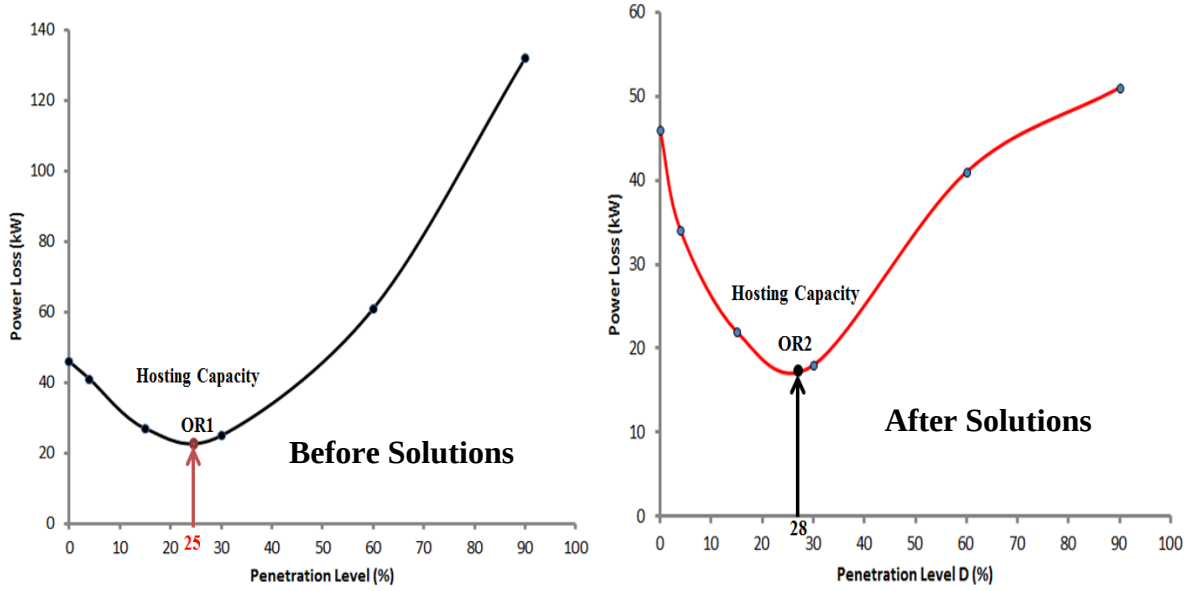

Figure 4.38: Orust Grid Power Loss-Concentrated and Distributed PV Plants

According Figure 4.38 results, there was grid loss reduction by shifting from the planned installation to distributed PV power plants. In addition, by considering the voltage level, line loading and power loss for the grid, there was a shift of the grid hosting capacity from point OR1 to point OR2 as shown in Figure 4.38. The hosting capacity of the grid increased from 25 to 28 percent penetration level by implementation of transformer tap changer control, feeder cable upgrade and distribution of the solar PV power plants on the distribution grid.

Other Possible Solutions

Other possible solutions that could mitigate problems at minimum load demand but were not implemented are [2], [12]:

- Reactive power/voltage control by use of either series or shunt flexible alternating current transmission systems (FACTS) devices in distribution grids (SVC or D-STATCOM).
- Use of PV inverter controls and advanced additional custom control functions for control of voltage, active and reactive power in unison with grid demand pattern.

- Distribution grid re-organisation/re-arrangement. That is conversion of a radial grid to a meshed or loop distribution grid to increase hosting capacity and control voltage levels.

These possible solutions work on the principle of reactive power and voltage control in the grid. For example, SVC or STACOM has the capability of either consuming or producing reactive power in order to control the voltage of the grid under normal operating conditions or under a faulty condition [15]. Use of advanced inverter control of voltage, active and reactive power could solve the impacts under different operating conditions for the PV plant [12], [26]. This could be used in operation with other plants.

In summary, grid re-organisation which is possible for small grids could solve the problem of reverse power flow in a radial grid. This could be done by conversion of the radial grid to a meshed or loop system [11].

5 Conclusions and Future Work

Having studied the impacts of solar PV power integration to an existing grid with focus on the distribution grids from Mölndal and Orust energy utility companies, this chapter presents conclusions and some work that can be done in the future to comprehend this study.

5.1 Conclusions

From the study conducted on the distribution grids to determine the impacts of solar PV power integration, the following conclusions were formulated for the given grid data by Orust and Mölndal energy companies:

- The integration of solar PV power to the distribution grids caused an increase in voltage level and voltage profile, a decrease in voltage drop and a decrease in grid losses for the grids. Additionally, the integration improved the steady state voltage stability. For line loading, two conclusions resulted. With integration of rooftop solar PV power, the line loading of the main feeder cable of the grid substation and that of the load were decreased while for utility integrated solar PV power plant the line loading for the main feeder cable for the substation of coupling increased. With integrated PV at different penetration levels (0%, 30%, 60% and 90%), for Mölndal area 1 and 2 in Mölndal, voltage level and profile increased with increase in penetrations while there was a decrease in voltage drops and grid losses. The steady state voltage stability improved with increase in PV penetration levels for the grids under study (Mölndal and Orust grids). For Orust area distribution grid, the increase in PV penetration level in the area planned for installation by the utility company caused an increase in voltage level and profile. There was an increase in the loading of the main feeder cable while the grid losses showed mixed results. Initially, the grid losses decreased with increased penetration level up to a certain penetration level. At this penetration level, the losses increased with increase PV penetration. In addition, for radial distribution grid of Mölndal area 1 the increase in PV penetration level caused reverse power flow at 60% penetration level.
- The hosting capacities for the grids were determined. The hosting capacity for Mölndal area 1 distribution grid was 30% penetration level, 40% for Mölndal area 2 and 25% for Orust energy grid.
- To curb the impacts and increasing the hosting capacity, reactive power consumption, line feeder upgrade, distribution/optimal location of utility PV plants and grid voltage control solutions need to be implemented. These are use of reactors, OLTC, inverter control, feeder upgrade, SVC and D-STATCOM. These were implemented and achieved the objective of mitigating the impacts and increasing the hosting capacity.

5.2 Future Work

The thesis attempted to establish the steady state impacts of integrating solar PV power to the distribution grids of Mölndal and Orust energy on voltage level, voltage profile, voltage drop,

losses, line loading and steady state voltage stability. In future, the study could be extended to investigate:

- Impacts on power quality/harmonic content, fault currents and grid protection system.
- Impacts on parameters studied in this thesis but with focus on variability of solar PV power production under varying climatic conditions (dynamics).
- Impacts on yearly grid losses and optimal PV plants location on Orust energy grid to minimise grid losses.

References

[1] J. Widen, E. Wäckelgård, J. Paatero and P. Lund, “Impacts of distributed photovoltaics on network voltages: Stochastic simulations of three Swedish low-voltage distribution grids,” *Electric power systems research,* vol. 80, pp. 1562-1571, 2010.

[2] T. Walla, J. Widen, J. Johansson and C. Bergerland, “Determining and Increasing the PV Hosting Capacity for Photovoltaics in the Swedish Distribution Grids,” in *European Photovoltaic Solar Energy Conference and Exhibition*, Frankfurt, 2012.

[3] A. Hoke, R. Butler, J. Hambrick and B. Kroposki, “Steady-State Analysis of Maximum Photovoltaic Penetration Levels on Typical Distribution Feeders,” *IEEE Transactions on Sustainable Energy,* vol. 4, no. 2, pp. 350 - 357, 2012.

[4] OGJ Editors,”BP Energy Outlook 2014,” BP, London, 2014.

[5] M. Suri, T. Cebecauer, A. Skoczek, R. Marais, U. Mushwana, J. Reinecke and R. Meyer, “Cloud Cover Impact on Photovoltaic Power Production in South Africa”, Stellenbosch University, 2014.

[6] M. Paulescu, E. Paulescu, P. Gravila and V. Badescu, "Weather Modeling and Forcasting of PV Systems Operation," London: Springer-Verlag, 2013.

[7] R. A. Shalwala, “PV Integration into Distribution Networks in Saudi Arabia”, PhD Thesis, University of Leicester, Leicester, 2012.

[8] R. Shaha, N. Mithulananthana, C. R. Bansalb and V. K. Ramachandaramurthy, “A review of key power system stability challenges for large-scale PV integration,” in *Renewable and Sustainable Energy Reviews-Elsevier*, vol. 41, pp. 1423-1436, 2015.

[9] F. Katiraei and J. R. Agüero, “Solar PV Integration Challenges,” *IEEE Power and Energy Magazine,* vol. 9, no. 3, pp. 62 - 71, 2011.

[10] J. Schoene, V. Zheglov, D. Houseman, J. C. Smith and A. Ellis, “Photovoltaics in Distribution Systems-Integration Issues and Simulation Challenges,” *in Power and Energy Society General Meeting (PES), IEEE,* 2013.

[11] H. L. Willis, "Power Distribution Planning Reference Book", Raleigh,North Carolina: CRC Press, 2004.

[12] M. Bollen och H. Fainan, "Integration of Distributed Generation in the Power System", Hoboken, New Jersey: John Wiley and Sons, Inc, 2011.

[13] J. Solanki, S. K. Solanki and V. Ramachandran, “Steady State Analysis of High Penetration PV on Utility Distribution Feeder,” in *IEEE Conference*, 2012.

[14] P. Kundur, "Power System Stability and Control", New York: McGraw-Hill, Inc., 1994 Edition.

[15] T. V. Cutsem and C. Vournas, Voltage Stability of Electric Power Systems, Kluwer Academic Publishers, 1998.

[16] Y. Xue, M. Manjrekar, C. Lin, M. Tamayo and J. N. Niang, “Voltage Stability and Sensitivity Analysis of Grid-Connected Photovoltaic Systems,” in *Power and Energy Society General Meeting*, San Diego,CA, 2011.

[17] Enernex, ”Integration Issues and Simulation Challenges of High Penetration PV,” Enernex, Knoxville, 2011.

[18] E. Pihl, “Concentrating Solar Power,” Energy Committee of Royal Swedish Academy of Sciences, Stockholm, 2009.

[19] R. Boylestad and L. Nashelsky, "Electronic Devices and Circuit Theory", New Jersey: Pearson Prentice Hall, 2009.

[20] K. Giannouloudis and E. Mulenga, “PV Systems and Applications,” ENM-095: Sustainable Power Production and Transportation Scientific Paper, Gothenburg, 2014.

[21] C. R. Nave, “The P-N Junction,” Physics World, 2012. [Online]. Available: http://hyperphysics.phy-astr.gsu.edu/hbase/solids/pnjun.html#c3.[Accessed 20 September 2014].

[22] S. Dubey, J. N. Sarvaiya and B. Seshadri, “Temperature Dependent Photovoltaic (PV) Efficiency and Its Effect on PV Production in the World,” *Energy Proceedings*, vol. 33, no. 1, pp. 331-321, 2012.

[23] H. Saadat, "Power System Analysis", New York-USA: PSA Publishing, 2010.

[24] T. Soubdhan, R. Emilion and R. Calif, "Classification of daily solar radiation distributions using a mixture of Dirichlet distributions", HAL-Aricle soumis `a Solar Energy, 2008.

[25] J. S. Stein, C. W. Hansen and M. J. Reno, "The Variability Index: A New and Novel Metric for Quantifying Irradiance and PV Output Variability,” Sandia National Laboratories, Albuquerque, 2012.

[26] L. Xu, “Case Studies of Experiences with Distributed Resource Interconnections on Distribution Systems,” in *IEEE PES General Meeting*, MD, 2014.

[27] J. Urbanetza, P. Brauna and R. Ruther, “Power Quality Analysis of Grid-Connected Solar PV Generators in Brazil,” in *Energy Conversion and Management-Elsevier*, 2012.

[28] Power Analytics Corporation, “*Paladin Designbase 3.0 Software User Manual*”, 2012.

[29] NEPLAN AG,”*NEPLAN Software Help Topics User Manual*”, Switzerland 2014

[30] www.google.se/maps

[31] www.eniro.se

[32] www.pvsyst.com/en

[33] www.poweranalytics.com

[34] www.neplan.ch

[35] Lecture no.8 in, “SPPT (part 1 and 2),” Chalmers University of Technology, 2014.

APPENDIX A Grid Areas and Circuit Diagrams

Figure A.1 : Ellös Area-Orust [30]

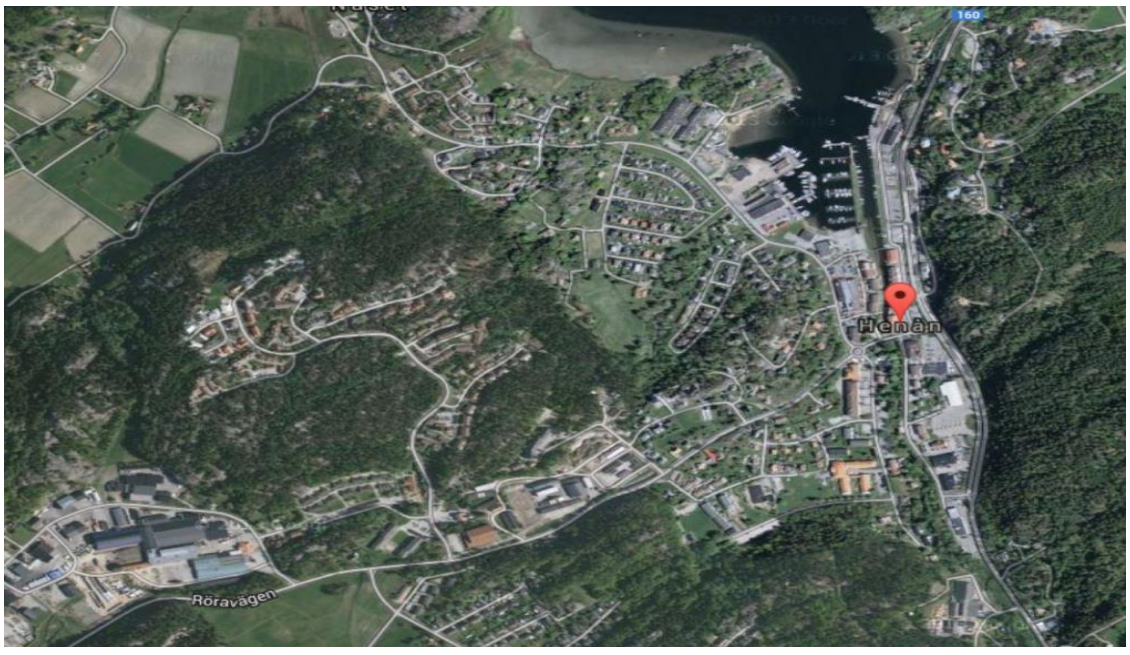

Figure A.2: Henån Area-Orust [30]

Figure A.3: Hälleviksstrand Area-Orust [30]

Figure A.4: Mollösund Area-Orust [30]

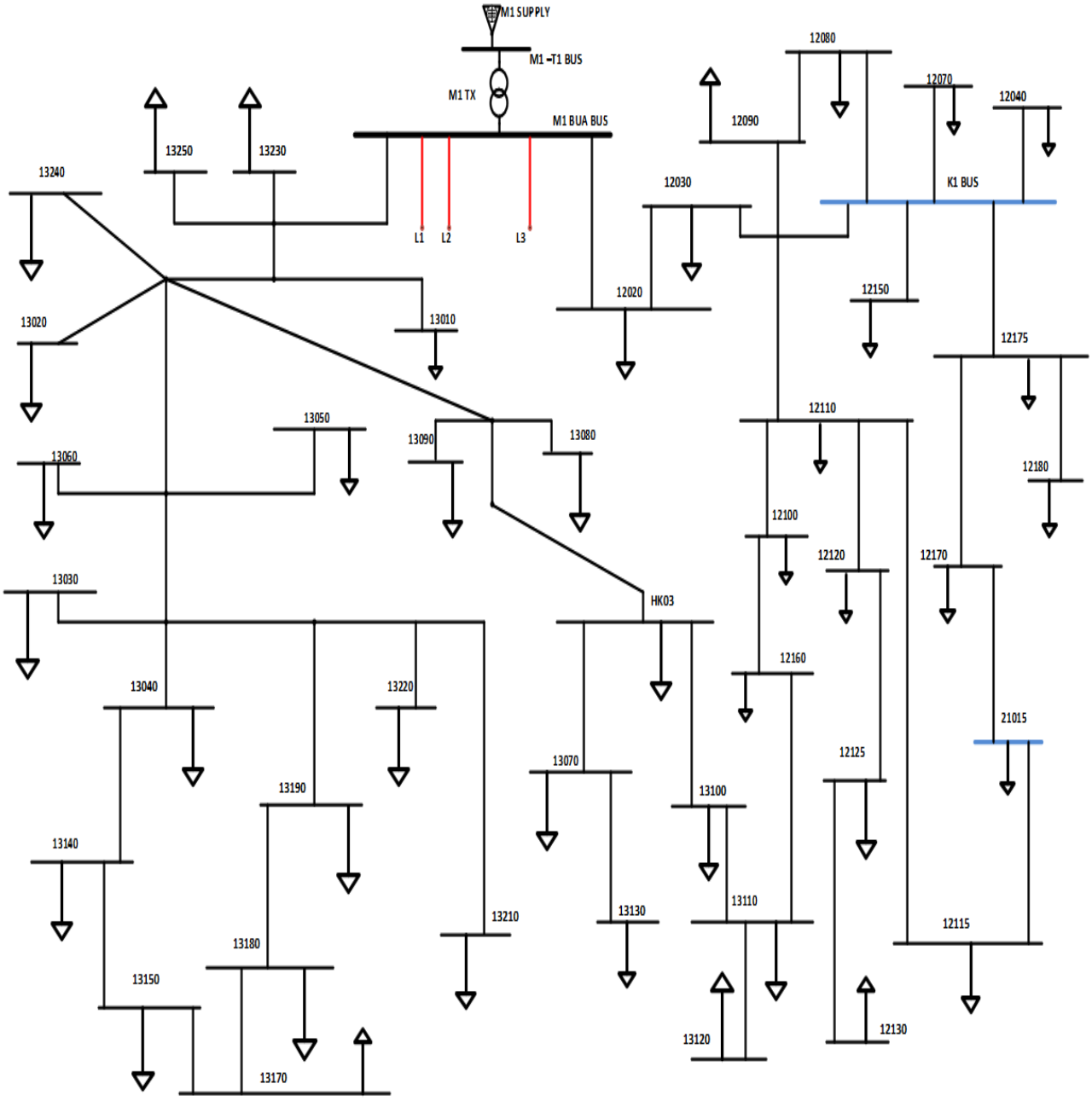

Figure A.5: Orust Grid 1

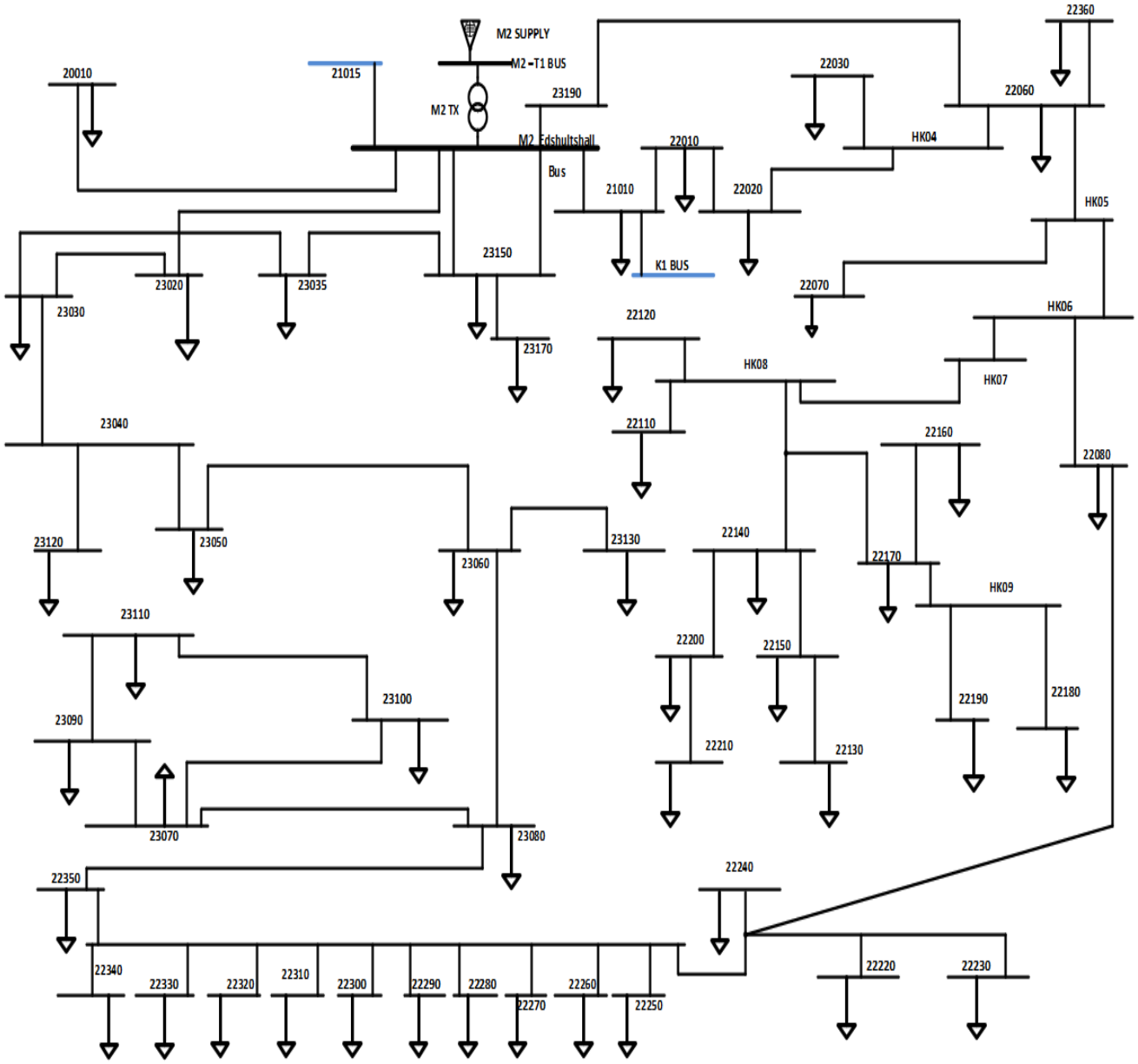

Figure A.6: Orust Grid 2

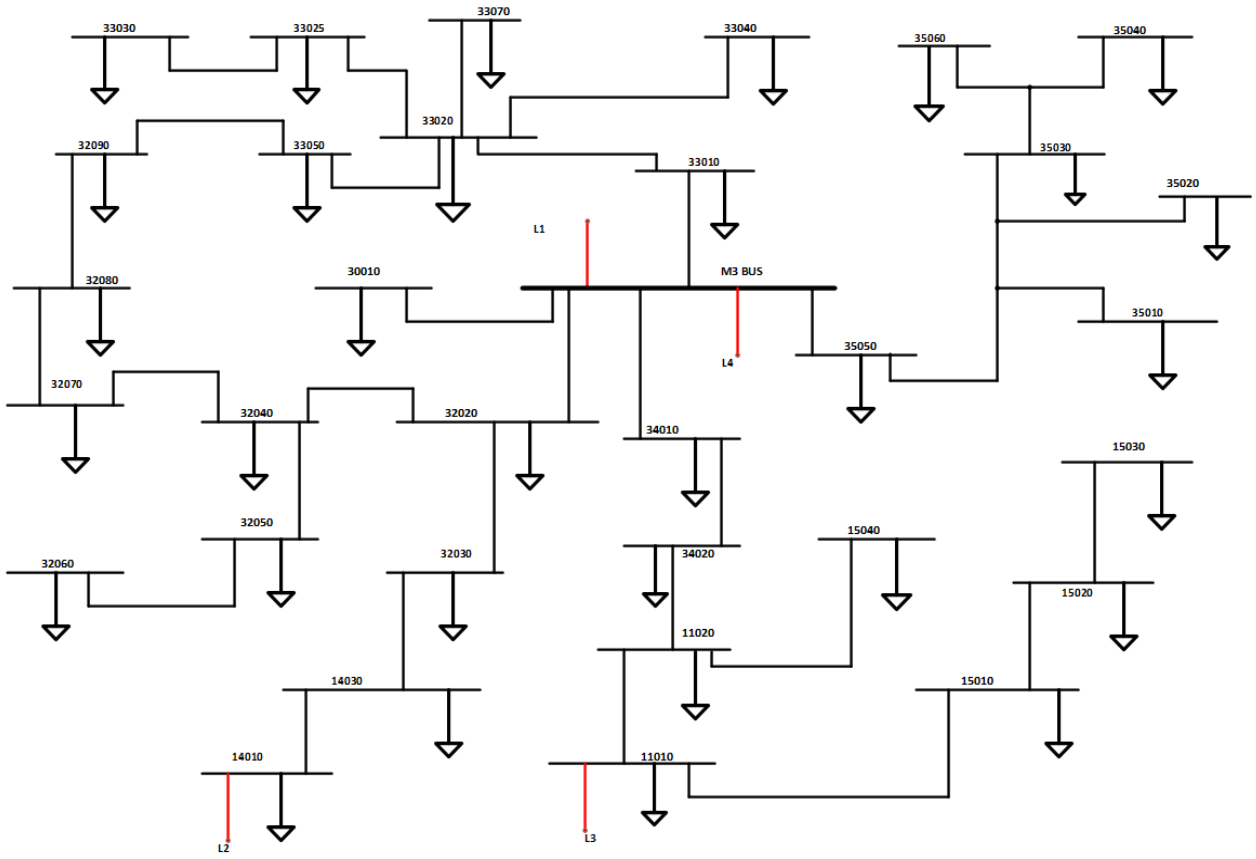

Figure A.7: Orust Grid 3

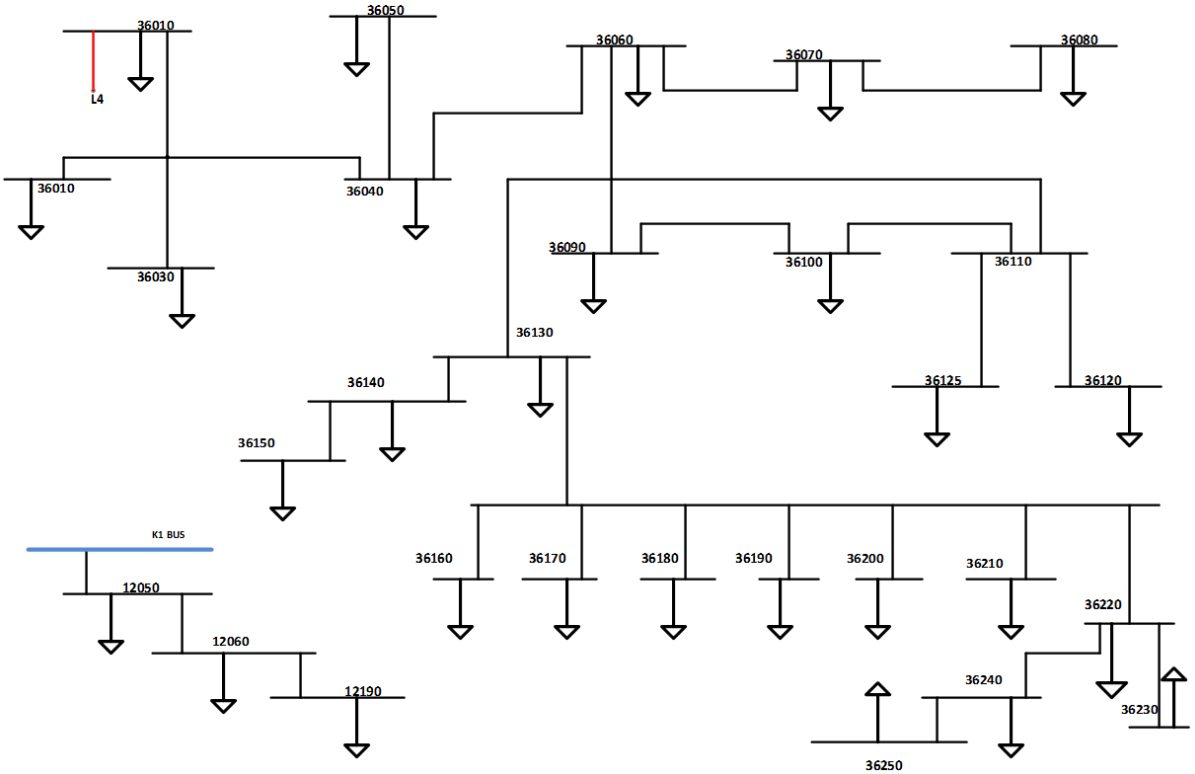

Figure A.8: Orust Grid 4

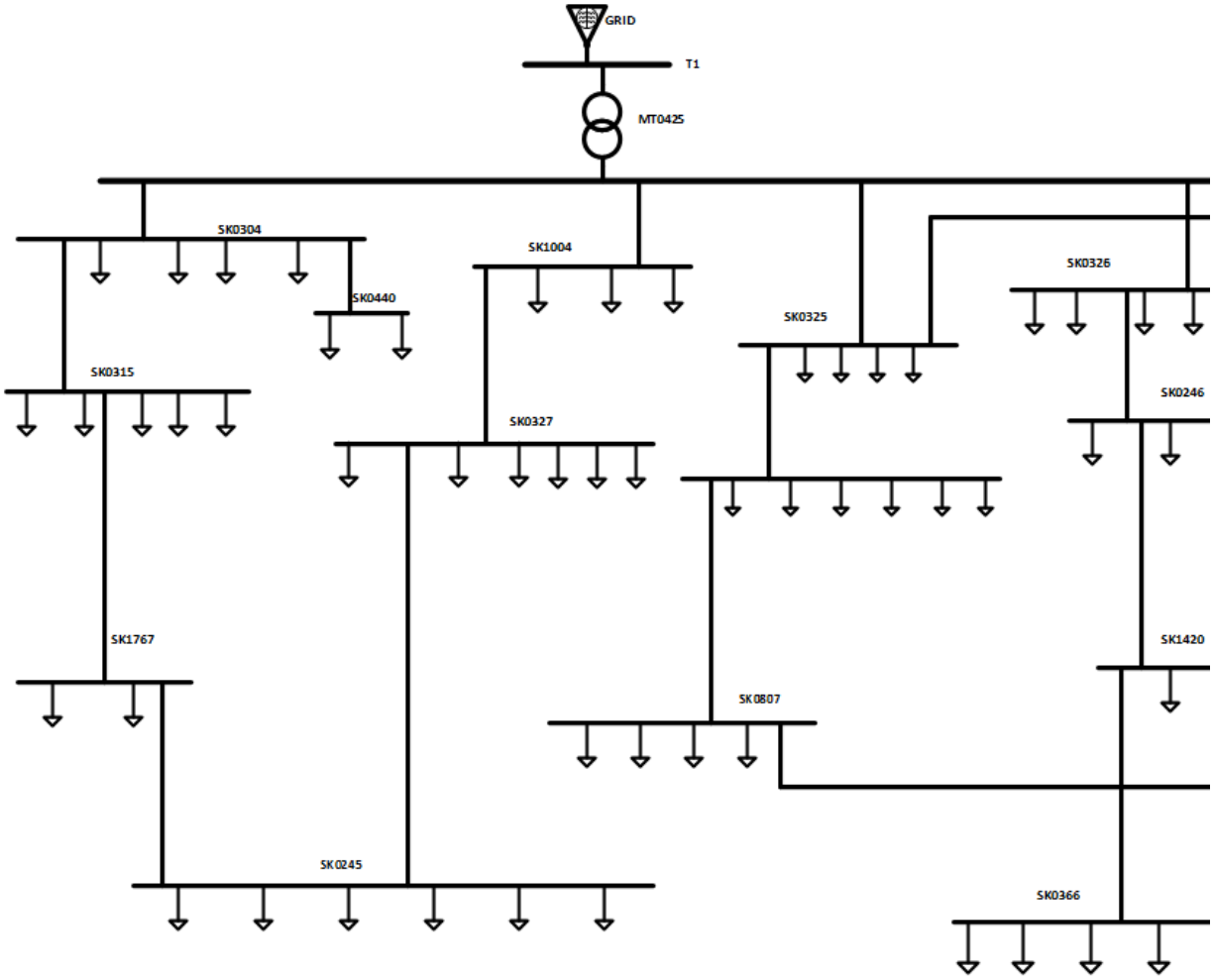

Figure A.9: Mölndal Meshed Circuit Diagram (Paladin-pg1)

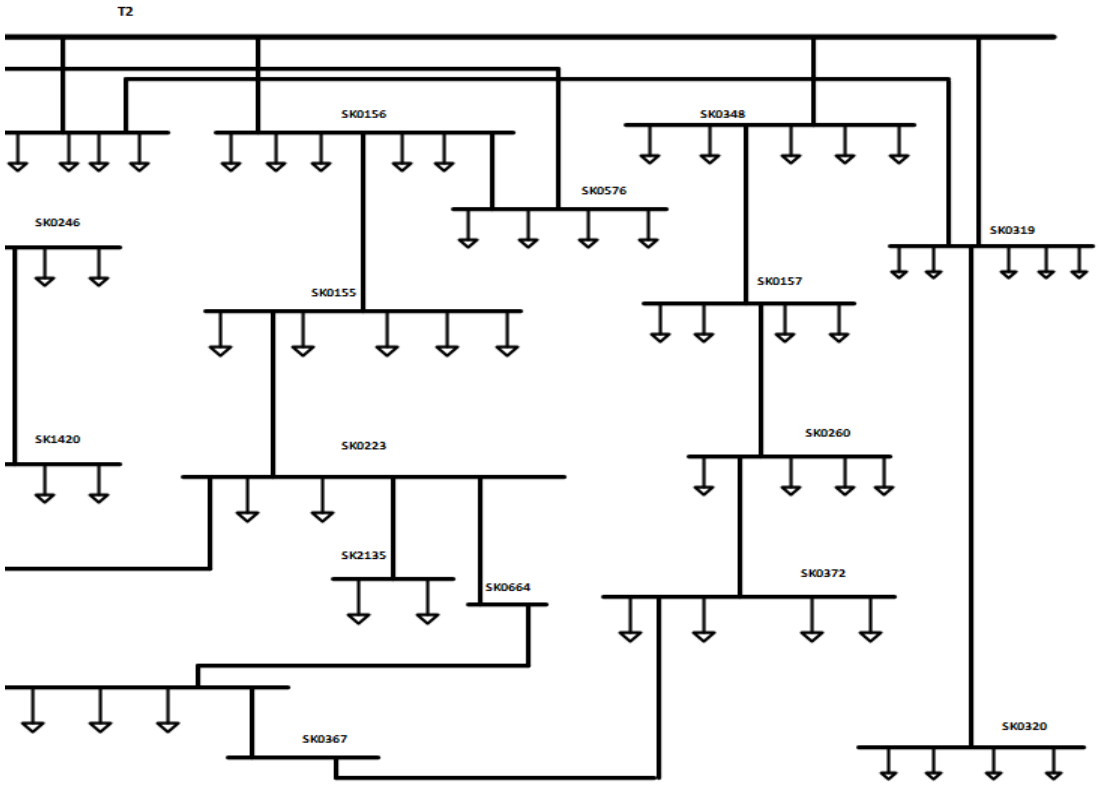

Figure A.10: Mölndal Meshed Circuit Diagram (Paladin pg2)

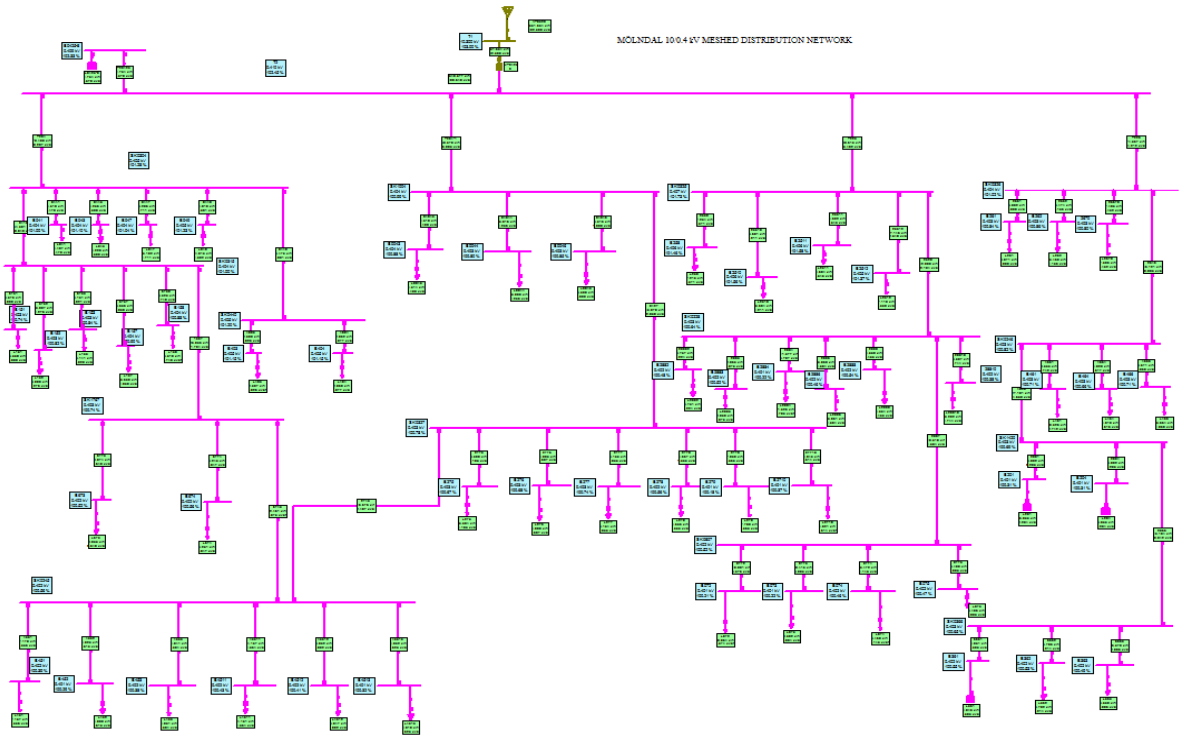

Figure A.11: Mölndal Meshed Circuit Diagram (NEPLAN pg1)

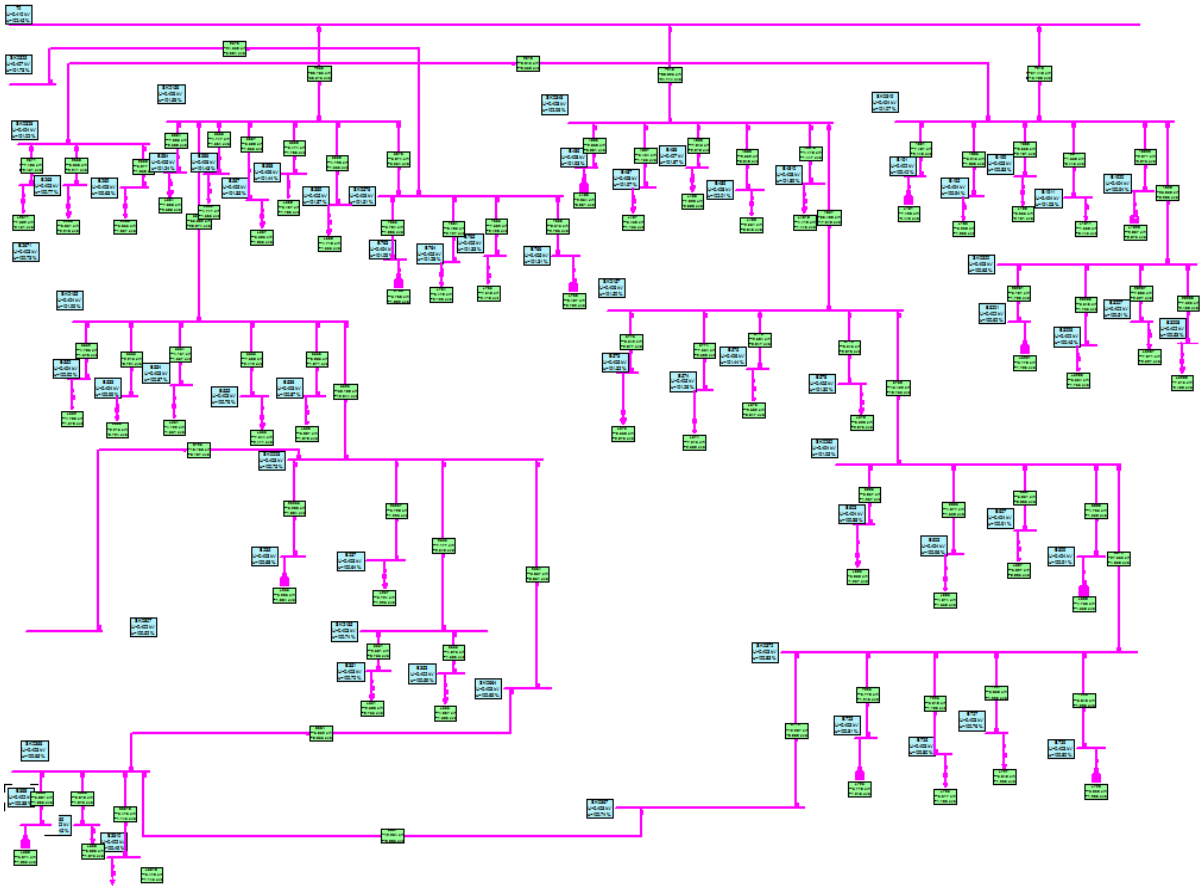

Figure A.12: Mölndal Meshed Circuit Diagram (NEPLAN pg2)

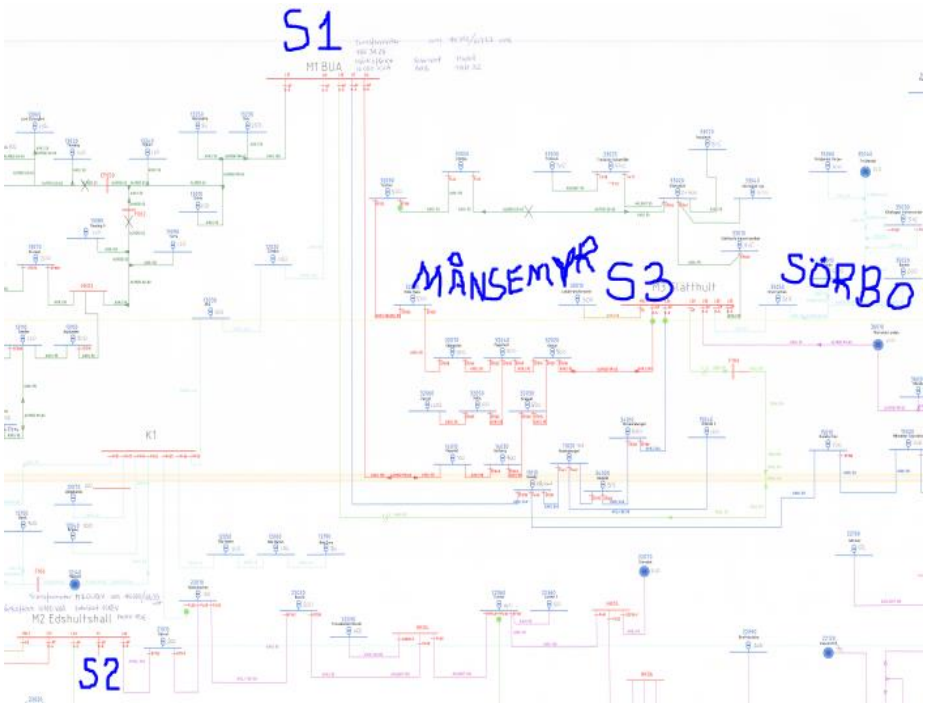

Figure A.13: Part of Orust Grid-As Built Circuit Diagram

APPENDIX B Grids Data

Table B.1: Mölndal Grid Data Area 1

MÖLNDAL AREA 1 SAMPLE DATA					
FROM	TO	LENGTH (m)	CABLE TYPE	X-AREA (m^2)	SUB-X-AREA
MT0546	LSKARV2695	16.00	N1XV	150	
LSKARV2695	SK2034	152.00	AKKJ	150	41
SK2034	SK2193	235.00	AKKJ	150	41
SK2193	2193-1	26.00	EKKJ	10	10
SK2193	2193-2	22.00	EKKJ	10	10
SK2193	SK2859	102.00	AKKJ	150	41
SK2859	SK2194	83.00	AKKJ	150	41
SK2194	2194-1	33.00	EKKJ	10	10
SK2194	SK2195	240.00	AKKJ	150	41
SK2195	2195-1	80.00	FKKJ	16	16
SK2194	2194-4	18.00	EKKJ	10	10
SK2859	2859-2	279.00	N1XE-5	16	
SK2859	2859-3	74.00	N1XE-5	16	
SK2193	2193-5	87.00	EKKJ	10	10
SK2034	SK2254	133.00	AKKJ	150	41
SK2254	SK2255	80.00	AKKJ	150	41
SK2255	2255-1	20.00	EKKJ	10	10
SK2255	2255-2	14.00	AKKJ	95	29
SK2254	SK2256	200.00	AKKJ	150	41

SK2256	2256-4	46.00	N1XE	10	
SK2256	2256-3	41.00	N1XE-5	10	
SK2254	2254-4	54.00	N1XV	10	
SK2034	2034-4	102.00	N1XE-5	10	
SK2034	2034-5	8.00	N1XE-5	10	
MT0546	L1745	125.00	AKKJ	50	15
L1745	L1743	90.00	ALUS	50	
L1743	SK2477	7.00	FKKJ	16	16
SK2477	2477-2	35.00	EKKJ	10	10
SK2477	LSKARV2502	7.00	EKKJ	10	10
LSKARV2502	L1742	54.00	ALUS	25	
L1742	2477-3	21.00	ALUS	25	
MT0546	SK0321	140.00	AKKJ	150	41
SK0321	0321-5	93.00	AKKJ-4	95	29
SK0321	SK2148	85.00	FKKJ	35	25
SK2148	2148-1	26.00	EKKJ	10	10
SK2148	SK0808	60.00	FKKJ	35	25
SK0808	0808-1	14.00	EKKJ	10	10
SK0808	0808-2	66.00	EKKJ	10	10
SK0808	0808-4	53.00	N1XE-5	10	
SK0808	0808-5	61.00	EKKJ	10	10
SK0808	0808-6	61.00	EKKJ	10	10

SK0808	0808-7	84.00	EKKJ	10	10
SK0808	0808-8	57.00	EKKJ	10	10
SK2148	2148-4	26.00	EKKJ	10	10
SK0321	L1746	30.00	FKKJ	16	16

Table B.2: Mölndal Grid Data Area 2

MÖLNDAL AREA 2 SAMPLE DATA					
FROM	TO	LENGTH (m)	CABLE TYPE	X-AREA (m^2)	SUB-X-AREA
SK0326	0326-1	23.00	EKKJ	10	10
MT0425	LSKARV1539	10.00	AKKJ	150	41
LSKARV1539	SK0319	175.00	FCJJ	70	35
SK0319	0319-1	76.00	ECJJ	10	10
SK0319	0319-20	40.00	ECJJ	10	10
SK0319	LSKARV1540	98.00	FCJJ	70	35
LSKARV1540	SK0320	2.00	FKKJ	70	35
SK0319	0319-5	36.00	N1XE-5	10	
SK0319	LSKARV1538	2.00	EKKJ	10	10
LSKARV1538	0319-9	32.00	ECJJ	10	10
SK0319	0319-11	30.00	EKKJ	10	10
MT0425	SK0156	190.00	AKKJ	240	72
SK0156	LSKARV1308	2.00	FKKJ	70	35
LSKARV1308	SK0576	63.00	FCJJ	70	35
SK0156	LSKARV1307	2.00	EKKJ	10	10

LSKARV1307	0156-4	38.00	ECJJ	10	10
SK0156	0156-6	24.00	ECJJ	10	10
SK0156	0156-7	33.00	ECJJ	10	10
SK0156	0156-8	19.00	ECJJ	10	10
SK0156	0156-9	35.00	ECJJ	10	10
SK0156	SK0155	45.00	FCJJ	70	35
SK0155	0155-2	53.00	FKKJ	16	16
SK0155	0155-3	37.00	ECJJ	10	10
SK0155	0155-4	45.00	ECJJ	10	10
SK0155	0155-5	31.00	EKKJ	10	10
SK0155	0155-6	43.00	FKKJ	16	16
SK0155	LSKARV1305	2.00	FKKJ	70	35
LSKARV1305	LSKARV1306	50.00	FCJJ	70	35
LSKARV1306	SK0223	2.00	FKKJ	70	35
SK0223	LSKARV2871	3.00	EKKJ	10	10
LSKARV2871	LSKARV2872	2.00	EKKJ	10	10
LSKARV2872	SK2135	7.00	EKKJ	10	10
SK2135	2135-1	16.00	EKKJ	10	10
SK2135	2135-3	27.00	EKKJ	10	10
SK0223	LSKARV1394	2.00	EKKJ	10	10
LSKARV1394	0223-5	19.00	ECJJ	10	10
SK0223	0223-7	36.00	EKKJ	10	10
SK0223	LSKARV1125	2.00	FKKJ	70	35
LSKARV1125	LSKARV1124	33.00	FCJJ	70	35
LSKARV1124	LSKARV1123	23.00	FCJJ	50	35

LSKARV1123	SK0053	2.00	FKKJ	70	35
SK0223	LSKARV1395	81.00	FCJJ	35	25
LSKARV1395	SK0664	2.00	FKKJ	35	16
MT0425	SK0304	160.00	AKKJ	240	72
SK0304	LSKARV1510	2.00	EKKJ	10	10
LSKARV1510	0304-1	53.00	ECJJ	10	10
SK0304	0304-3	37.00	EKKJ	10	10
SK0304	SK0440	86.00	FCJJ	70	35
SK0304	SK0315	54.00	AKKJ	240	72

Table B.3: Orust Grid Data

ORUST SAMPLE DATA					
FROM	TO	LENGTH (m)	CABLE TYPE	X-AREA (m^2)	SUB-X-AREA
M1	11010	1.170.00	AXKJ	240	12
11010	15010	1.004.00	AXCEL	50	12
15010	15020	983.00	AXCEL	50	12
15020	15030	357.00	AXKJ	50	12
11010	11020	760.00	AXKJ	240	12
11020	15040	741.00	AXLJ-SE	50	12
11020	34020	643.00	AXKJ	240	12
34020	34010	630.00	AXKJ	240	12
34010	M3	522.00	AXKJ	240	12
M1	OBJ_13754	600.00	AXKJ	150	12
OBJ_13754	12020	424.00	AXCEL	240	12

12020	12030	535.00	AXCEL	240	12
12030	K1	1.454.00	AXCEL	240	12
K1	3AE	187.00	AXKJ	95	12
3AE	OBJ_13218	135.00	AlMgSi	62	12
OBJ_13218	5U	41.00	AlMgSi	62	12
5U	OBJ_13210	241.00	AlMgSi	99	12
OBJ_13210	12080	61.00	Axclight-FLT	150	12
12080	OBJ_13210	61.00	Axclight-FLT	150	12
OBJ_13210	21F	832.00	AlMgSi	99	12
21F	12090	297.00	AXKJ	95	12
12090	12100	432.00	FCJJ	70	12
12100	OBJ_13647	1.384.00	AXKJ	50	12
OBJ_13647	HK02	1.647.00	AXKJ-SH	50	12
HK02	S100103	1.802.00	AXKJ-SH	50	12
S100103	12110	923.00	AXKJ-SH	50	12
M2	21015	1.076.00	AXKJ	150	12
21015	12170	882.00	AXKJ-SM	95	12
12170	12175	441.00	AXLJ-SE	95	12
12175	OBJ_11827	129.00	AXKJ	50	12
OBJ_11827	12180	173.00	AXLJ-SE	95	12
M2	S100106	455.00	AXCEL	240	12

S100106	21010	96.00	AXLJ-SE	240	12
21010	S100107	96.00	AXLJ-SE	240	12
S100107	22010	572.00	AXCEL	240	12
22010	S10006	1.114.00	AXLJ-SE	150	12
S10006	22020	560.00	AXKJ	95	12
22020	S100117	453.00	AXKJ	95	12
S100117	HK04	189.00	Axclight-FLT	150	12
HK04	22030	24.00	AXKJ	50	12
HK04	22060	1.093.00	Axclight-FLT	150	12
22060	S100112	267.00	AXKJ	95	12
S100112	HK05	565.00	Axclight-FLT	150	12
HK05	S100116	946.00	Axclight-FLT	150	12
S100116	HK06	51.00	Axclight-FLT	150	12

Table B.4: Solar PV Power Potential-Mölndal Area 1

Load	**Roof Top Area (m^2)**	**Solar PV Power Potential (kWp)**
2193-1	259.65	44
2193-2	1401.82	235
2194-1	314.26	53
2195-1	294.41	50

2194-4	103.93	16.5
2859-2	32.77	5.5
2859-3	45.63	7.7
2193-5	98.11	16
2255-1	225	41.8
2255-2	400	74
2254-4	97.39	16
2477-2	215	40
2477-3	417.22	77.5
0321-5	473	87
2148-1	202.21	37.5
0808-1	224.48	41.8
0808-2	214.06	40
0808-4	159.29	29.6
Load	**Roof Top Area (m^2)**	**Solar PV Power Potential (kWp)**
0808-5	97.65	16
0808-6	112.8	20.7
0808-7	144.34	26.8
0808-8	134.35	25
2148-4	203.93	37
2683-1	272.96	50
2683-2	161.28	29
2683-3	149.3	27.8
2811-3	229.3	42.7
2811-4	205.5	37

2811-5	228.8	42
2812-2	249.79	46.4
2812-3	195	36.3
2812-4	241.22	44.8
2812-5	260.57	48.5
MT0546-5	449.5	83.6

Table B.5: Solar PV Power Potential-Mölndal Area 2

Load	**Roof Top Area (m^2)**	**Solar PV Power Potential (kWp)**
0319-1	214.04	39.6
0319-5	93	17.4
0319-9	190.56	35.4
0319-11	39	7.3
0319-20	85.04	15.6
03120-1	149.04	27.8
03120-6	153.52	28.4
03120-7	203.56	37.8
03120-8	216.28	40.3
0156-4	225.33	41.8
0156-6	135.75	25
0156-7	160	29.9
0156-8	156.51	29
0156-9	135	25
0576-3	165.5	30.8

0576-4	185.23	34.5
0576-5	210.41	39
0576-6	243.36	45.1
0155-2	137.84	25.6
0155-3	63.62	11.6
0155-4	118.42	22
0155-5	211.15	39.3
0155-6	172.14	32
0223-5	94.52	17.4
0223-7	107.05	19.8
Load	**Roof Top Area (m^2)**	**Solar PV Power Potential (kWp)**
2135-1	66.21	12.2
2135-3	140	25.9
0304-1	129	24.1
0304-3	121.28	22.6
0304-7	149	27.8
0304-9	137.99	25.6
0440-3	72	13.4
0440-4	85	15.9
0315-1	182.58	33.9
0315-2	111.7	20.7
0315-3	176.29	32.6
0315-7	161.57	29.9
0315-8	152.81	28.4
1767-3	231.86	43

1767-4	179.14	33.2
0245-1	206	38.4
0245-2	141.34	26.2
0245-3	139.25	25.9
0245-11	119.58	22.3
0245-12	87.84	16.2
0245-13	141.86	26.2
0325-8	206.38	38.4
0325-10	105.32	19.5
0325-11	134.02	25
0325-12	203.78	37.8
0228-2	107.39	19.8
Load	**Roof Top Area (m^2)**	**Solar PV Power Potential (kWp)**
0228-3	85.13	15.9
0228-4	332.21	61.6
0228-6	114.14	21.4
0228-8	125.22	23.2
0228-10	152.44	28.4
0807-2	313.23	58.3
0807-3	270.45	50.3
0807-4	100	18.6
0807-5	157.89	29.3
0348-6	83.58	15.6
0348-7	97.94	18
0348-8	226.21	42.1

0348-9	72.6	13.4
0348-10	125.77	23.2
0157-3	181.25	33.5
0157-4	209.44	38.7
0157-5	74.2	13.7
0157-8	181.26	33.5
0260-3	109.88	20.1
0260-5	116.79	21.7
0260-7	86.99	15.9
0260-9	136.41	25.3
0372-3	108.67	20.1
0372-5	103.86	19.2
0372-7	110.54	20.4
0372-9	113.12	21
1004-3	129.58	24.1
Load	**Roof Top Area (m^2)**	**Solar PV Power Potential (kWp)**
1004-4	109.47	20.1
1004-5	158.29	29.3
0327-5	103.48	19.2
0327-6	140.79	25.9
0327-7	90.78	16.8
0327-8	133.94	24.7
0327-9	224.6	41.8
0327-10	141.72	26.2
0326-2	99.51	18.3

0326-1	174.24	32.3
0326-70	106.12	19.8
0326-71	106.12	19.8
0326-8	196.15	36.6
0326-9	171.23	31.5
0246-1	239.43	44.5
0246-4	141.57	26.2
0246-6	162.93	30.2
1420-1	200.23	37.2
1420-4	200.23	37.2
0366-1	139.52	25.9
0366-2	106.62	19.8
0366-3	183.15	34.2
0366-8	172.07	32
0366-9	172.97	32
0366-10	100	18.6
MT0425-8	50	9.2

Table B.6: Typical PV System Production-Mölndal Area 1

Mölndal Area 1

Monthly Hourly averages for E_Grid [kW]

	0H	1H	2H	3H	4H	5H	6H	7H	8H	9H	10H	11H	12H	13H	14H	15H	16H	17H	18H	19H	20H	21H	22H	23H
January	0.0	0.0	0.0	0.0	0.0	0.0	0.0	0.0	0.0	2.6	6.0	7.5	8.2	7.6	5.9	1.9	0.0	0.0	0.0	0.0	0.0	0.0	0.0	0.0
February	0.0	0.0	0.0	0.0	0.0	0.0	0.0	0.0	1.7	6.1	8.8	11.3	11.7	14.1	11.4	7.1	2.3	0.0	0.0	0.0	0.0	0.0	0.0	0.0
March	0.0	0.0	0.0	0.0	0.0	0.0	0.1	2.7	8.5	13.6	16.5	19.2	20.4	19.0	16.5	14.3	8.7	2.0	0.0	0.0	0.0	0.0	0.0	0.0
April	0.0	0.0	0.0	0.0	0.0	0.2	2.3	7.5	12.7	18.1	22.2	23.1	23.2	22.0	21.1	17.7	12.2	5.5	0.7	0.0	0.0	0.0	0.0	0.0
May	0.0	0.0	0.0	0.0	0.1	1.6	4.6	11.4	17.7	23.1	26.2	25.1	25.5	25.4	22.8	18.4	13.0	7.4	2.1	0.4	0.0	0.0	0.0	0.0
June	0.0	0.0	0.0	0.0	0.6	2.0	4.8	11.3	17.2	21.7	25.7	26.1	25.6	23.5	21.5	18.2	13.2	7.4	2.1	1.2	0.1	0.0	0.0	0.0
July	0.0	0.0	0.0	0.0	0.2	1.6	4.3	10.7	16.4	20.8	24.0	24.6	24.9	24.0	20.5	16.4	12.1	7.3	2.2	0.9	0.0	0.0	0.0	0.0
August	0.0	0.0	0.0	0.0	0.0	0.5	2.8	8.4	14.2	18.2	22.7	23.0	24.5	21.9	19.8	16.0	11.4	5.7	1.3	0.1	0.0	0.0	0.0	0.0
Septembe	0.0	0.0	0.0	0.0	0.0	0.0	0.8	5.4	10.6	15.4	17.3	18.2	18.7	22.4	19.6	14.4	8.5	2.5	0.0	0.0	0.0	0.0	0.0	0.0
October	0.0	0.0	0.0	0.0	0.0	0.0	0.0	1.3	6.4	9.5	12.1	13.0	13.4	16.4	14.1	8.2	2.0	0.0	0.0	0.0	0.0	0.0	0.0	0.0
Novembe	0.0	0.0	0.0	0.0	0.0	0.0	0.0	0.0	0.8	3.6	5.6	6.4	7.5	10.3	7.8	2.1	0.0	0.0	0.0	0.0	0.0	0.0	0.0	0.0
Decembe	0.0	0.0	0.0	0.0	0.0	0.0	0.0	0.0	0.0	1.9	4.8	6.3	6.3	6.8	4.8	0.0	0.0	0.0	0.0	0.0	0.0	0.0	0.0	0.0
Year	0.0	0.0	0.0	0.0	0.1	0.5	1.7	4.9	8.9	12.9	16.0	17.0	17.5	17.8	15.5	11.2	7.0	3.2	0.7	0.2	0.0	0.0	0.0	0.0

Mölndal Area 1

Hourly maximum values for E_Grid [kW]

	0H	1H	2H	3H	4H	5H	6H	7H	8H	9H	10H	11H	12H	13H	14H	15H	16H	17H	18H	19H	20H	21H	22H	23H
January	0.0	0.0	0.0	0.0	0.0	0.0	0.0	0.0	0.0	14.2	22.4	28.7	28.5	29.2	23.8	12.8	0.0	0.0	0.0	0.0	0.0	0.0	0.0	0.0
February	0.0	0.0	0.0	0.0	0.0	0.0	0.0	0.0	12.7	22.9	29.9	35.9	36.0	32.5	29.6	22.4	11.1	0.0	0.0	0.0	0.0	0.0	0.0	0.0
March	0.0	0.0	0.0	0.0	0.0	0.0	0.9	10.3	21.4	30.7	37.3	40.6	42.2	40.7	35.7	28.5	18.6	6.7	0.0	0.0	0.0	0.0	0.0	0.0
April	0.0	0.0	0.0	0.0	0.0	1.0	4.5	14.9	24.8	32.9	38.7	41.2	41.7	40.0	35.6	31.3	21.0	9.2	2.4	0.0	0.0	0.0	0.0	0.0
May	0.0	0.0	0.0	0.0	0.7	2.6	6.5	17.0	26.7	35.0	38.7	40.8	41.0	39.4	35.5	29.3	20.8	10.9	3.1	1.2	0.0	0.0	0.0	0.0
June	0.0	0.0	0.0	0.0	1.1	3.1	6.3	16.3	27.2	34.6	37.7	43.2	40.8	39.3	38.5	29.9	21.6	12.2	3.8	2.2	0.3	0.0	0.0	0.0
July	0.0	0.0	0.0	0.0	0.9	2.7	6.3	15.8	26.0	32.5	37.5	40.1	40.4	38.8	35.3	29.5	21.4	11.9	3.8	2.1	0.2	0.0	0.0	0.0
August	0.0	0.0	0.0	0.0	0.0	1.8	4.2	14.2	23.1	31.1	36.6	39.1	39.9	37.9	34.3	28.4	20.7	10.7	2.9	0.7	0.0	0.0	0.0	0.0
Septembe	0.0	0.0	0.0	0.0	0.0	0.0	3.2	13.3	23.2	31.7	37.1	39.6	40.1	38.2	33.9	27.2	18.0	7.5	0.3	0.0	0.0	0.0	0.0	0.0
October	0.0	0.0	0.0	0.0	0.0	0.0	0.0	6.9	20.0	28.3	34.6	37.2	34.1	32.3	28.4	17.8	7.9	0.0	0.0	0.0	0.0	0.0	0.0	0.0
Novembe	0.0	0.0	0.0	0.0	0.0	0.0	0.0	0.0	6.3	16.0	22.0	24.4	25.9	25.9	24.4	15.2	0.0	0.0	0.0	0.0	0.0	0.0	0.0	0.0
Decembe	0.0	0.0	0.0	0.0	0.0	0.0	0.0	0.0	0.0	12.4	20.7	25.2	25.8	21.9	16.4	0.0	0.0	0.0	0.0	0.0	0.0	0.0	0.0	0.0
Year	0.0	0.0	0.0	0.0	1.1	3.1	6.5	17.0	27.2	35.0	38.7	43.2	42.2	40.7	38.5	31.3	21.6	12.2	3.8	2.2	0.3	0.0	0.0	0.0

Table B.7: Typical PV System Production-Mölndal Area 2

Mölndal Area 2

Monthly Hourly averages for E_Grid [kW]

	0H	1H	2H	3H	4H	5H	6H	7H	8H	9H	10H	11H	12H	13H	14H	15H	16H	17H	18H	19H	20H	21H	22H	23H
January	0.0	0.0	0.0	0.0	0.0	0.0	0.0	0.0	0.0	2.1	4.7	5.8	6.3	5.8	4.5	1.4	0.0	0.0	0.0	0.0	0.0	0.0	0.0	0.0
February	0.0	0.0	0.0	0.0	0.0	0.0	0.0	0.0	1.4	4.8	6.8	8.7	9.0	10.7	8.6	5.4	1.7	0.0	0.0	0.0	0.0	0.0	0.0	0.0
March	0.0	0.0	0.0	0.0	0.0	0.0	0.1	2.3	6.7	10.5	12.7	14.6	15.5	14.4	12.4	10.7	6.4	1.5	0.0	0.0	0.0	0.0	0.0	0.0
April	0.0	0.0	0.0	0.0	0.0	0.3	2.0	5.9	9.9	14.0	17.0	17.6	17.6	16.6	15.9	13.2	9.0	4.0	0.7	0.0	0.0	0.0	0.0	0.0
May	0.0	0.0	0.0	0.0	0.3	1.4	3.9	9.0	13.7	17.8	20.0	19.1	19.3	19.2	17.1	13.7	9.7	5.3	1.7	0.6	0.0	0.0	0.0	0.0
June	0.0	0.0	0.0	0.0	0.7	1.6	4.0	8.9	13.3	16.7	19.6	19.8	19.4	17.8	16.2	13.7	9.8	5.4	1.6	1.1	0.2	0.0	0.0	0.0
July	0.0	0.0	0.0	0.0	0.4	1.4	3.6	8.5	12.7	16.0	18.3	18.7	18.9	18.1	15.4	12.3	9.0	5.4	1.6	0.9	0.1	0.0	0.0	0.0
August	0.0	0.0	0.0	0.0	0.0	0.6	2.4	6.7	11.1	14.0	17.4	17.5	18.5	16.6	14.9	12.0	8.4	4.2	1.1	0.2	0.0	0.0	0.0	0.0
Septembe	0.0	0.0	0.0	0.0	0.0	0.0	0.8	4.4	8.3	11.9	13.2	13.9	14.2	16.9	14.7	10.7	6.3	1.8	0.1	0.0	0.0	0.0	0.0	0.0
October	0.0	0.0	0.0	0.0	0.0	0.0	0.0	1.1	5.1	7.5	9.3	9.9	10.2	12.4	10.6	6.1	1.5	0.0	0.0	0.0	0.0	0.0	0.0	0.0
Novembe	0.0	0.0	0.0	0.0	0.0	0.0	0.0	0.0	0.7	2.9	4.4	5.0	5.8	7.8	5.9	1.6	0.0	0.0	0.0	0.0	0.0	0.0	0.0	0.0
Decembe	0.0	0.0	0.0	0.0	0.0	0.0	0.0	0.0	0.0	1.6	3.8	4.9	4.9	5.2	3.6	0.0	0.0	0.0	0.0	0.0	0.0	0.0	0.0	0.0
Year	0.0	0.0	0.0	0.0	0.1	0.4	1.4	3.9	6.9	10.0	12.3	13.0	13.3	13.5	11.7	8.4	5.2	2.3	0.6	0.2	0.0	0.0	0.0	0.0

Mölndal Area 2

Hourly maximum values for E_Grid [kW]

	0H	1H	2H	3H	4H	5H	6H	7H	8H	9H	10H	11H	12H	13H	14H	15H	16H	17H	18H	19H	20H	21H	22H	23H
January	0.0	0.0	0.0	0.0	0.0	0.0	0.0	0.0	0.0	11.1	17.3	21.9	21.6	22.0	17.7	9.4	0.0	0.0	0.0	0.0	0.0	0.0	0.0	0.0
February	0.0	0.0	0.0	0.0	0.0	0.0	0.0	0.0	10.1	17.8	23.0	27.3	27.2	24.6	22.2	16.6	8.1	0.0	0.0	0.0	0.0	0.0	0.0	0.0
March	0.0	0.0	0.0	0.0	0.0	0.0	1.3	8.5	16.8	23.7	28.5	30.9	31.9	30.6	26.7	21.1	13.6	4.7	0.0	0.0	0.0	0.0	0.0	0.0
April	0.0	0.0	0.0	0.0	0.0	1.0	4.0	11.9	19.4	25.3	29.5	31.3	31.5	30.1	26.7	23.2	15.3	6.4	1.8	0.0	0.0	0.0	0.0	0.0
May	0.0	0.0	0.0	0.0	0.8	2.0	5.4	13.6	20.8	26.9	29.5	30.9	31.0	29.6	26.6	21.8	15.2	7.6	2.4	1.1	0.2	0.0	0.0	0.0
June	0.0	0.0	0.0	0.0	1.1	2.3	5.4	13.0	21.2	26.6	28.8	32.8	30.8	29.6	28.9	22.2	15.9	8.6	2.9	1.7	0.6	0.0	0.0	0.0
July	0.0	0.0	0.0	0.0	0.9	2.1	5.4	12.6	20.3	25.0	28.7	30.4	30.6	29.2	26.5	22.0	15.7	8.5	2.8	1.7	0.5	0.0	0.0	0.0
August	0.0	0.0	0.0	0.0	0.0	1.4	3.6	11.4	18.1	24.0	28.0	29.7	30.2	28.6	25.7	21.1	15.2	7.5	2.2	0.8	0.0	0.0	0.0	0.0
Septembe	0.0	0.0	0.0	0.0	0.0	0.0	2.8	10.8	18.2	24.4	28.4	30.1	30.3	28.7	25.4	20.2	13.1	5.1	0.5	0.0	0.0	0.0	0.0	0.0
October	0.0	0.0	0.0	0.0	0.0	0.0	0.0	5.6	15.7	21.8	26.4	28.2	25.8	24.3	21.2	13.1	5.6	0.0	0.0	0.0	0.0	0.0	0.0	0.0
Novembe	0.0	0.0	0.0	0.0	0.0	0.0	0.0	0.0	5.0	12.4	16.8	18.6	19.6	19.4	18.2	11.1	0.0	0.0	0.0	0.0	0.0	0.0	0.0	0.0
Decembe	0.0	0.0	0.0	0.0	0.0	0.0	0.0	0.0	0.0	9.7	15.9	19.2	19.5	16.4	12.1	0.0	0.0	0.0	0.0	0.0	0.0	0.0	0.0	0.0
Year	0.0	0.0	0.0	0.0	1.1	2.3	5.4	13.6	21.2	26.9	29.5	32.8	31.9	30.6	28.9	23.2	15.9	8.6	2.9	1.7	0.6	0.0	0.0	0.0

Table B.8: Typical PV System Production-Orust Area

Orust

Monthly Hourly averages for E_Grid [kW]

	0H	1H	2H	3H	4H	5H	6H	7H	8H	9H	10H	11H	12H	13H	14H	15H	16H	17H	18H	19H	20H	21H	22H	23H
January	0.00	0.00	0.00	0.00	0.00	0.00	0.00	0.00	0.00	0.28	0.79	1.12	1.37	1.96	1.57	0.39	0.00	0.00	0.00	0.00	0.00	0.00	0.00	0.00
February	0.00	0.00	0.00	0.00	0.00	0.00	0.00	0.00	0.21	0.86	1.47	2.42	2.43	3.04	2.71	1.70	0.49	0.00	0.00	0.00	0.00	0.00	0.00	0.00
March	0.00	0.00	0.00	0.00	0.00	0.00	0.01	0.86	2.84	4.43	5.68	6.14	6.38	6.37	5.29	4.26	2.40	0.55	0.00	0.00	0.00	0.00	0.00	0.00
April	0.00	0.00	0.00	0.00	0.00	0.03	0.64	2.65	4.47	6.33	8.02	8.62	8.32	7.84	6.79	5.40	3.60	1.42	0.13	0.00	0.00	0.00	0.00	0.00
May	0.00	0.00	0.00	0.00	0.03	0.35	1.48	3.55	5.68	6.71	7.68	8.26	8.70	8.50	7.78	6.09	4.32	2.15	0.43	0.11	0.00	0.00	0.00	0.00
June	0.00	0.00	0.00	0.00	0.15	0.55	1.67	3.83	5.69	7.38	8.51	8.34	8.03	7.67	6.60	5.56	4.13	2.37	0.57	0.25	0.00	0.00	0.00	0.00
July	0.00	0.00	0.00	0.00	0.06	0.37	1.31	3.38	5.17	6.57	7.57	7.40	7.49	7.25	6.78	5.61	4.12	2.51	0.71	0.27	0.01	0.00	0.00	0.00
August	0.00	0.00	0.00	0.00	0.00	0.08	0.78	2.50	4.28	5.77	6.73	6.83	6.91	6.81	6.12	4.74	3.36	1.74	0.31	0.02	0.00	0.00	0.00	0.00
Septembe	0.00	0.00	0.00	0.00	0.00	0.00	0.19	1.73	3.54	4.85	5.84	6.36	6.20	6.47	6.38	5.04	3.13	0.94	0.00	0.00	0.00	0.00	0.00	0.00
October	0.00	0.00	0.00	0.00	0.00	0.00	0.00	0.42	1.69	3.01	4.09	4.64	4.43	4.71	3.82	2.29	0.59	0.00	0.00	0.00	0.00	0.00	0.00	0.00
Novembe	0.00	0.00	0.00	0.00	0.00	0.00	0.00	0.00	0.48	0.91	1.52	1.85	1.56	1.73	1.29	0.34	0.00	0.00	0.00	0.00	0.00	0.00	0.00	0.00
Decembe	0.00	0.00	0.00	0.00	0.00	0.00	0.00	0.00	0.00	0.01	0.85	1.14	1.11	0.98	0.53	0.00	0.00	0.00	0.00	0.00	0.00	0.00	0.00	0.00
Year	0.00	0.00	0.00	0.00	0.02	0.12	0.51	1.59	2.85	3.94	4.91	5.27	5.26	5.29	4.65	3.46	2.19	0.98	0.18	0.05	0.00	0.00	0.00	0.00

Orust

Hourly maximum values for E_Grid [kW]

	0H	1H	2H	3H	4H	5H	6H	7H	8H	9H	10H	11H	12H	13H	14H	15H	16H	17H	18H	19H	20H	21H	22H	23H
January	0.0	0.0	0.0	0.0	0.0	0.0	0.0	0.0	0.0	3.6	6.1	7.8	8.7	7.5	5.1	3.3	0.0	0.0	0.0	0.0	0.0	0.0	0.0	0.0
February	0.0	0.0	0.0	0.0	0.0	0.0	0.0	0.0	2.5	6.3	9.1	10.8	11.2	10.6	8.6	6.9	3.5	0.0	0.0	0.0	0.0	0.0	0.0	0.0
March	0.0	0.0	0.0	0.0	0.0	0.0	0.2	2.7	6.7	8.6	10.9	12.2	12.4	11.7	10.6	8.6	5.9	2.1	0.0	0.0	0.0	0.0	0.0	0.0
April	0.0	0.0	0.0	0.0	0.0	0.2	1.4	4.5	7.9	10.5	12.1	13.0	13.2	12.7	11.3	9.1	6.0	2.7	0.6	0.0	0.0	0.0	0.0	0.0
May	0.0	0.0	0.0	0.0	0.2	0.7	2.1	5.4	8.7	11.1	12.4	12.9	13.0	12.5	11.2	9.2	6.3	3.6	0.8	0.5	0.0	0.0	0.0	0.0
June	0.0	0.0	0.0	0.0	0.6	1.2	2.4	5.8	8.9	11.0	12.1	12.4	12.4	11.9	10.8	9.0	6.4	3.4	1.1	0.6	0.0	0.0	0.0	0.0
July	0.0	0.0	0.0	0.0	0.3	0.9	2.1	5.3	8.2	10.6	12.0	12.2	12.4	12.0	11.0	9.3	6.8	3.6	1.6	0.6	0.1	0.0	0.0	0.0
August	0.0	0.0	0.0	0.0	0.0	0.4	1.2	4.6	8.2	10.2	11.2	12.0	12.2	11.7	10.6	8.8	6.2	3.2	0.8	0.1	0.0	0.0	0.0	0.0
Septembe	0.0	0.0	0.0	0.0	0.0	0.0	0.7	4.1	7.2	9.8	11.5	12.3	12.4	11.9	10.5	8.4	5.6	2.2	0.0	0.0	0.0	0.0	0.0	0.0
October	0.0	0.0	0.0	0.0	0.0	0.0	0.0	2.3	5.6	8.6	10.4	11.0	10.5	9.9	9.3	6.6	3.1	0.0	0.0	0.0	0.0	0.0	0.0	0.0
Novembe	0.0	0.0	0.0	0.0	0.0	0.0	0.0	0.0	3.2	6.1	7.0	7.2	7.6	6.7	5.8	3.0	0.0	0.0	0.0	0.0	0.0	0.0	0.0	0.0
Decembe	0.0	0.0	0.0	0.0	0.0	0.0	0.0	0.0	0.0	0.2	4.9	6.0	6.3	4.8	2.8	0.0	0.0	0.0	0.0	0.0	0.0	0.0	0.0	0.0
Year	0.0	0.0	0.0	0.0	0.6	1.2	2.4	5.8	8.9	11.1	12.4	13.0	13.2	12.7	11.3	9.3	6.8	3.6	1.6	0.6	0.1	0.0	0.0	0.0

APPENDIX C Normal Case Results

Mölndal Area 1

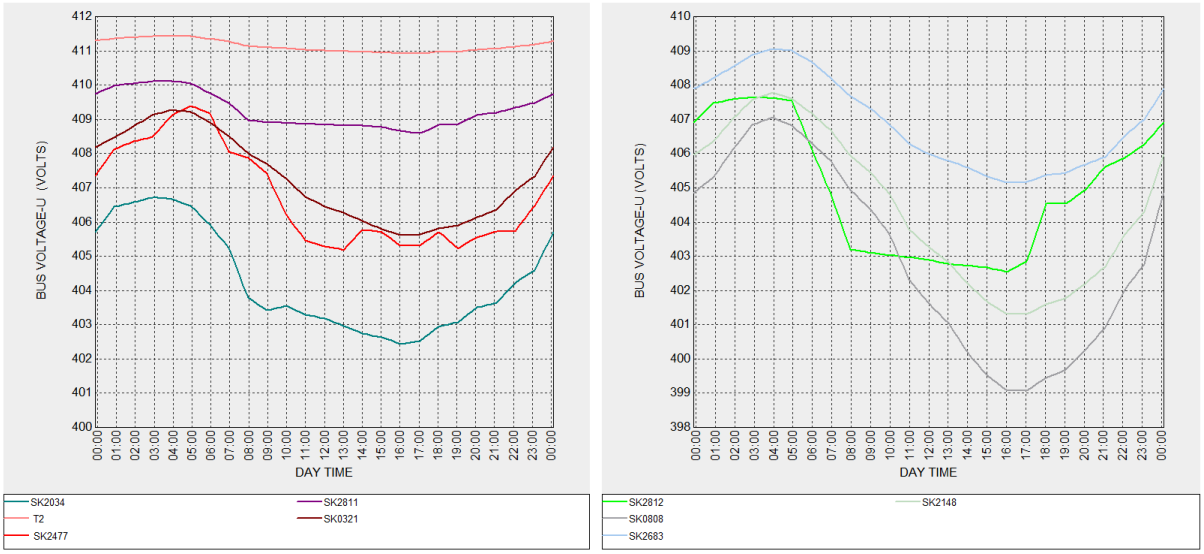

Figure C.1: Bus Voltage Profiles-Mölndal Area 1

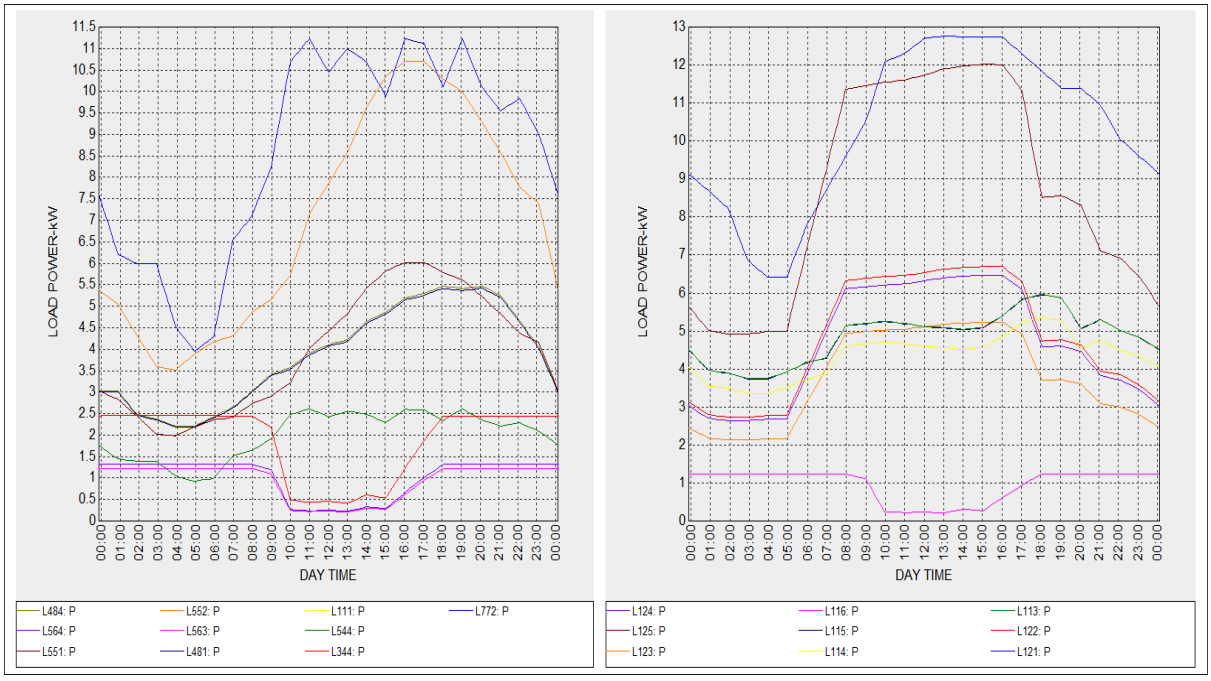

Figure C.2: Load Power Profiles-Mölndal Area 1

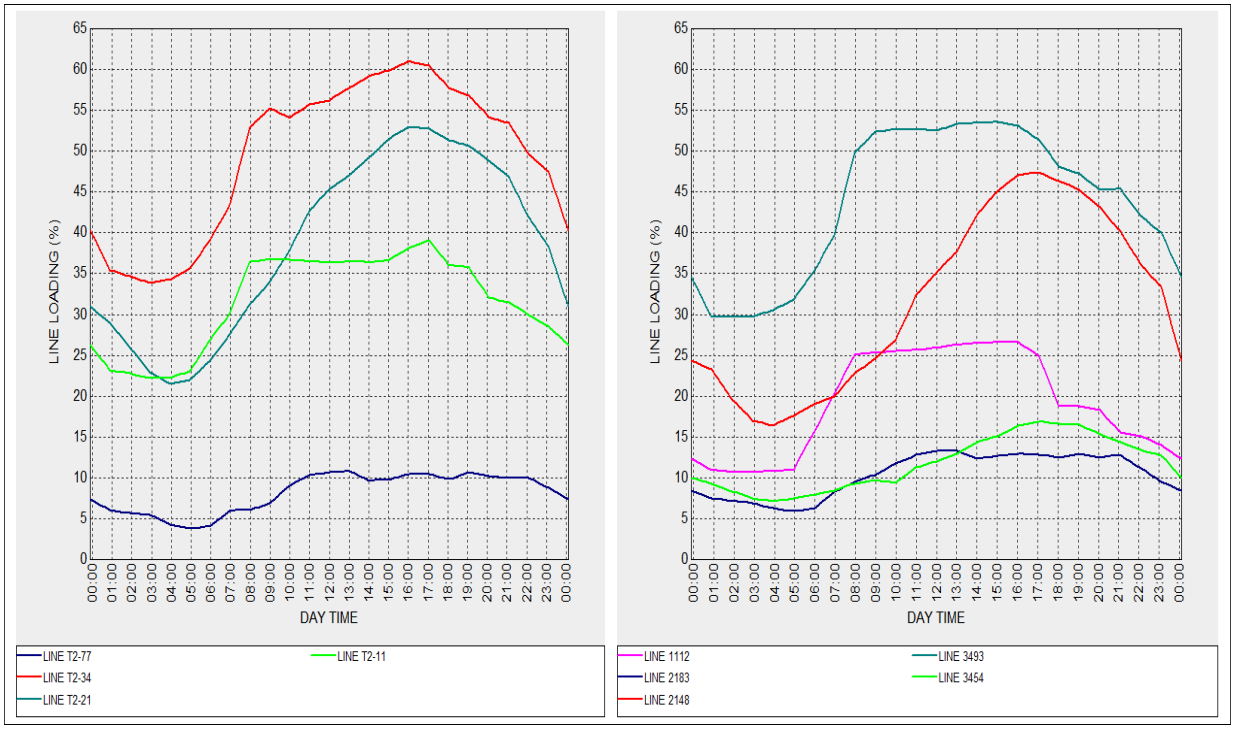

Figure C.3: Line Loading-Mölndal Area 1

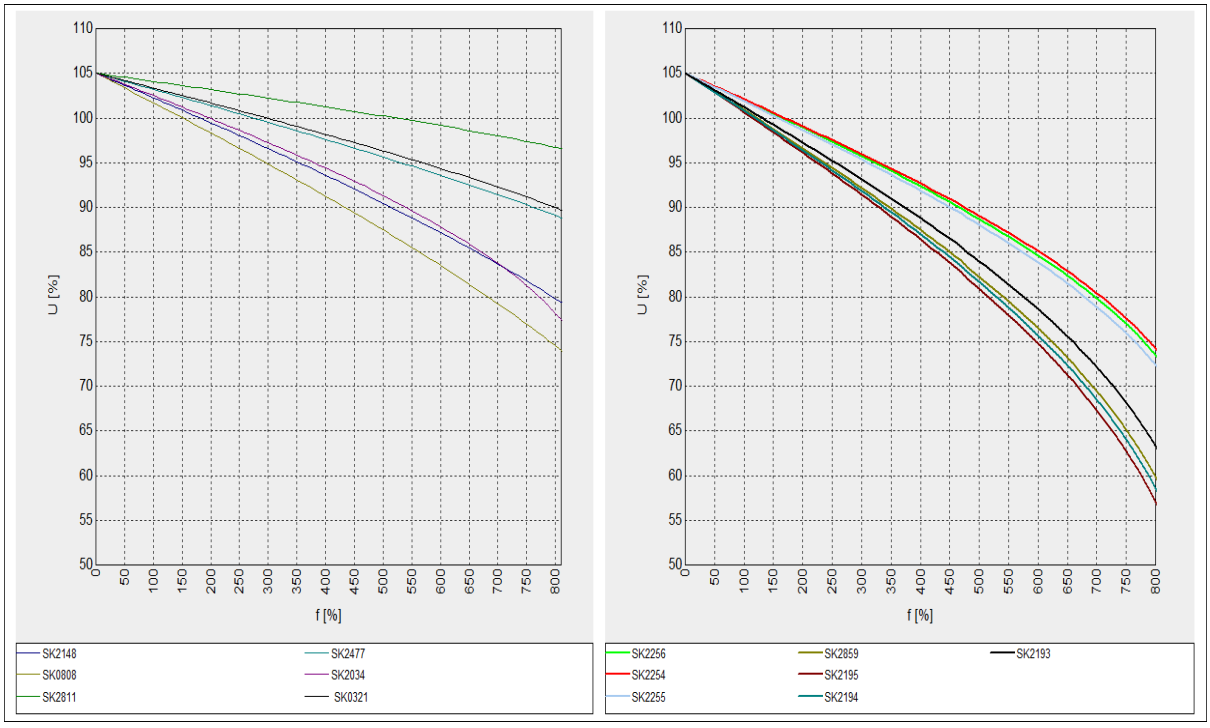

Figure C.4: P-U Curves-Mölndal Area 1

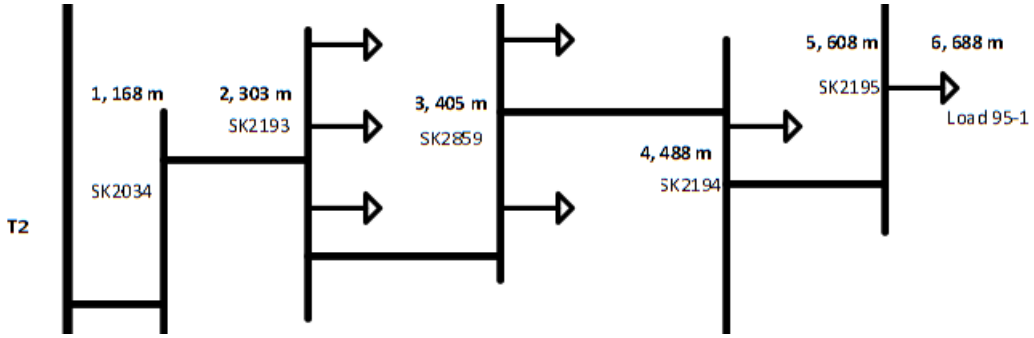

Figure C.5: Voltage Profile Diagram along Feeders-Mölndal Area 1

Mölndal Area 2

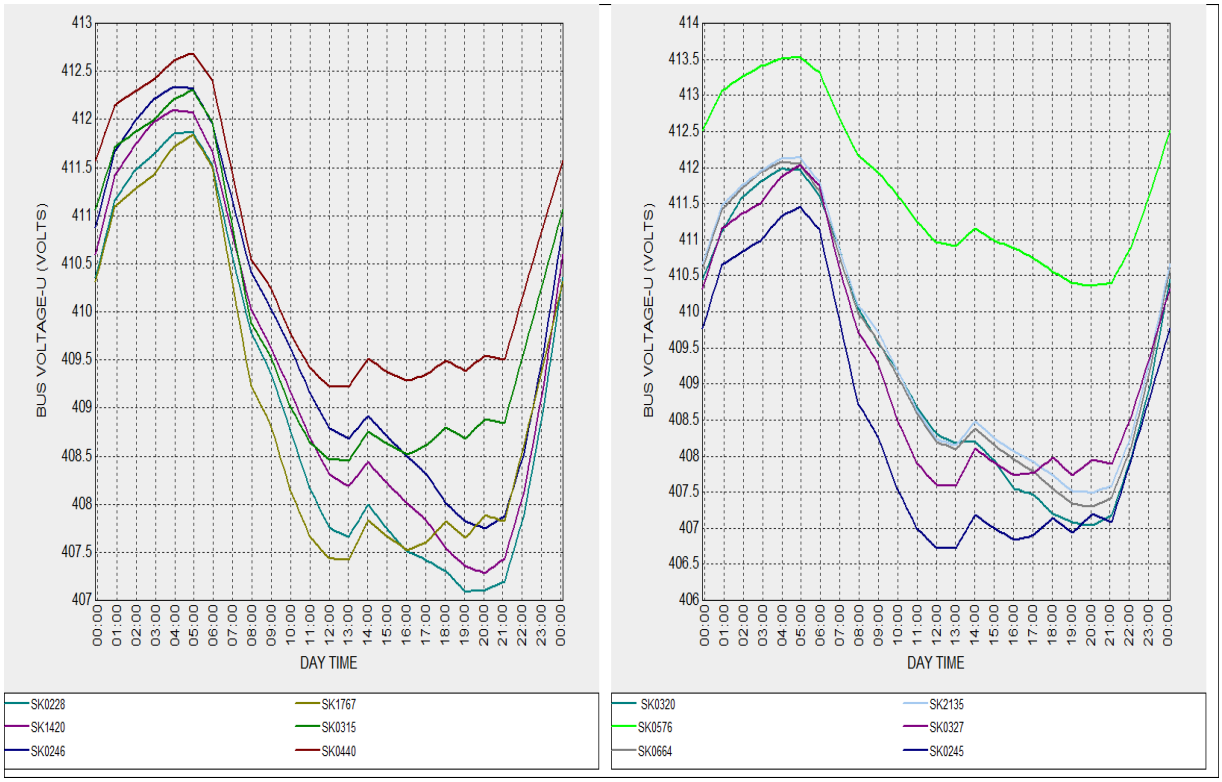

Figure C.6: Bus Voltage Profile-Mölndal Area 2

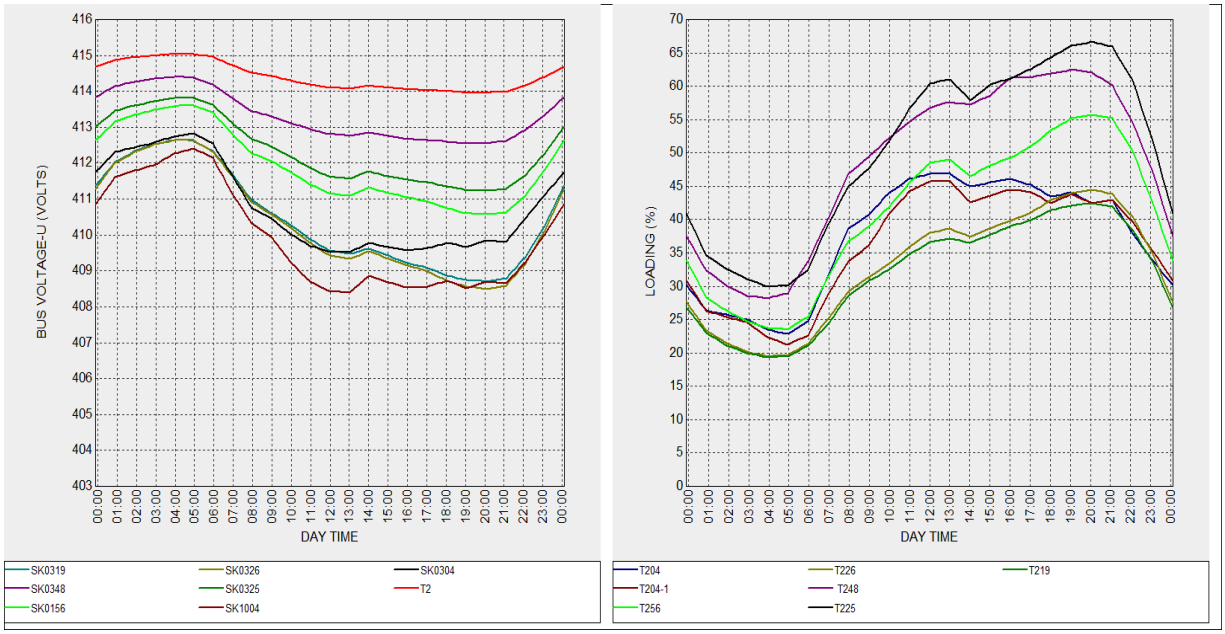

Figure C.7: Bus Voltage Profile/Line Loading-Mölndal Area 2

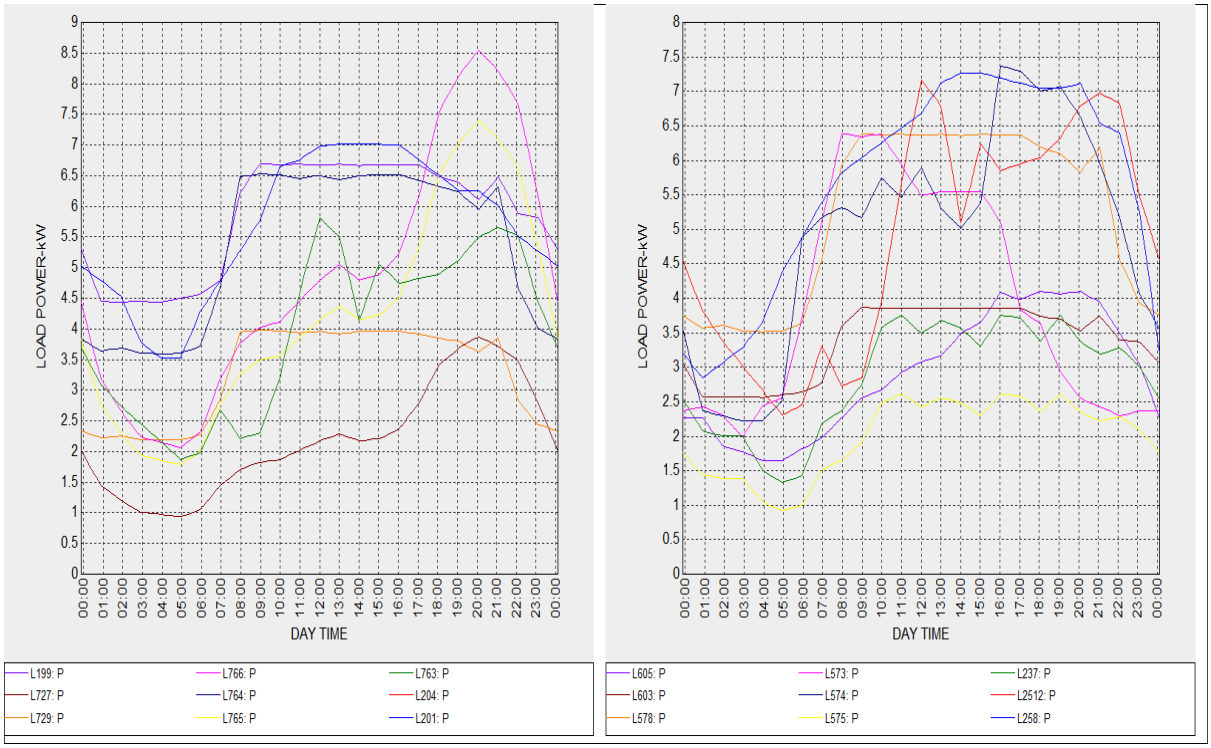

Figure C.8: Load Power Profiles-Mölndal Area 2

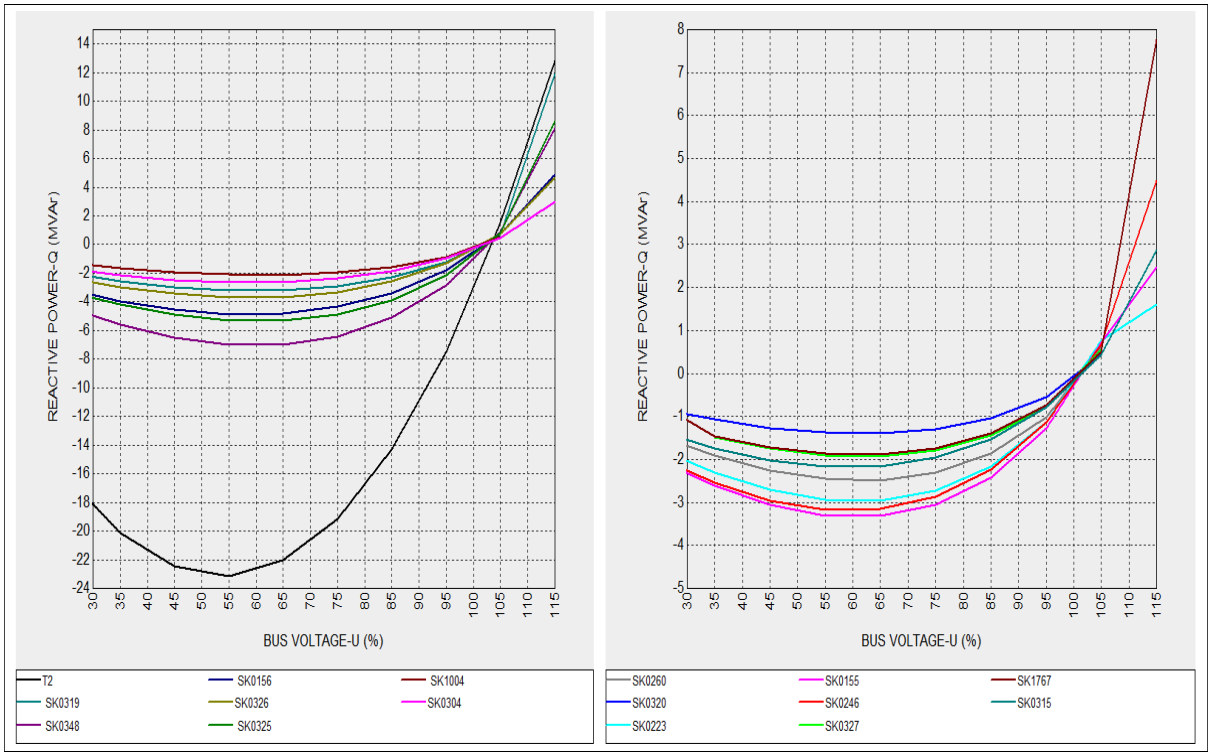

Figure C.9: Q-U Curves-Mölndal Area 2

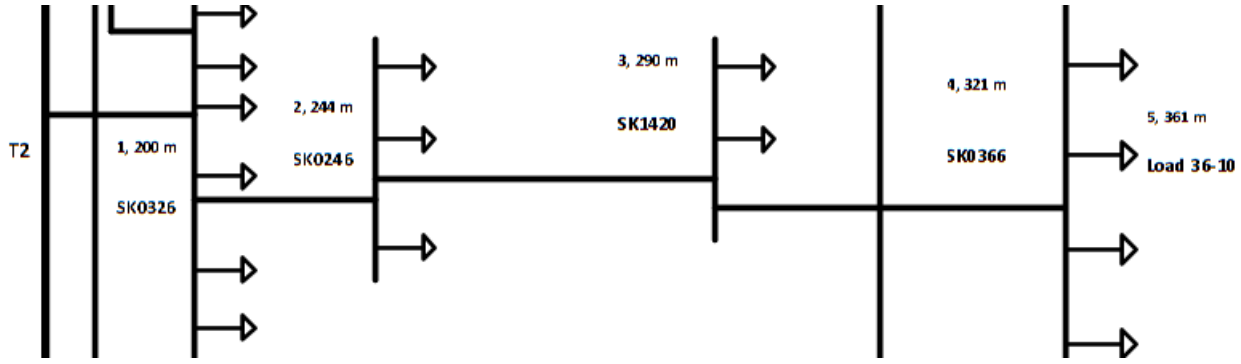

Figure C.10: Voltage Profile Diagram along Feeders-Mölndal Area 2

Orust

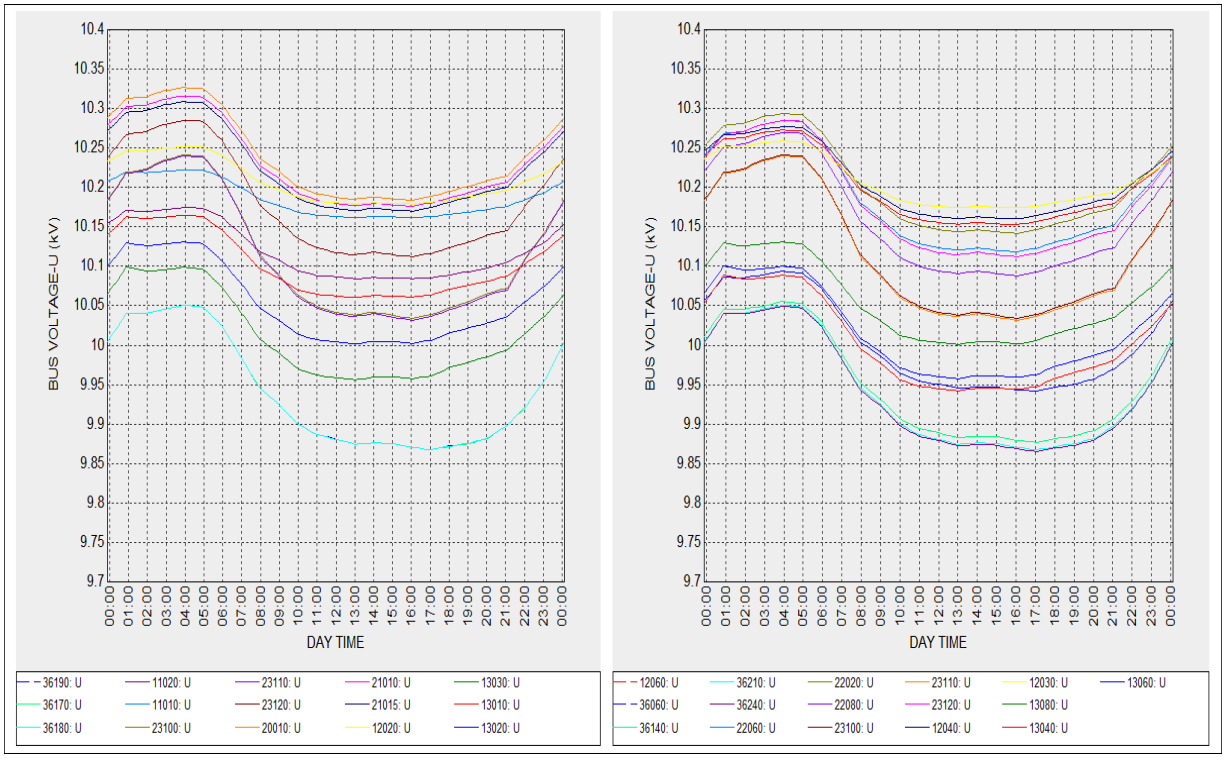

Figure C.11: Selected Buses Voltage Profile-Orust Area

Figure C.12: Selected Line Loading-Orust Area

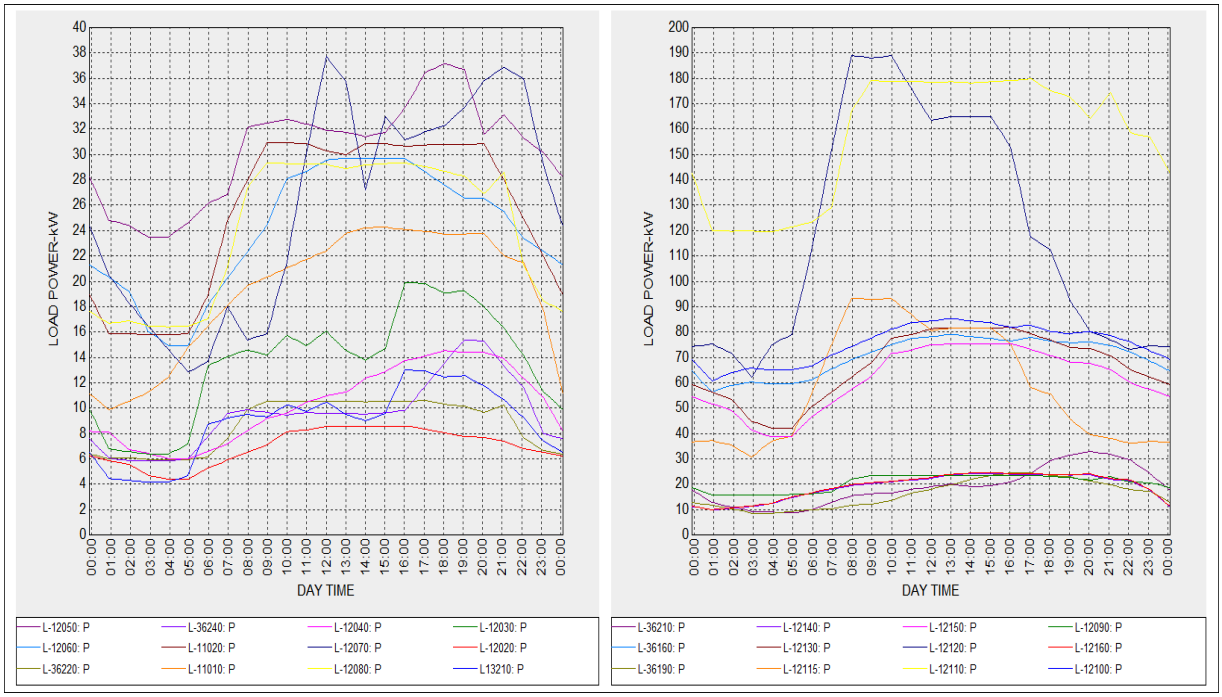

Figure C.13: Load Power Profiles 1-Orust

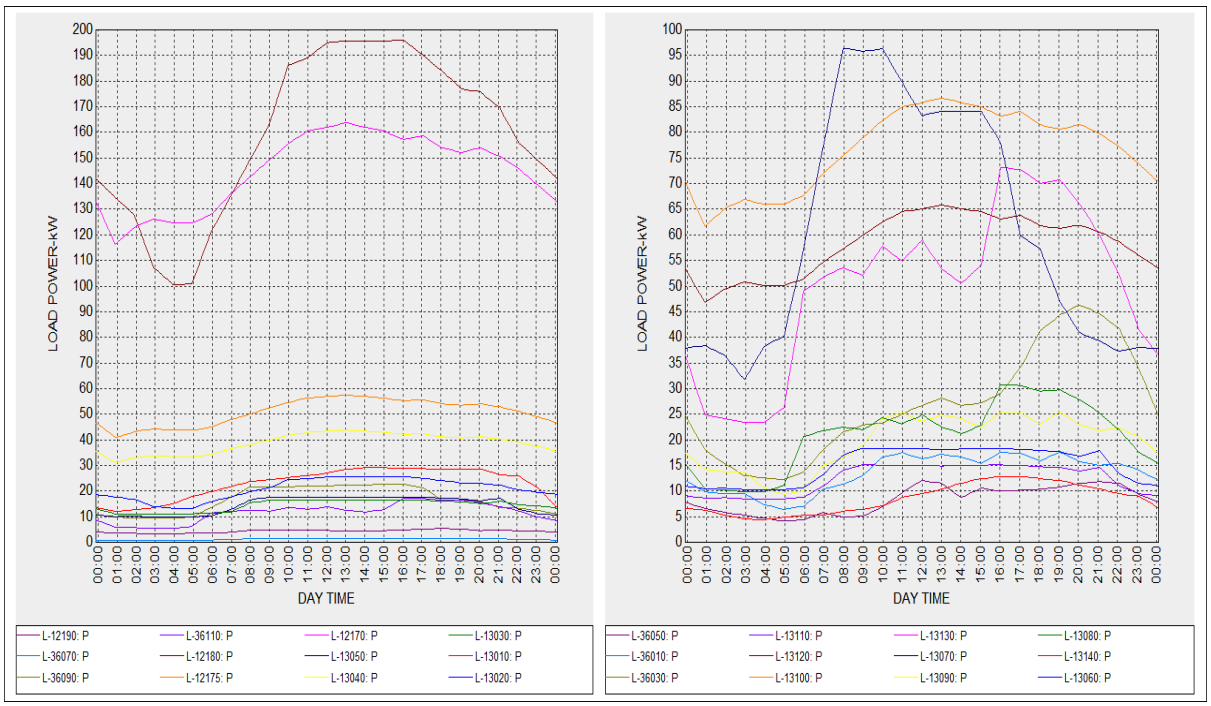

Figure C.14: Load Power Profiles 2-Orust

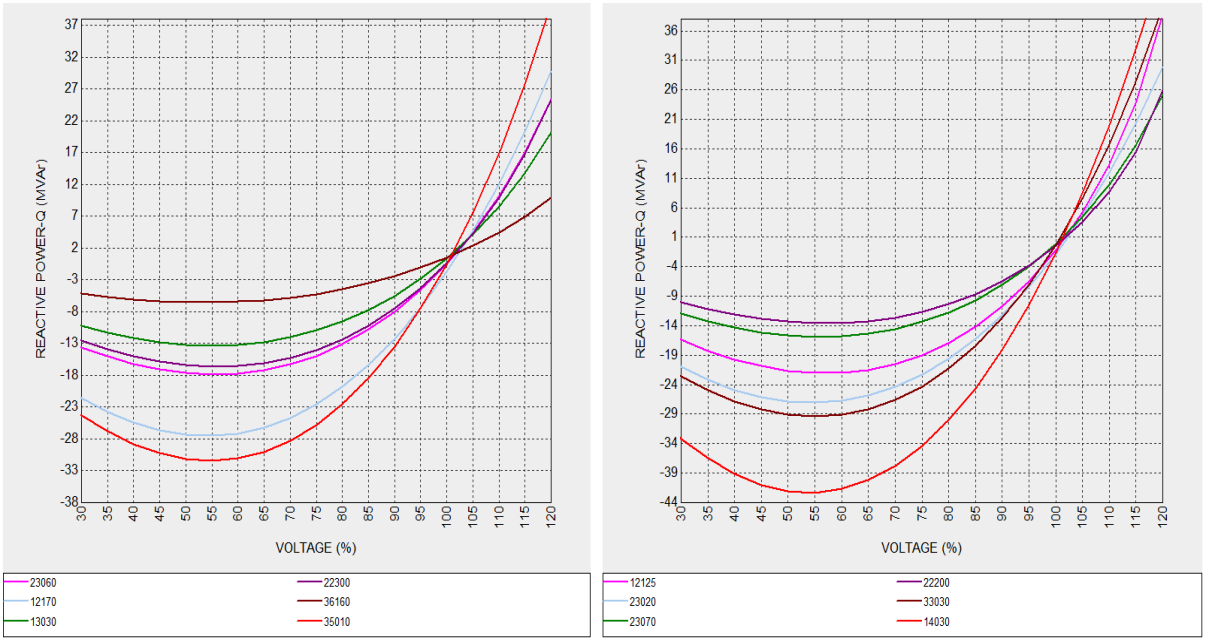

Figure C.15: Q-U Curves for Selected Buses 1

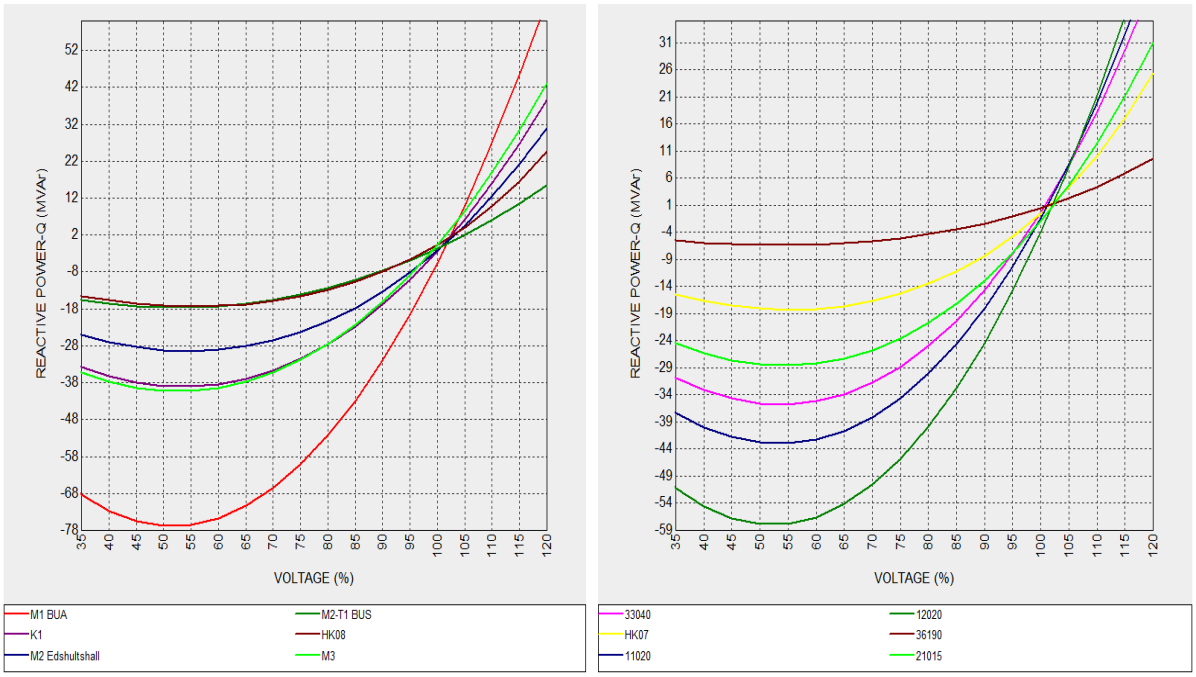

Figure C.16: Q-U Curves for Selected Buses 2

APPENDIX D Results with Solar PV Power

Mölndal 1

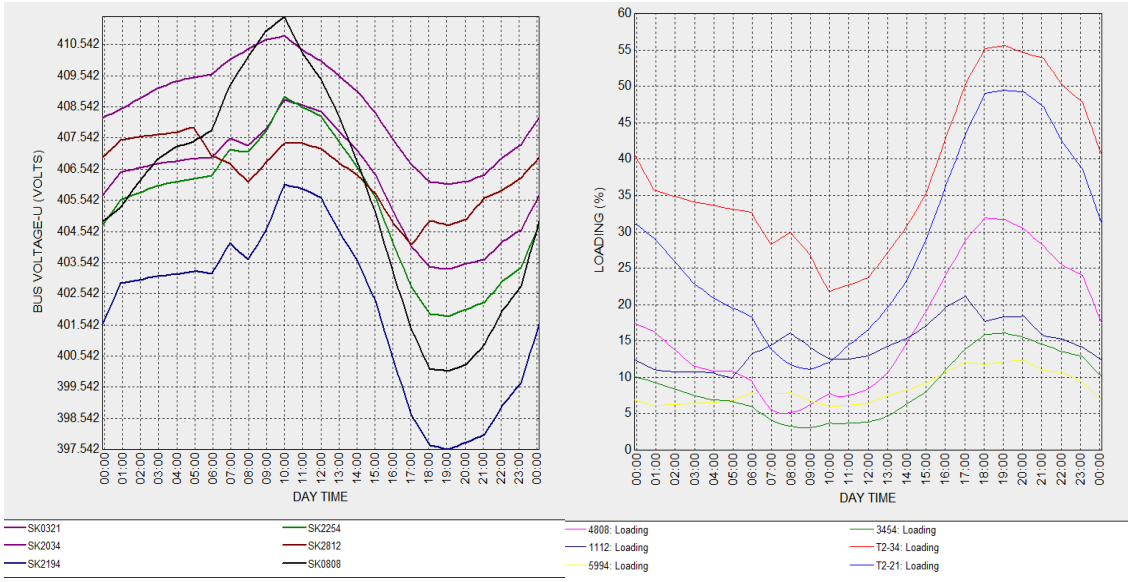

Figure D.1: Voltage Profile and Line Loading (60 % Penetration)

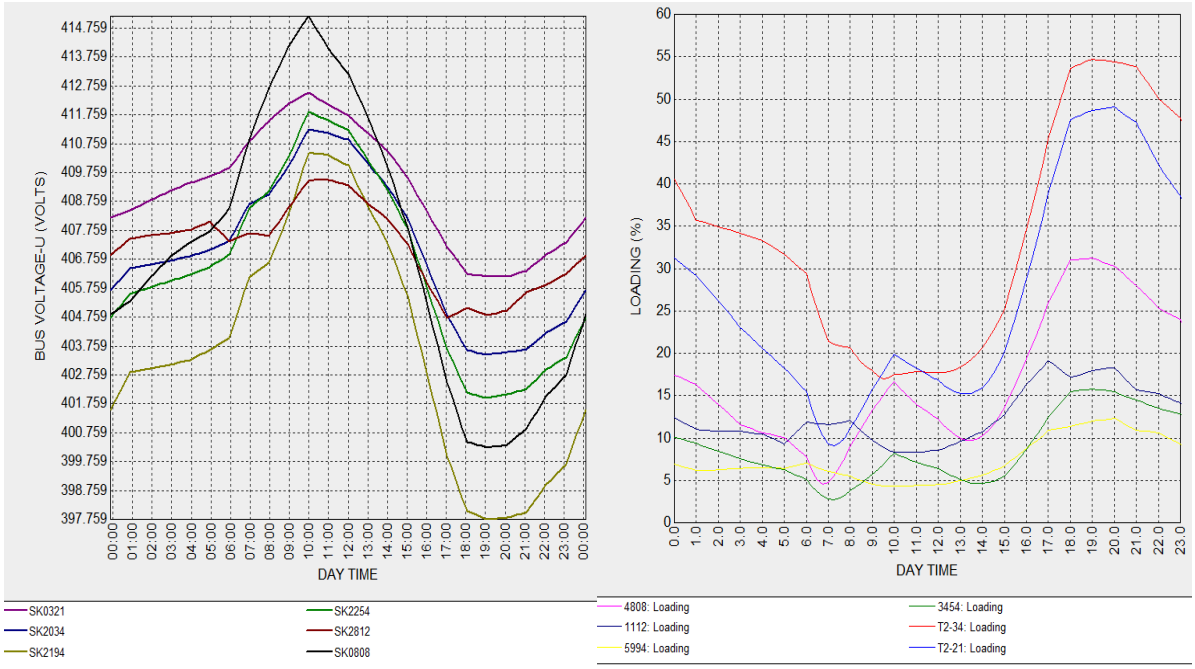

Figure D.2: Voltage Profile and Line Loading (90 % Penetration)

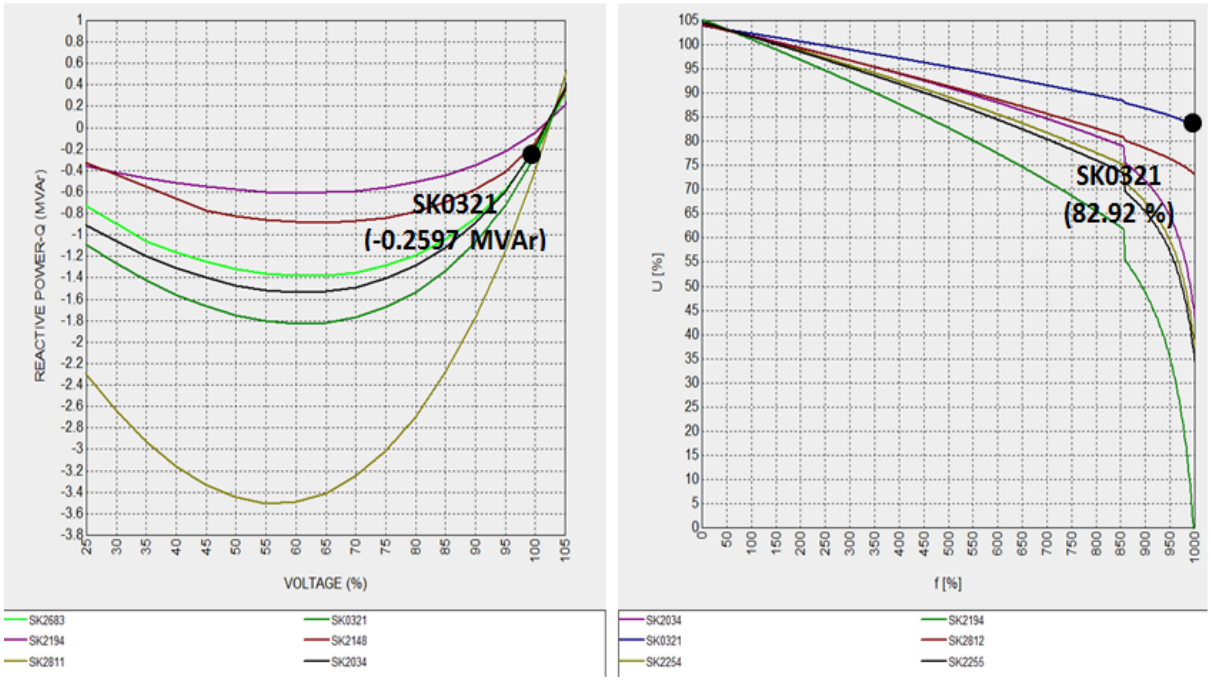

Figure D.3: Q-U and P-U curves at 60 % PV Penetration-Mölndal Area 1

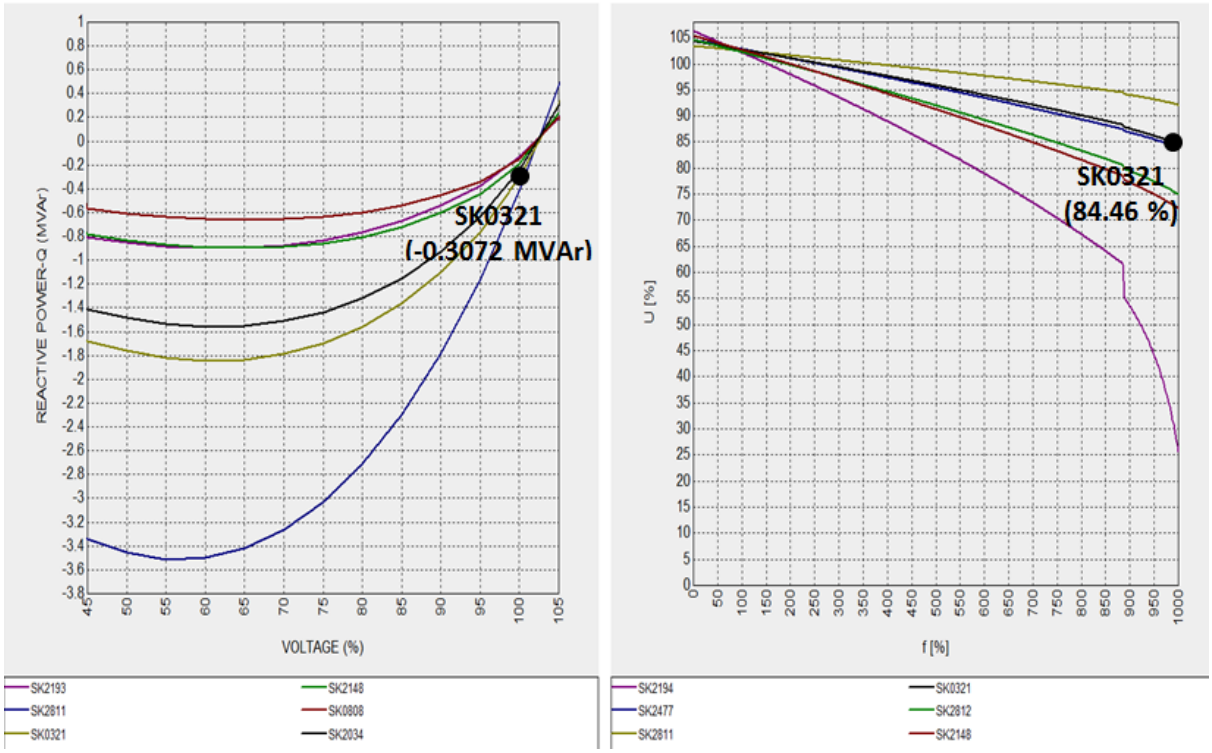

Figure D.4: Q-U and P-U curves at 90 % PV Penetration-Mölndal Area 1

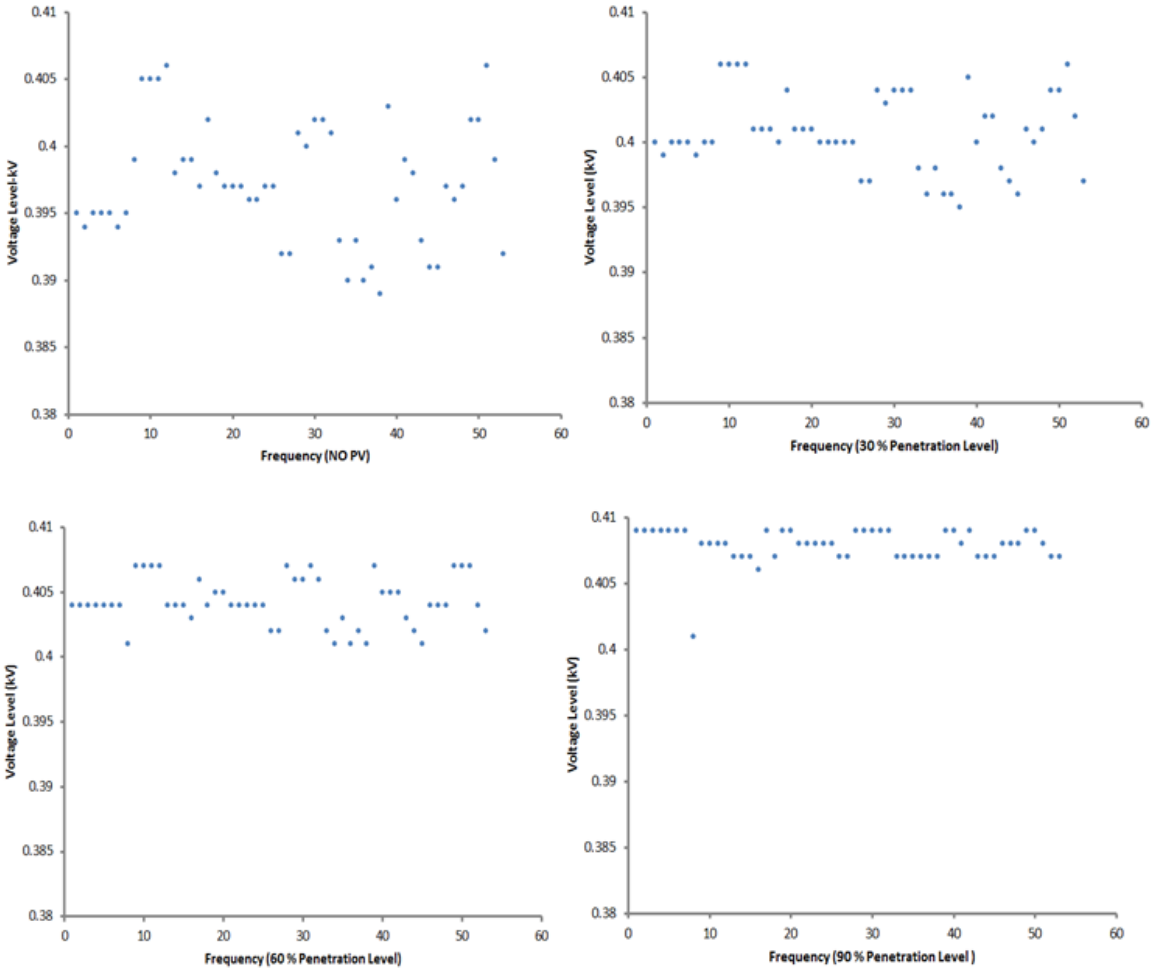

Figure D.5: Voltage Scatter Plots-Mölndal Area 1

Mölndal 2

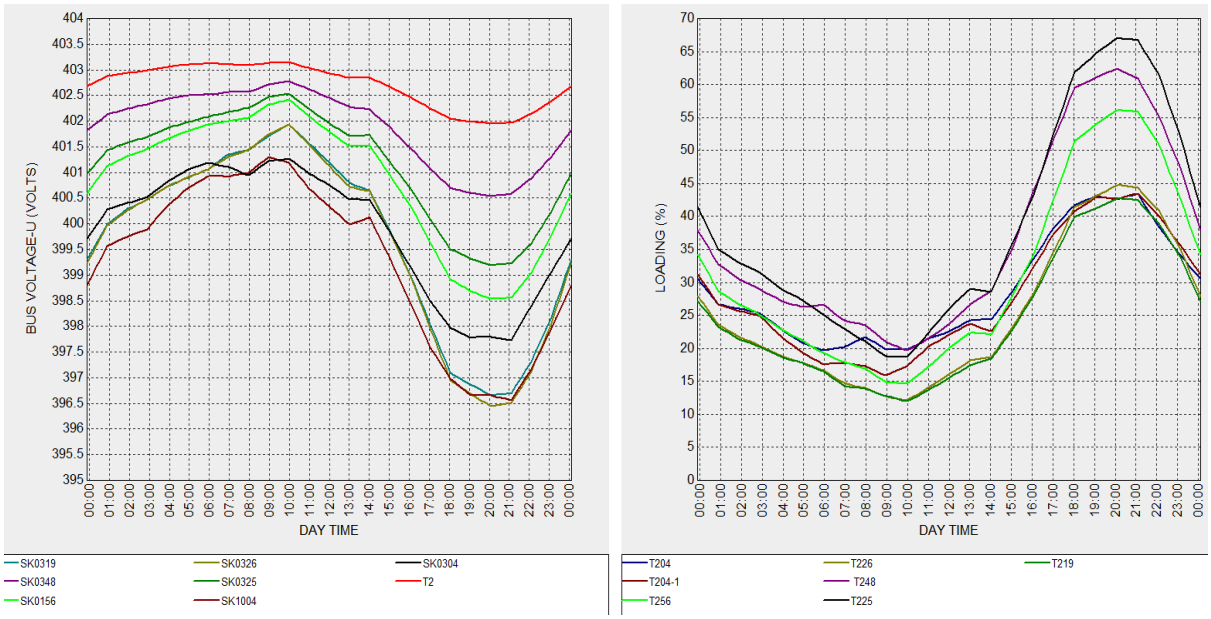

Figure D.6: Voltage Profile and Line Loading (60 % Penetration)-Mölndal Area 2

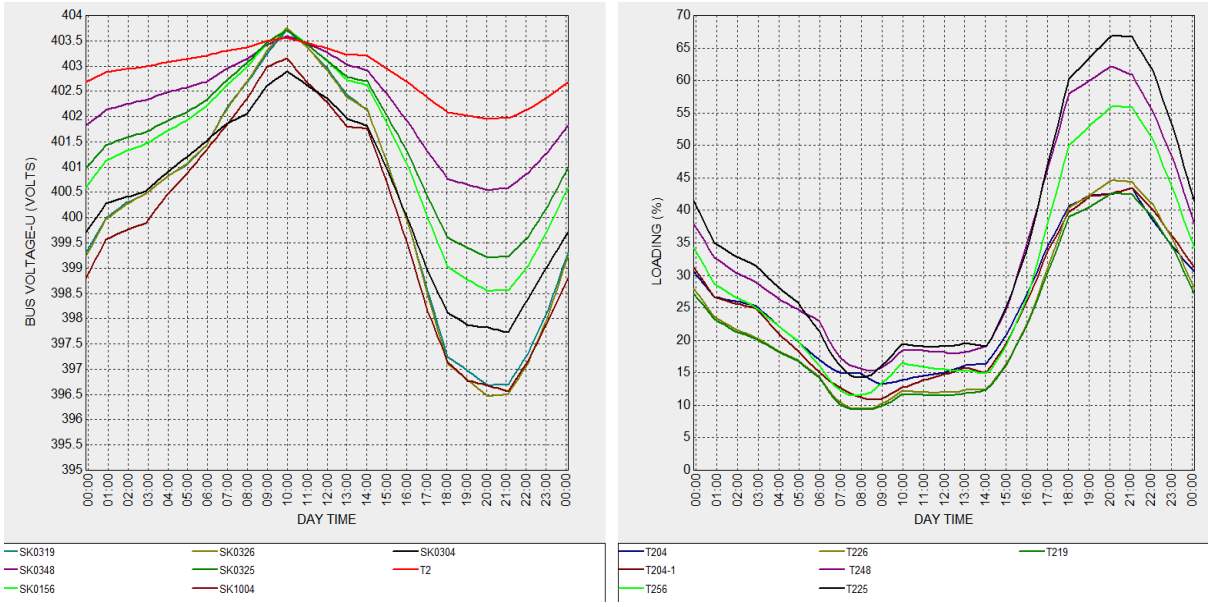

Figure D.7: Voltage Profile and Line Loading (90 % Penetration)-Mölndal Area 2

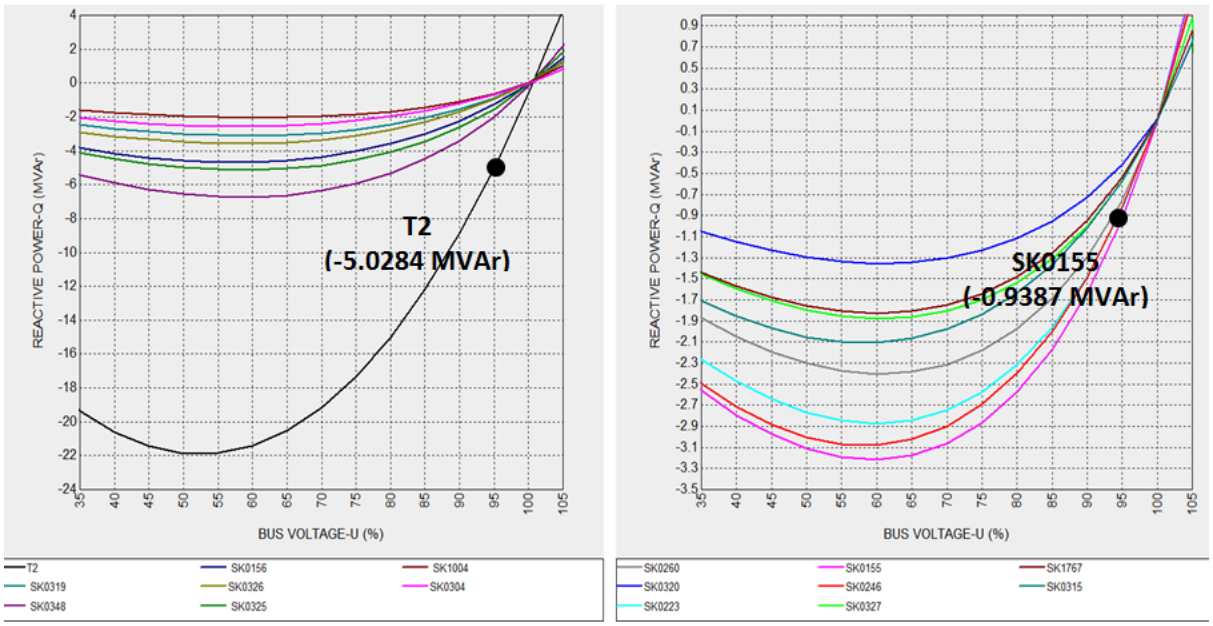

Figure D.8: Q-U curves at 60 % PV Penetration-Mölndal Area 2

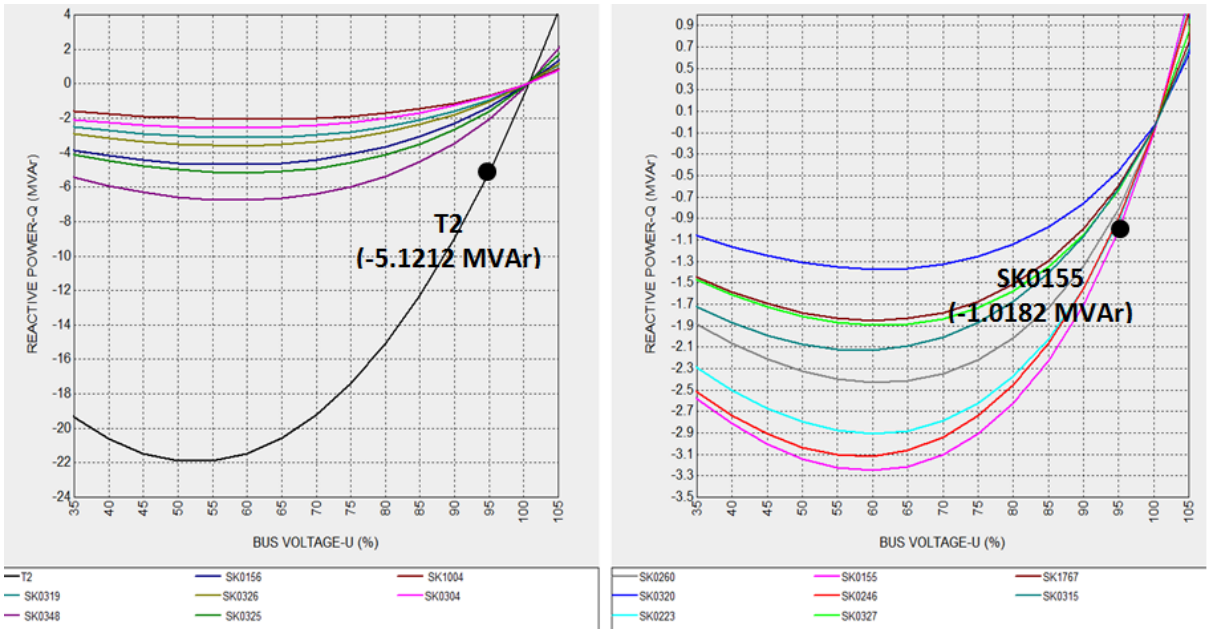

Figure D.9: Q-U curves at 90 % PV Penetration-Mölndal Area 2

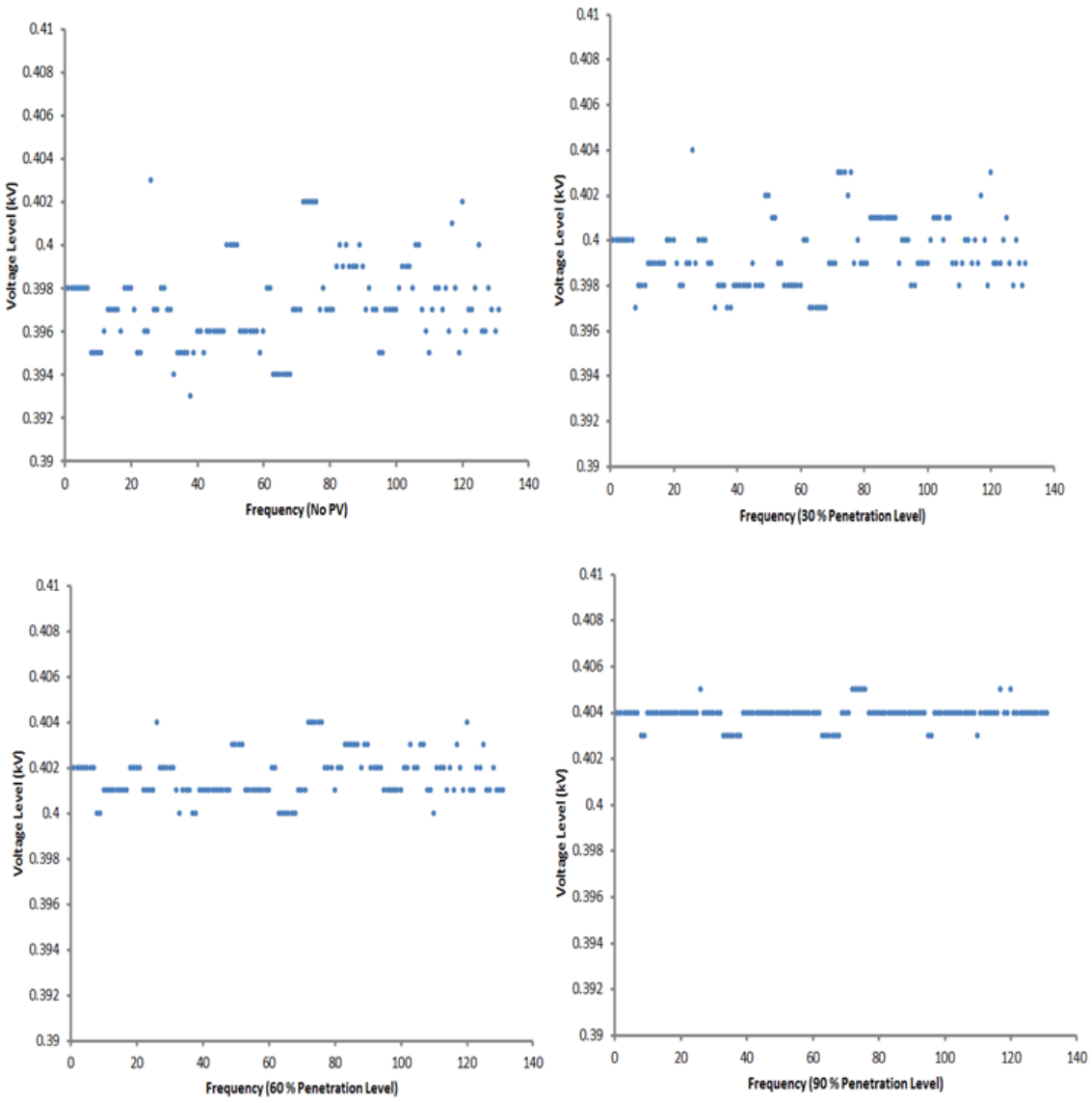

Figure D.10: Voltage Scatter Plots-Mölndal Area 2

Orust

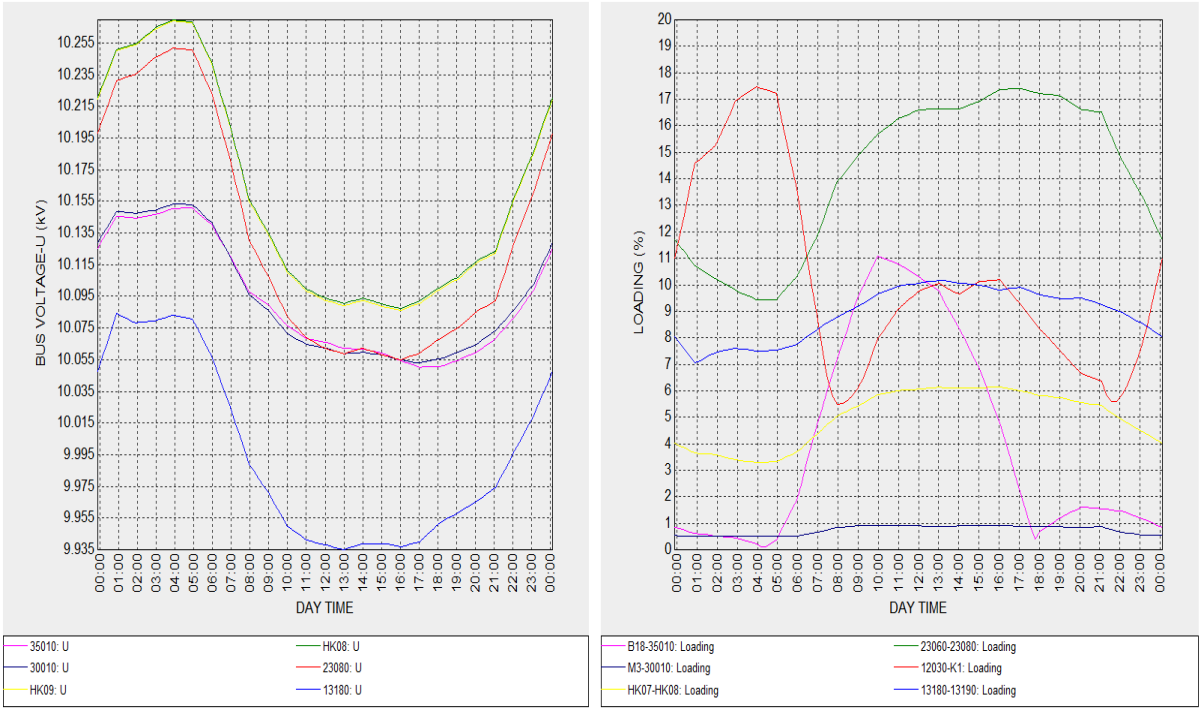

Figure D.11: Voltage Profile and Line Loading (4 % Penetration)-Orust

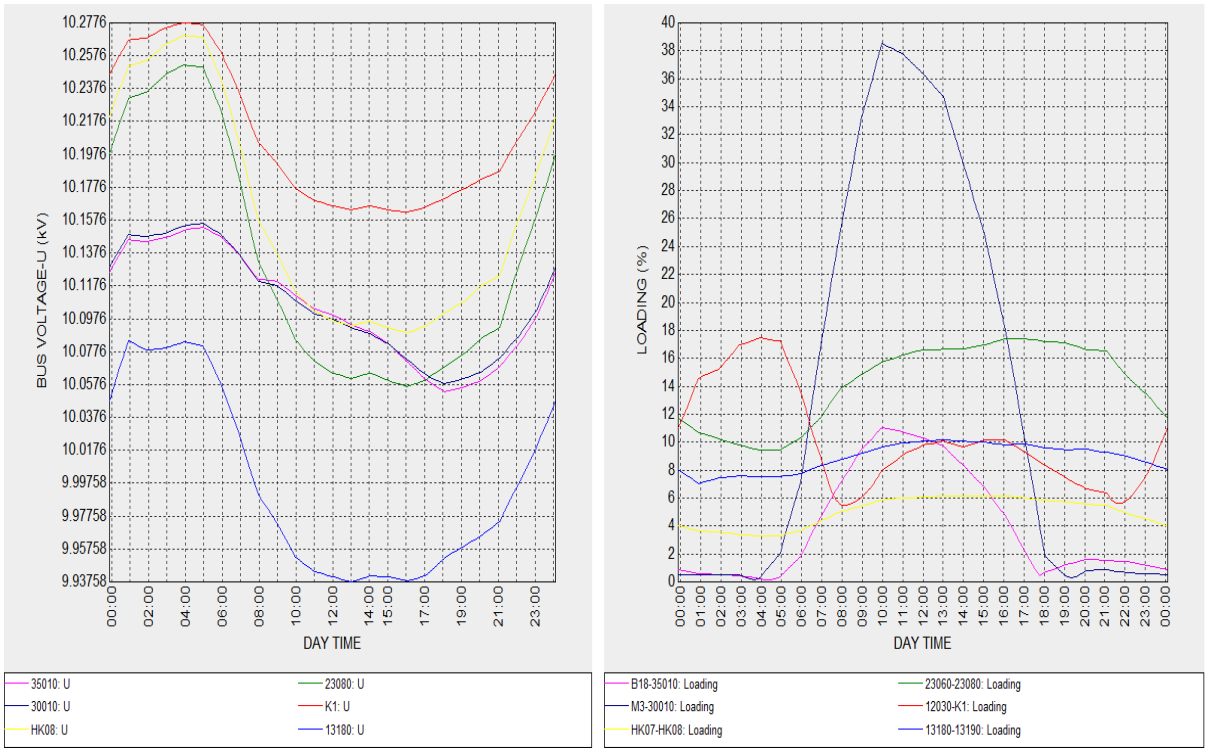

Figure D.12: Voltage Profile and Line Loading (15 % Penetration)-Orust

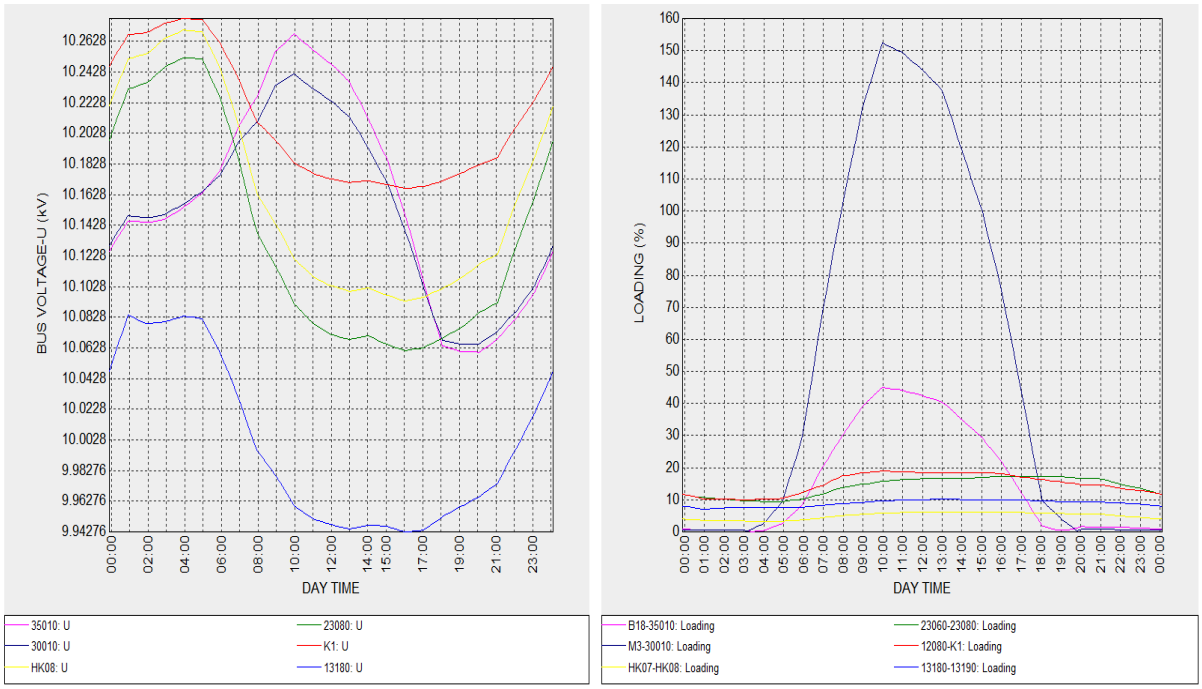

Figure D.13: Voltage Profile and Line Loading (60 % Penetration)-Orust

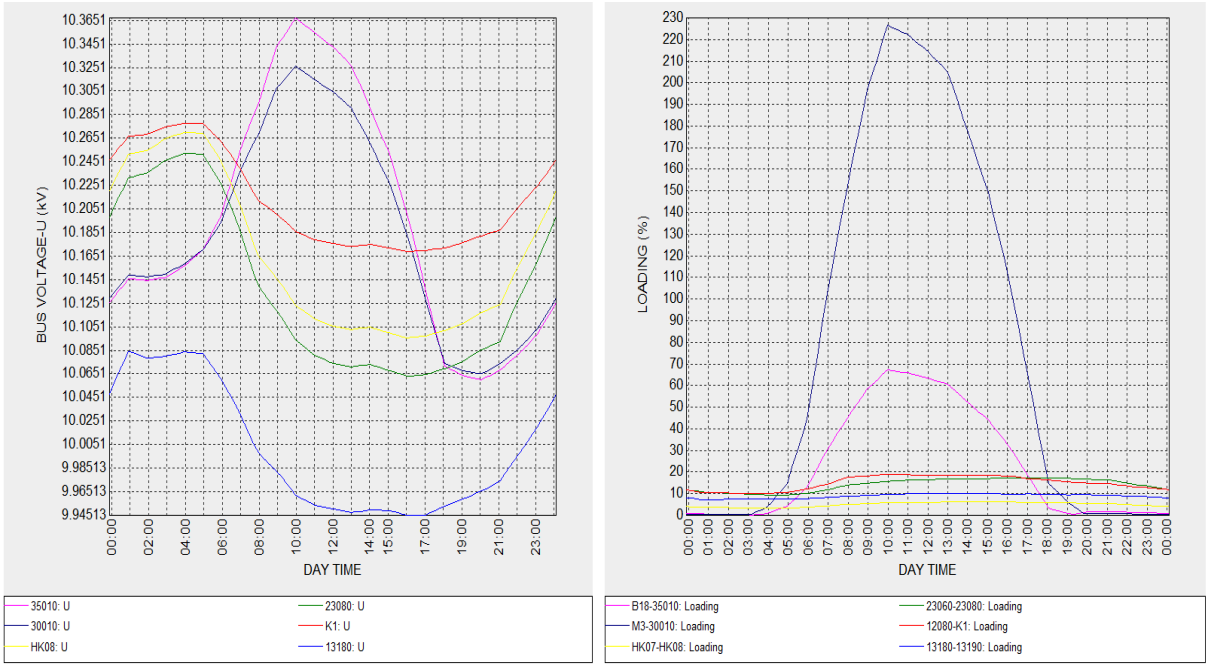

Figure D.14: Voltage Profile and Line Loading (90 % Penetration)-Orust

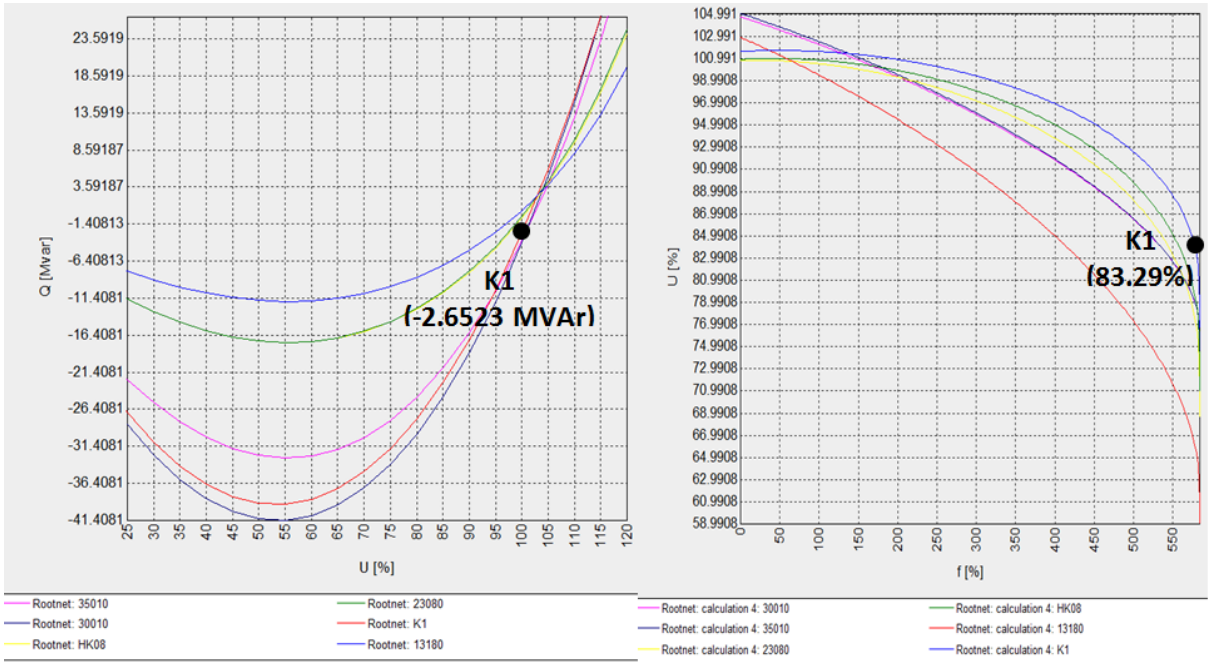

Figure D.15: Q-U and P-U curves at 60 % PV Penetration-Orust

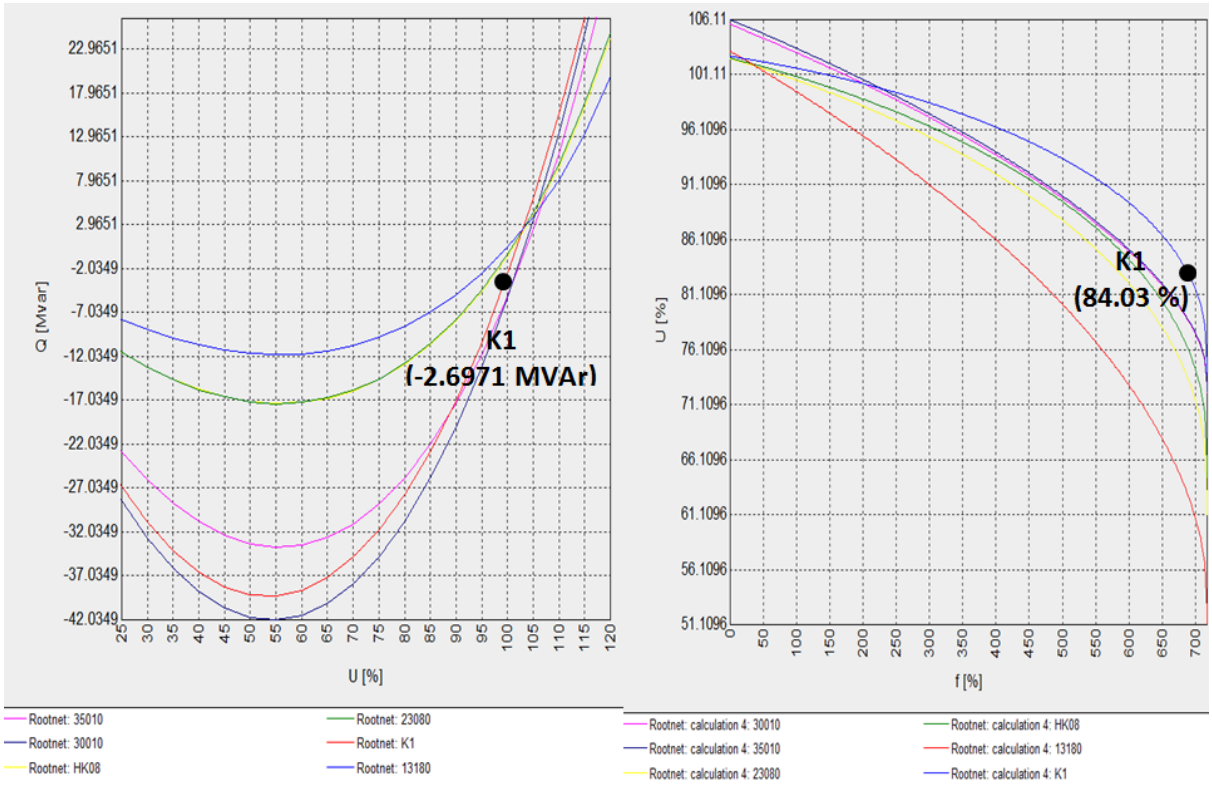

Figure D.16: Q-U and P-U curves at 90 % PV Penetration

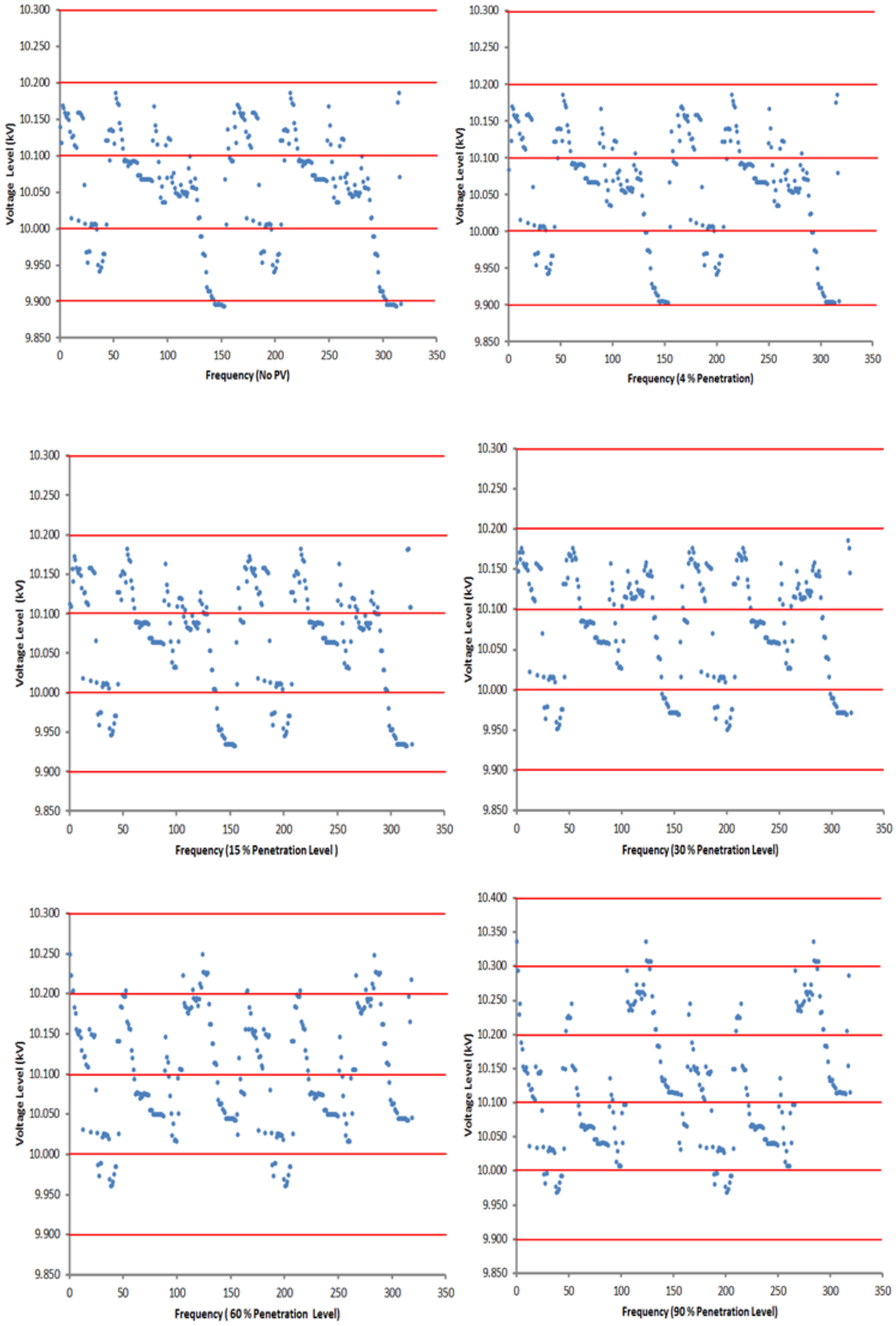

Figure D.17: Voltage Scatter Plots-Orust